UNIVERSITÀ DEGLI STUDI DI TRIESTE

XXIX CICLO DEL DOTTORATO DI RICERCA IN

Scienze della terra e meccanica dei fluidi

Assessing the role of local air-sea interaction over the South Asia region in simulating the Indian Summer Monsoon (ISM) using the new earth system model RegCM-ES

Settore scientifico-disciplinare: **FIS/06**

DOTTORANDO
Fabio Di Sante

COORDINATORE
Prof. Pierpaolo Omari

SUPERVISORE DI TESI
Dott. Erika Coppola

ANNO ACCADEMICO 2015/2016

Fabio Di Sante. *Assessing the role of local air-sea interaction over the South Asia region in simulating the Indian Summer Monsoon (ISM) using the new earth system model RegCM-ES.*

Ph.D. thesis. University of Trieste

EMAIL: fdi_sant@ictp.it

Contents

Introduction

The term "Monsoon" derives from the Arabic/Hindi word "Mausam" that means season. Initially used by sailors referring to the large variation in the direction of the wind with seasons, this word is now more extensively used by people living the regions affected by this phenomenon, to indicate the very large variation of precipitation during the rainy seasons.

The monsoon is actually considered as the manifestation of the seasonal migration of the Intertropical convergence zone (ITCZ) in response to the seasonal variation of the insolation (Chao and Chen [2001] ; Trenberth et al. [2000] ; Gadgil [2003]).

The understanding and prediction of the monsoon variability over South Asia region is one of the biggest challenges for climatologist and meteorologist today. Complex and vulnerable natural ecosystems are strictly dependent from its intensity and variability as well it is the economy and sustenance of the inhabitants of these regions. The South Asia is one of the areas dominated by the monsoon precipitation that divides the climate in two different seasons, the wet and dry seasons, and that influences the lives of billions of peoples. In the dry season, from December to April, there is hardly any rainfall that instead falls abundantly during the wet season spanning from June to September. The rainy season begins with the onset of the monsoon and terminates with its retreat. The monsoon, over India, exhibits spatial variation on its onset and retreat leading to a different lenghts of the rainy season. The Indian Summer Monsoon (ISM) has different temporal and spatial scales of variability and it is mainly driven by strong air sea interactions. The monsoon interannual variability (IAV) and the intraseasonal variability (ISV) of daily rainfall are the two most important scale of analysis of this phenomenon.

In this thesis we evaluate the performance of the new regional Earth System Model (ESM) RegCM-ES, in reproducing the main characteristics of the ISM rainfall (ISMR). We focus on the two main scale of variability (IAV and ISV) of precipitation that to a greater extent influence the life one of the most populated region in the world. We performed two set of simulations, one with the new RegCM-ES and another with the stand alone version of the atmospheric component i.e. the regional climate model (RCM) RegCM4. RegCM-ES is composed mainly by three components, the RegCM4, the ocean model MITgcm and the hydrological model HD. Another experiment, performed using RegCM-ES with a more high resolution hydrological model implemented ad hoc for this study, has been added to this two set of experiments. The climatological mean state of the monsoon is well represented by mostly all the experiments although not with the same skills. The most interesting results are observed in simulating the variability of the monsoon and here we highlight some of them.

The intraseasonal northward(eastward) propagation of the convection has been

analysed using lag/lead map of the regressed anomalies as a function of latitudes(longitudes). The two propagation are better reproduced by the set of ESM simulations thanks to the role of the air-sea coupling.

For what concerns the interannual variability of the ISMR the air-sea coupling plays an important role. The uncoupled simulations have no skills in reproducing the right signals of the standardized yearly rainfall anomalies over India. The time series of simulated anomalies by RCM exhibit no correlation with the observed anomalies obtained from the dataset of the Indian Meteorological Department (IMD) that is based on raingauges observations. On the other hand, the corresponding ESM simulations exhibits good skills in reproducing the IAV of ISMR and good correlation coefficients are observed with IMD.

One new finding of this study is a new source of predictability with one year lag for the ISMR. It is well-known that El Niño Southern Oscillation (ENSO) plays a quite important role in modulating the precipitation over most of the intertropical belt and over the South Asia region, but in this work a statistically significant correlation has been found between the Niño3.4 index for JJAS (June July August September) season and the ISMR standardised anomalies of the following year. The coupled simulations are used to explain the mechanism and investigate the models response.

The role of the new hydrological model (CHyM) implemented inside RegCM-ES on the ISMR is investigated in each section of the analysis using the comparison between the two twins experiments (two identically coupled simulations performed with RegCM-ES and with only the HD model changed with CHyM). Due to the main role that the freshwater discharge plays on the formation of a shallow mixed layer depth on the Bay of Bengal that influences the air-sea coupling and the formation of deep convection over this area, the correct estimation of the freshwater discharge is quite important. Although the new hydrological model produces a more realistic annual cycle of the discharge (verified only for a limited set of data due to the lack of observations over this region), as will be shown in chapter 3, this doesn't seem to have a relevant effect on both the mean climatological state of the monsoon and in its variability. A possible explanation for this comes from a missing representation of the barrier layer (BL) in the Bay of Bengal (BoB) due to many different reasons. Two of them are a not enough resoluted ocean model as well as a too strong wind stress forcing that doesn't allow the formation of the BL.

After an introduction of the main features of the ISM and a review of the recent literature in chapter 1, we will describe the data and the methology in chapter 2 while the analysis and discussion of the experimental results will be presented in chapter 3. To conclude, a summary will be given in the last chapter.

Chapter 1

The Indian summer monsoon

1.1 The monsoon system

Indian Summer Monsoon (ISM) is an integral part of the Asian monsoon system and presents some unique characteristic features. An Administrative divisions map of India (Fig. 1.1) and a physical geography map of part of South Asia region has been added (Fig. 1.2) to make the followig description clearer.

The "Trough zone", also called "Monsoon zone" or "Monsoon trough", is a belt of minimum atmospheric pressure spanning over India peninsula and extending from north Bay of Bengal (BoB) to the region of Rajasthan (Rao [1976]). As shown in Fig. 1.3 highest rainfall amount are observed over the Western Ghats on the Deccan Plateau, while lowest rainfall amounts are recorded over western Rajasthan (the Thar Desert) increasing gradually as we move towards Southeast.

Accordingly to the Indian Meteorological Department (IMD) we can observe four different precipitation seasons over India: Winter Season (January-February), Pre Monsoon Season (March-May), Southwest Monsoon Season (June-Semptember) and Post Monsoon Season (October-December). This four seasons have different spatial patterns for the mean rainfall as shown in Figure 1.3. During the winter season the rain belt, associated to the Tropical Convergence Zone (TCZ), is located around 5°S, over the Equatorial Indian Ocean (EIO) and the Indian territory is free from rain. Associated with the northward migration of the TCZ, during the pre monsoon season, the precipitation begins to approach the south and north-east part of India (Figure 1.3(b)). Two rainbelts are observed in Figure 1.3(c) during the summer monsoon season. The first one covers the EIO and extent from 60°E till the South East asia region. The other one located over India is responsible for the strong precipitations and takes the name of Indian Summer Monsoon Rainfall (ISMR). During this season we can identify a subseason that we will call peak monsoon period (July-August) when the rainfall covers most of the India. The monsoon, during the peak period, exhibits wetter (active spells) and drier (break spells) days as will be explained more in detail in a dedicated section. The topography plays a big role in triggering very high rainfall amounts over the winward Western Ghats and over the northeastern region (figure 1.3(c)). While the rainfall occurs mainly during the summer monsoon season in almost the whole India, over Southeastern peninsula the main rainy season is shifted at the end of the year (figure 1.3(d) ; October-December) and takes the name of Northeast monsoon season (also called post monsoon season).

Figure 1.1. Administrative divisions of India (figure taken from https://en.wikipedia.org/wiki/File:India-map-en.svg)

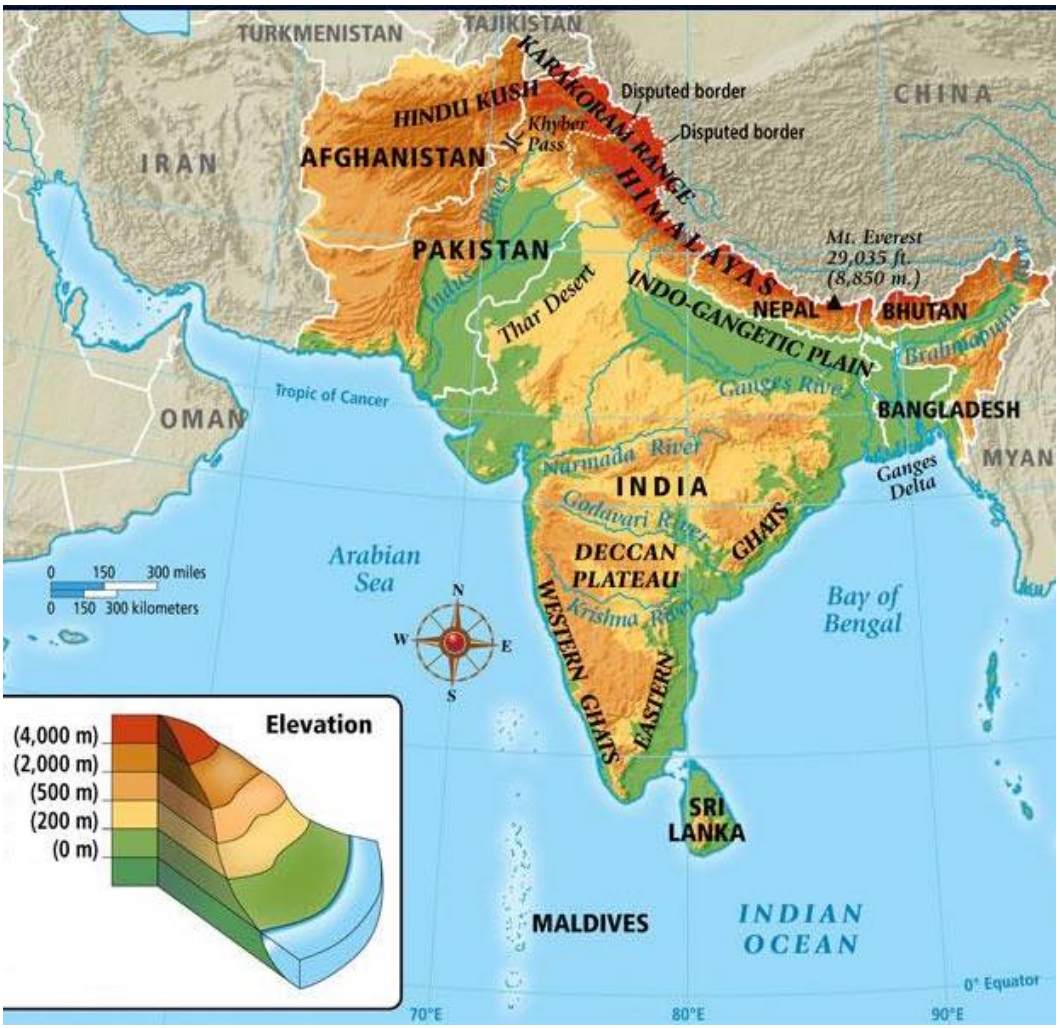

Figure 1.2. Physical Geography of India(figure taken from https://sites.google.com/a/ehschools.org/global-9/unit-1/ancient-india-ch-3/3-1)

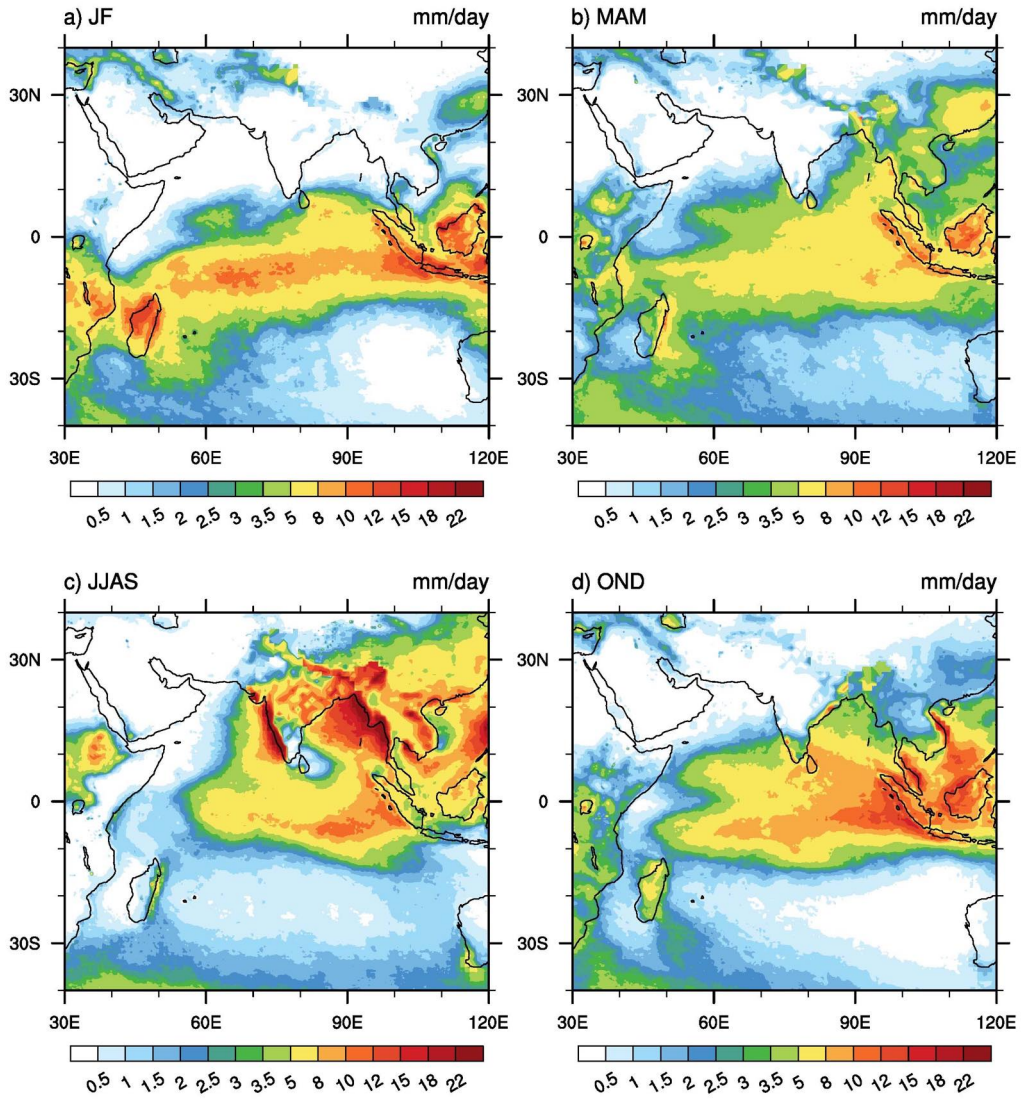

Figure 1.3. Climatological precipitation (mm/day) for the 4 seasons: (a) winter season (JF; January, February), (b) pre monsoon season (MAM; March, April and May), (c) southwet monsoon season (JJAS; June, July, August and September) and (d) post monsoon season (OND; October, November and December); from the Indain Meteorological Departhment (IMD) dataset (1980-2007) over India and the Tropical Rainfall Measuring Mission (TRMM ; 1998-2013) elsewhere.

Another important feature of the ISM is the monsoon onset that is associated with the reversal of the meridional gradient of upper tropospheric temperature south of the Tibetan Plateau (Li and Yanai [1996]).

The onset of the ISM is identified with an abrupt increase in rainfall in the south Kerala state reliably every year, also known as monsoon onset over Kerala (MOK). The mean date of the MOK for the last century is around 1 June with a standard deviation of about 9 days (Ananthakrishnan and Soman [1988])(fig. 1.4).

The MOK is associated with a large area of organized rainfall related to a deep convection belt extending from south Arabian Sea (AS) to south China trough the Bay of Bengal (BoB; Joseph et al. [1994]).

During the boreal spring, before the monsoon starts, the Indian subcontinent gets hot under the high insolation and an heat low develops over the continent. During the monsoon onset the heat low turns in a dynamic trough with deep cyclonic vorticity above the boundary layer and deep convection activity associated to it. During the MOK there is an overturning in the thermal and pressure gradients over India and the monsoon starts (Ananthakrishnan and Thiruvengadathan [1968] Ananthakrishnan et al. [1983]).

During the summer monsoon season the Tropical Convergence Zone (TCZ) has two favoured locations over the South Asia region and it is expressed as two maxima in seasonal mean precipitation. The northern band is located along the monsoon trough extending to the north Bay-of-Bengal, the other is located between 0° and 10°S over the Indian Ocean warm water (Sikka and Gadgil [1980] Goswami [1994]).

The Maximum Cloud Zone (MCZ), forming over the monsoon trough, is also called Continental Tropical Convergence zone (CTCZ; from the main position over the Indian subcontinent). The CTCZ life-span is not more than one month, during this period it can oscillates north and south over the trough (between 15° and 25° N), and can be replaced by the northward movement of a secondary MCZ forming over the Equatorial Indian Ocean (EIO) (Sikka and Gadgil [1980]). The oceanic TCZ is important in supporting the persistence of the CTCZ but it could also be the case that, between this two convergence zones, a competition starts and the strengthening of the oceanic TCZ make rise to a dry spell over the India subcontinent (Sikka and Gadgil [1980]).

The northward propagation of the well organised convective systems from EIO plays a major role for both, during the transition phases of the ISM (onset and retreat), and during its peak (Sikka and Gadgil [1980]). Synoptic disturbances forming over the Bay of Bengal (BoB) and over the monsoon trough, have also a major role in maintain alive the CTCZ over the trough zone and hence the active phases of ISM(Sikka and Gadgil [1980]) about which we will discuss in greater detail in the section 1.2.2.

To ensure the development of organized deep convection a threshold of 28°C in the SST is needed (Gadgil et al. [1984]). In the work of Waliser et al. [1993], deep clouds has been observed over warmer sea but the convection decreases with increases SST above the threshold of 29.5°C. This comes from the fact that the warmest ocean areas lie under clear sky conditions.

When the SST threshold of 27.5°C is reached the dynamics plays a major role in inducing convection and the convergence (divergence) in the low level winds became the limiting condition for convection (no convection) situations (Graham and Barnett [1987]).

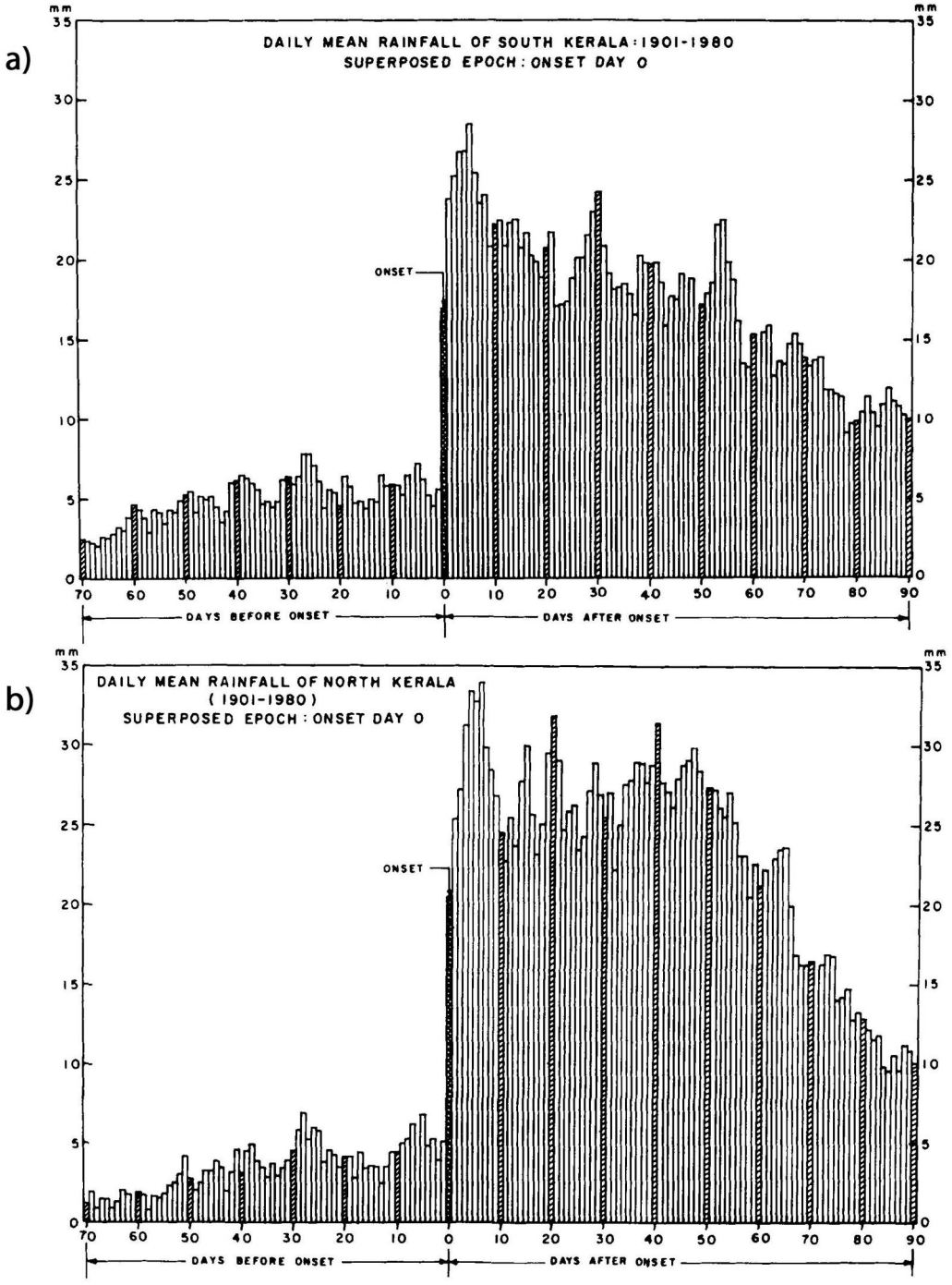

Figure 1.4. (a) Mean daily rainfall (mm) over south Kerala after superposing onset dates of the southwest monsoon for the period 1901-1980. (b) Mean daily rainfall (mm) over north Kerala after superposing onset dates of the southwest monsoon for the period 1901-1980(figure taken from Ananthakrishnan and Soman [1988]).

Two clear examples of this two limiting conditions are observed during the ISM. The West AS (WAS), that shows temperature under the minimum temperature threshold (27.5°C), remains under dry conditions while in some area of the EIO (Equatorial Indian Ocean) where the temperature are above this threshold, the rainfall variations are independent from the SST variations.

Over the Northwest part of Indian subcontinent and Pakistan, during the ISM, is often observed an heat low with dry weather conditions and hot temperatures (Rao [1976]). The name heat low arises from the need of distinguishing it from the dynamical low that is instead associated with moist convection. The heat low has low-pressure values on the surface but ascending motion only in the low troposphere with subsidence conditions over 3 km hight that suppresses the convection. The heat low together with the dynamic low, extending from to the BoB westward, forms the monsoon trough.

Making use of reanalyses for divergent winds and associated vertical motions, from the National Centers for Environmental Prediction-National Center for Atmospheric Research (NCEP-NCAR; Kalnay et al. [1996]) and European Centre for Medium-Range Weather Forecasts (ECMWF; Gibson et al. [1997]), Trenberth et al. [2000] identified two main monsoon modes during the year. The first mode, which accounts for 60% of the annual variance and migrates and evolves considerably with the seasons, is associated to a deep wind convergence in the lower and middle troposphere and a maximum in wind divergence at 150 mb. At the second mode corresponds a shallow lower overturning cell and it accounts only for the 20% of the variance. The overturning patterns identified in this study are associated with the surface trough in the tropics and provide a bases to delimit monsoon regions of the world.

1.2 Variability of the monsoon

The monsoon has different temporal and spatial scales of variability. Ranging from large-scale subseasonal variations to interdecadal oscillations.

1.2.1 The intraseasonal oscillations of the Indian summer monsoon

In addition to the fluctuations of weather that occur with a timescale of 5-7 days (synoptic disturbances), the Indian Summer monsoon exhibits, in almost of all its elements, westward propagating fluctuations around a quasi-biweekly period range (Krishnamurti and Bhalme [1976], Krishnamurti and Ardanuy [1980] Chen and Chen [1993]). The quasi-biweekly oscillations appears to be related to fluctuations that arise from feedbacks involving clouds (Krishnamurti and Bhalme [1976]). The dry and moist instabilities, which arise from the eating of the soil due to insolation, trigger the cumulus convection. The slow increase of cloudiness on the other hand gradually shields the incoming short wave and as a consequence the moist and dry instabilities start to be reduced as well as the cumulus convection associated. Besides the westward propagating mode (10-20 days oscillation), a 30-60 days (sub-monthly range) northward propagating mode is seen in cloudiness and precipitation (Yasunari [1979] Yasunari [1980] Yasunari [1981] Sikka and Gadgil [1980]). The northward propagation of the precipitation belt happens every year regardless if it is a good or a weak monsoon season, furthermore it plays a role in the onset, retreat and revival from break situations of the monsoon. Poleward propagations of the TCZ

were firstly simulated by Webster and Chou [1980b] and Webster and Chou [1980a], using a zonally symmetric ocean-atmosphere-land climate model. The 30-60 days model of monsoon has been observed over a large part of the tropics and it is related to the MJO (Madden-Julian Oscillation). The MJO is characterized by a traveling pattern of anomalous rainfall propagating eastwards manifesting its effects over the warmest water of Indian, Pacific oceans and less frequently over the west coast of Central America and Atlantic Ocean (Pai et al. [2011]). The bimodality in the TCZ (occurrence of two favorable zones for convergence, one over the equatorial oceans and another over the continent) observed during the ISM as well as the poleward propagations of the TCZ, appears to be a basic features in the seasonal oscillations of the TCZ only over the Asian summer monsoon region (Gadgil and Srinivasan [1990]).

The eastward and northward propagations take part approximately equally to the total Intraseasonal Variability (ISV) in the South Asian monsoon region and they strongly modulate the synoptic activity. The two propagation modes are responsible of the Intraseasonal Oscillations (ISO) of the monsoon that occur during the ISM, dictating, along with the synoptic disturbances that have a short "life-cycle", the active and break phases of the ISMR. During an active phase of the ISO the conditions for cyclogenesis are 3.5 times more favorable and more clustered over the monsoon trough zone compared to a break condition (Goswami et al. [2003]). The strong modulation of the synoptic activity by ISO has been demonstrated also by Krishnamurthy and Shukla [2007] and Krishnamurthy and Ajayamohan [2010].

1.2.2 The Active and Break phase of the ISMR

The superposition of multiple time scale variations of ISM (from synoptic to sub-monthly), give life to the break and active phases of ISM. The first reference describing a monsoon break dates back to Blandford [1886], he described the fluctuation in the rainfall over the monsoon trough zone. Blandford [1886] referred to the periods between two active spells as "intervals of droughts" that occur "when northwesterly and westerly winds interrupt the monsoon in north-western and central India, it (the trough of low pressure) is pushed northward to the foot of the hills". Ramamurthy [1969] describes a weak spell as a condition that occur every year associated to a less cyclonic vorticity and rainfall over the monsoon trough and defines a break in the monsoon as a particular case of weak spell, that doesn't happen every year, having well defined circulation features. More recently, Ramamurthy [1969] and Raghavan [1973] identified the large-scale circulation changes associated with the active (abundant) and break (scanty) spells of the ISM. In general, a break (active) phase of the monsoon is associated with a decrease (increase) of pressure over the monsoon trough zone resulting in decreased (increased) cyclonic vorticity over the monsoon region and a strengthening (weakening) of the moisture-laden Low Level Jet (LLJ) (Ramamurthy [1969] Raghavan [1973]).

The recovery from a break occurs mainly trough two disctint processes: The first, suggested by Ramamurthy [1969], happens in the 45-55% of the situations and starts with the formation of a synoptic disturbancies over the BoB, while the second one occurs with the northward propagation of the TCZ (Sikka and Gadgil [1980]).

Many criteria are used in literature to define active and break phases of the SAM, each one with its own pro and contra. The comprehensive work by Webster

et al. [1998] refers to an active and break condition following definition by Magana and Webster [1996] where they used a zonal wind anomalies and outgoing longwave radiation anomalies over the central part of India (65-95°E, 10-20°N) to identify these events. Rajeevan et al. [2010] suggested criteria for identification of active and break events of the ISM on the basis of normalized anomaly of the rainfall during the peak monsoon months of July and August over a critical area called the monsoon core zone. This criterion is chosen so as to ensure a large overlap with the traditional breaks documented by Ramamurthy [1969] and De et al. [1998]. Active and break are defined as period longer than 3 days where the normalized anomaly of the rainfall over the monsoon areaa (65-88°E, 18-28°N) exceeds 1 or is less than -1 respectiveley. This new criteria is applied by Indian Meteorological Department (IMD) to monitor the alternation of active and break events on an operational basis (Rajeevan et al. [2010]). The area chosen by Rajeevan et al. [2010] is highly correlated with the interannual and intraseasonal variability of ISMR over all India and doesn't include the Himalayas foothills, that receives large amount of precipitations also during the ISM break. During the break days, the precipitations increase and concentrate over the foothills of Hymalaya, the north east of India and the east peninsula and are negatively correlated with the rainfall of the monsoon core zone (Rajeevan et al. [2010]). Composite analyses of monsoon rainfall based on days on which the Low Pressure Systems (LPSs), forming in the BoB and AS, are present and days on which they are absent, show how the LPSs may determine the active and break phases of the monsoon (Krishnamurthy and Ajayamohan [2010]). This last study offers a broad method of defining the active and break monsoon phases and explains the role of these tropical disturbances on seasonal monsoon rainfall over India.

Break typically occurs during the monsoon peak (July-August) and may last for a prolonged period than active spells causing severe dry condition over large part of India (Rajeevan et al. [2010]). In the derived high resolution daily gridded rainfall dataset over India examined by Rajeevan et al. [2010], spanning from (1951-2007), it has been observed an average of 7 days of active and break events during the period July and August. The number and life-span of the breaks in a monsoon season make that a good or a weak monsoon season (Krishnamurti and Bhalme [1976] Sikka [1980] Gadgil and Joseph [2003] Rajeevan et al. [2010]).

To summarize, during a typical break day it can be observed:

- a totally absence of the easterlies winds over India up to 3 km
- the absence of the monsoon trough
- the presence of a ridge over the western part of India
- anticyclonic vorticity at 850hpa hight
- decrease of the north-south gradient of surface pressure
- large negative anomalies of precipitations over the monsoon trough
- positive anomalies over the southeastern India and Himalayan foothills

During a typical active day it can be observed:

- synoptic low systems over the monsoon trough
- positive precipitation anomalies over the trough
- cyclonic vorticity at 850hpa hight

(Ramamurthy [1969] Rao [1976] Sikka and Gadgil [1980]).

1.2.3 The interannual variability of the Indian summer monsoon

It is possible to define a drought(flood) year if the ISMR (Indian Summer Monsoon Rainfall) departs significantly, less than -1(greater than +1) normalized values, from its long term mean. External forcing as the El Niño-Souther Oscillation (ENSO; Walker [1925]) may contribute to the intensity of the ISM but the interannual varibility of mean ISMR seems to be governed by internal chaotic dynamics that manifests in the form of "active" and "break" spells wihtin the summer monsoon season (Gadgil and Joseph [2003]). Supporting this thesis is the study of Rajeevan et al. [2010], he founded that the number of break days results to be significantly correlated with the ISMR. He also showed how there are important differences between the spatial patterns of the active/break spells and those characteristic of interannual variation associated with the link to ENSO. The influences of ENSO on ISMR has been investigated since the beginning of eighties (Sikka [1980]; Rasmusson and Carpenter [1983]). In the last decades of the last century the correlation between the ISMR and ENSO has weekened probably due to the shift in the Walker circulation (Walker and Bliss [1932]) anomalies as well as an increase of land-ocean thermal gradient linked with the global warming trend (Kumar et al. [1999]). More recent studies have indicated, as responsible of the weakening of the teleconnection between the ENSO and ISM, the natural variability rather than, as suggested earlier, the antropogenic forcing inducing stronger thermal gradient between land and sea (Annamalai et al. [2007]; Turner et al. [2007]). In addition to the ENSO-ISMR relationship, the EQUatorial INdian Ocean Oscillation (EQUINOO) has a contribution in the Interannual Variability (IAV) of the ISMR (Gadgil et al. [2003] Gadgil et al. [2004]). The EQUINOO is the atmospheric response to the Indian Ocean Dipole (IOD) that is characterized by anomalies in the SST and SSH (sea surface height) in the eastern and western parts of EIO (Equatorial India Ocean) (Saji et al. [1999] Webster et al. [1999]). Looking at the 1997-1998 years investigated by Webster et al. (1999) it is possible to note that a positive phase of the EQUINOO is associated at an enhanced convection over West Equatorial Indian Ocean (WEIO), where there were positive SST anomalies in the autumn 1997, inducing a suppression of convection in the opposite side of the ocean i.e. the East Equatorial Indian Ocean (EEIO). Viceversa the opposite happened on summer 1998 (negative phase of the EQUINOO), where positive SST anomalies over EEIO induced suppression of convection over the WEIO (fig. 1.5).

The positive phases of the EQUINOO are associated to a positive anomalies on ISMR whereas negative phases are associated to a negative anomalies(Gadgil et al. [2004] ; Ihara et al. [2007]. Considering the June to September averages of EQUINOO index (EQWIN) and ENSO index (NINO3) it is possible to note as the correlation between the two is not significant (-0,09) and they can be considered as independent modes (Gadgil et al. [2004]). The two modes together better represent

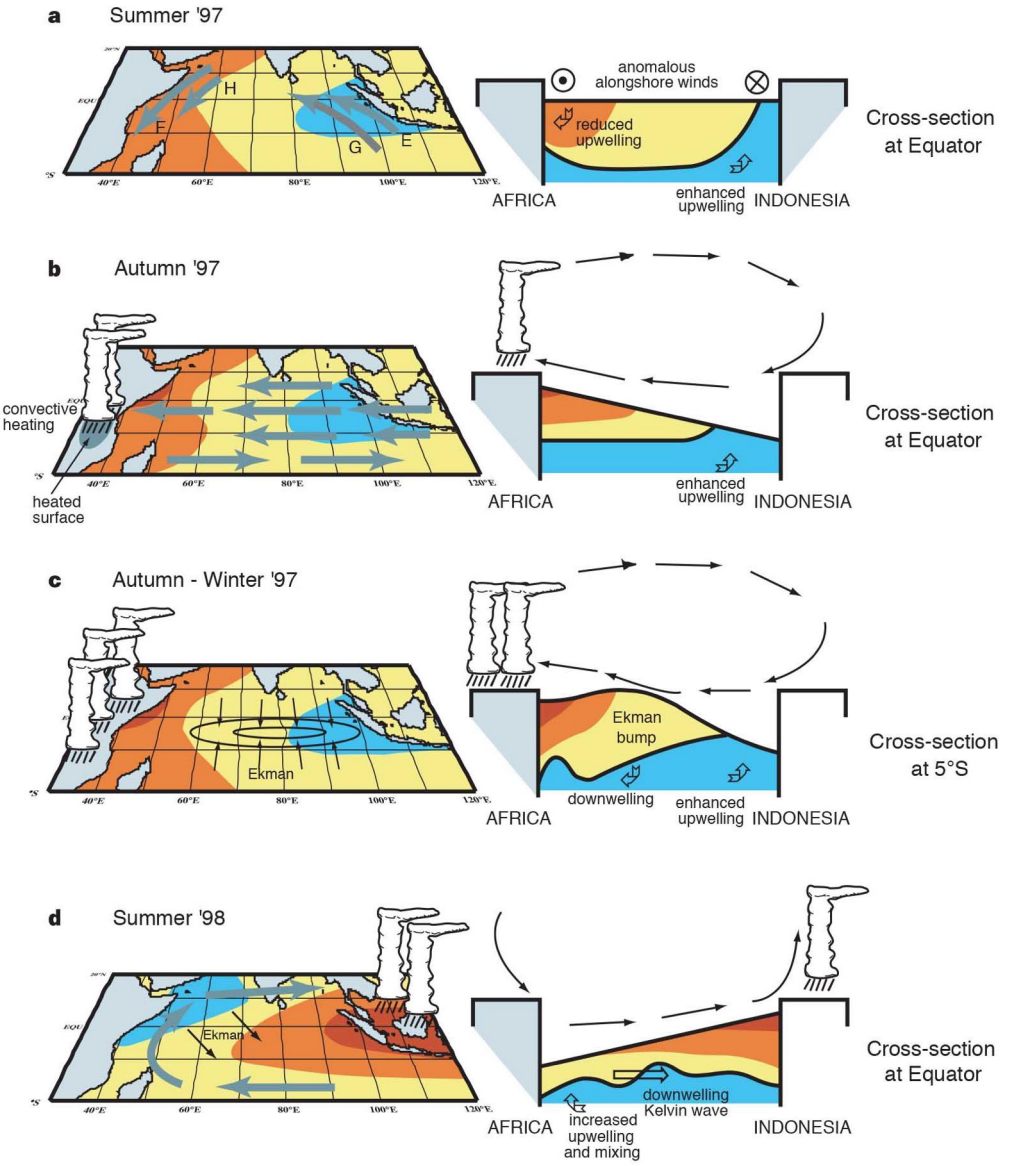

Figure 1.5. Diagram of the sequence of events in 1997/98 (Coupled ocean-atmosphere dynamics in the Indian Ocean during 1997/98, figure taken from Webster et al. [1999]).

the IAV of the ISMR respect to consider only on of the two (Ihara et al. [2007]). ENSO typically starts to develop in boreal summer and have its maximum anomalies values in boreal winter. Induced SST anomalies over the North Indian Ocean outlast more than a season after the ENSO peak and lasting until the next summer (Nigam and Shen [1993] ; Du et al. [2009]). This wide warming/cooling over the Indian Ocean induced by ENSO, constitutes the dominant mode of SST variability over the Tropical Indian Ocean (TIO) and takes the name of Indian Ocean basin mode (IOBM ; Klein et al. [1999] ; Yang et al. [2007]). The IOD mode is the second mode of SST variability over TIO (Webster et al. [1999] ; Saji et al. [1999]). The IOD effect is concurrent with that of IOBM and has been suggested to have a potential negative influence with its impact in the ISMR (Bracco et al. [2005] ; Bracco et al. [2007] ; Cherchi et al. [2007] ; Cherchi and Navarra [2013]). The correlation of Indian ocean SST with the NDJ(0) Niño-3.4 index shows two maximum peaks, one occurring during the concurrent boreal winter and the other during the following summer (Du et al. [2009]). Here the numerical 0 between parenthesis denote the year of the developing positive Niño-3.4 index anomalies while the numerical 1 will denote the following year. Many studies in the last decade are focused in the concurrently correlation between the main EOF mode of the ISMR and the ENSO indices (Mishra et al. [2012] ; Syed and Kucharski [2016]) less deeply investigated is the correlation that ENSO has with ISM in the summer following the period of its peak (DJF) (Xie et al. [2009]). The processes involved are the same founded in other studies(Izumo et al. [2008] ; Xie et al. [2009]) and a review of these mechanisms with the recent advances can be found in Xie et al. [2016]. In this study the late response in the ISMR is related to the capacitor capability of the Indian Ocean (Xie et al. [2009]). In spring and summer, WAS coastal zone, exibits a minimum in the mixed layer depth and SST gets prone to upwelling variations (Montégut et al. [2007] ; Fischer et al. [2002]). The WIO and AS SST plays an important role in modulating the ISMR, a decrease in upwelling in these areas causes an intensification of precipitation over the Indian Western Ghats (Izumo et al. [2008]). The increase of rainfall over Western Ghats is principally due to the increase of SST over IO that follows an El Niño event and a major contribution to the outlast Warmer SST anomalies over this basin during the Pre-Monsoon season results from easterlies anomalies over the north part of IO associated with the IO-TNWP AAC (Indian Ocean - Tropical North Western Pacific anomalous anticyclone). The resulting weakened westerlies during the pre-monsoon season reduce surface evaporation over the IO that induces the warming (Du et al. [2009]). Weare in 1979 using a statistical analysis of different SST datasets for the period 1949-1972 showed how there is a strong link between pacific SST anomalies and Indian Ocean SST's. Higher Indian SST's generally follow higher Pacific SST's by a season after an El Niño event. He suggests that periods with higher than normal SST's over IO, usually accompanied by positive anomalies in MSLP, is a possible explanation to why higher Indian SST's are usually not associated with a stronger than normal precipitation over India. A recent study correlates the weakening trend of the ISMR in the last century to the warming SST over the Western Indian Ocean (Roxy et al. [2015]). This confirms the finding of Kucharski et al. [2006] that trough Atmospheric General Circulation Models (AGCM) simulations showed how a meridional gradient in Indian Ocean SST's is responsible for changes in the local Hadley circulation affecting in turn the ISMR.

1.3 Numerical modeling

The atmosphere numerical models are developing fast and with them the increase of skills in forecasting the ISM. Some models such as the Coupled Forecast System model version 2 (CFSv.2) of the US National Centers for Eviromental Prediction for example, are now able to simulate with some reliability characteristics of the ISO of the monsoon (Sabeerali et al. [2013] ; Sharmila et al. [2013]). Moreover, the atmospheric models are a very useful tools to study the characteristics and feedbacks of this complex phenomenon. Here we present a brief review of some of the advancements reached in the last few decades.

The skills on simulating the IAV of all-India region by 32 Atmospheric General Circulation Models (AGCM) being part of the Atmospheric Model Intercomparison Project (AMIP, Gates [1992]) have been evaluated by Sperber and Palmer [1996]. The ensemble simulations for the period 1979-88, using prescribed SST boundary conditions, was obtained from perturbation of both model formulation and initial conditions. The results showed how the simulation of IAV of the ISM is a very tough task for the AGCMs and how the skill in simulating ISMR were poor. These results come in part from the lack of air-sea interaction in the AIMP experimental design.

The relationship between the rainfall and SST, in AGCMs where the atmosphere is forced by prescribed lower boundary condition, over the BoB, is not reproduced correctly and most of the AMIP models simulate rainfall anomalies positively correlated with SST anomalies whereas they are inversely related in the reality (Wang et al. [2004]). Moreover, the poor representation of the mean rainfall pattern and of the IAV of precipitation, over the Indian region, comes out from the lack of air-sea interaction as elucidated by different studies (Gadgil and Sajani [1998] Fu et al. [2002]). In the warm pool of Indo-Pacific ocean the SST anomalies are forced by atmosphere anomalies and this partially explains the unsuccessful simulations of asian pacific summer monsoon rainfall by the AMIP (Wang et al. [2005]). When a coupled atmosphere-ocean model is used improvements can be observed in simulating climatological ISO for the Asian Summer Monsoon. The main improvements come from a better representation of the two rainbelts (related to the CTCZ and the oceanic TCZ) and the poleward-propagation associated with them (Fu et al. [2002]). In a later study Fu et al. [2007], making use of an atmosphere-ocean coupled model, assessed that the implementation of the coupling increases the predictability in simulating the monsoon ISO (MISO) respect to an atmosphere-only model as was previously supposed by Kemball-Cook and Wang [2001]. A fully coupling between the dynamic ocean and the atmosphere appears to be necessary to reproduce the IAV related to ENSO. Bracco et al. [2007] showed how the switch from an atmosphere-only model to a fully-coupled atmosphere-ocean model, improved significatively the interannual and interdecadal variability, linked with ENSO, of the Asian monsoon. From the just mentioned studies it has become clear the importance it has became clear the importance of considering the air-sea interaction for correctly representing monsoon processes. The development of coupled atmosphere-ocean-land-cryosphere climate models (AOGCMs) has vastly increased in the last decade to fill the gap, and the Coupled Model Intercomparison Project (CMIP) was initiated to provide a common framework in support of diagnosis, intercomparison, documentation and data access under the World Climate Research Programme (WCRP; `http://cmip-pcmdi.llnl.gov/index.html`).

To date the program has completed different phases, the third one (CMIP3; Meehl et al. [2005]) has collected the model output from simulations of different AOGCMs mostly during the years 2005 and 2006 and the papers written on the analisys of those models have been utilized to write the Fourth Assessment Report (AR4) of the Intergovernemtal Panel on Climate Change (IPCC). The fifth phase (CMIP5; Taylor et al. [2012]), the most recent one, has started in 2008 and completed in the following 5 years with the purpose of improving the CMIP3 model simulations, increasing the spatial resolution and moving towards the use of Earth System Models (ESMs; Stouffer et al. [2011]). The CMIP5 contributed to the Fifth Assessment Report (AR5) of IPCC.

An assessment of the skills on simulating the ISM for the period 1961-1999 by 25 CMIP5 and 22 CMIP3 models output and a comparison between the two set of output is presented in the work of Sperber et al. [2013]. A skill score system was employed and a multy-model means (MMM) of this skill was used to evaluate the performances. CMIP5 models MMM climatology and ENSO variability result in better agreement with the observations compared to CMIP3. The late monsoon onset, the poor representation of the annual cycle of ISMR and the inaccurate simulation of the oceanic TCZ are still present in both CMIP3 and CMIP5 models.

In the recent CMIP6, the sixth phase of the project, has been introduced a new contribution, the Global Monsoons Model Inter-comparison Project (GMMIP)(Zhou et al. [2016]). 21 international modeling groups are committed to joining GMMIP and its main focus is on monsoon climatology, variability, prediction and projection, which is relevant to four of the âĂIJGrand ChallengesâĂİ proposed by the World Climate Research Programme.

The delayed onset and late retrieval, in the annual cycle of rainfall over India, has been observed in many CMIP5 models simulations by other study as Sabeerali et al. [2013]. In their research the outputs of 32 different CMIP5 models have been analized for the period from 1986 to 2005. The simulation of a correct monsoon ISO variance is still a challenge by the majority of the models and most of them understimate its values over equatorial IO. The authors assert that a correct simulation of seasonal mean precipitation magnitude and pattern doesn't imply a correct representation of Boreal Summer Intraseasonal Oscillation (BSISO) in CMIP5 models. Less than 50% of the 32 models analized in this study are able to simulate the northward propagation of convection and emerges that the same models are also able to simulate the eastward propagation along the equatoial Indian Ocean showing a relation between the two propagations. In many models the northward propagation is resulted absent below 5°N.

The added value of finer spatial and vertical resolution model are well documented in the literature.The introductions of Regional Climate Models (RCMs) shows an improvement in simulating the spatial and temporal patterns of temperature and rainfall over India thanks to a better representation of the complex orography (Himalaya and Indian Western Ghats for example) and the fine scale atmospheric processes associated with them (Ratnam and Kumar [2005] ; Pattnayak et al. [2016] ; Dash et al. [2013] ; Dash et al. [2006]). The representation of tropical cyclones forming over BoB and equatorial IO is imporoved when the spatial resolution of the model is of the order of 50-60 km (Landman et al. [2005] ; Samson et al. [2014]) but the choice of the model domain and parametrization schemes remains of crucial importance for a better simulation of their intensities and traks (Goswami and

Mohapatra [2014]). The use of the coupled Atmospheric Ocean Regional Climate Models (AORCM) to assess the role of air-sea coupling in the representation of ISM is still limited and only few attemps are reported in the literature (Ratnam et al. [2009] ; Samala et al. [2013] ; Samson et al. [2014] ; Seo et al. [2009]). The still limited use of this models has not yet allowed the development and the distribution of RESM around the regional climate modeling community since the last years, when the new RESM RegCM-ES, described in a dedicated paper by Sitz et al. [2017], has been developed and distributed. As for the AGCM also for the RCM an added value is expected when we use a coupled RESM. In previous studies different models and methods has been used to couple the ocean and atmosphere regional models over the Indian domain and only short simulations have been completed. The RCM RegCM3 (Pal et al. [2007a]) has been coupled with the version 2.2 of ROMS (Shchpetkin and McWilliams [2005]) in the study of Ratnam et al. [2009] in order to simulate the ISM for four years (1997, 1998, 2002 and 2003) and the results show a better representation of the air-sea feedbaks over the IO that translate in a better representation of the ISM. As in the suty of Ratnam et al. [2009], Samala et al. [2013] in 2013 made use of a coupled model to assess the role of air-sea interaction during the ISM. For this study they made use of the Weather Research and Forecasting (WRF; Wang et al. [2004] ; Skamarock et al. [2005]) coupled with ROMS and completed eight different simulation with the same setting for eight consequent ISM (from may to september) and the results compared to the standalone version for both the components. The improvements shown in this study are related to the mean climatology of the ISMR togheter with a better simulation of the ISO of rainfall in the coupled version of the models. A longer simulation (1990-2009) to simulate the ISM has been completed and analized only more recently by Samson et al in 2014 using the new model NOW composed by Nucleos for European Modelling of the Ocean (NEMO; Madec et al. [2015]) and WRF coupled through OASIS3 (Valcke and Redler [2012]). In this study the improvements are related to the representation of ISV and IAV associated with IOD and ENSO. To conclude this section we want to highlight the study of Seo et al. [2009] that makes use of a ESM to evaluate the role of the large amount of fresh water discharge in influencing the Barrier Layer (BL) over BoB. The BL develops in the BoB thanks to the large contribution of the freshwater discharge, and limits the vertical mixing over this basin. The shallow vertical mixing is very important in modulating the ISMR as will be elucidated in the Chapter 3 with a dedicated section and the correct simulation of this phenomenon is crucial to correctly reproduce the monsoon ISO associated. The results from Seo et al. [2009] suggest that the river discharge over the BoB plays a role on affecting SST during the boreal summer resulting in an improved simulation of the winter monsoon rainfall. To date there are no studies that shows a comparison between the AOGCMs and ESMs in simulating the ISM and hence is not possible to assess the possible added values. In a very recent study (Singh et al. [2016]) the skills on reproducing te ISV by 9 RCMs from Coordinated Regional Climate Downscaling Experiment (CORDEX) have been compared with that of their relative driving CMIP5 models. As expected their results show no consistent improvements in the use of a regional climate model on simulating ISMR but even a worst representation of ISV. The worsening is in part explained by the lack of an active coupled dynamic ocean in the RCMs leadin to a poor representation of sea-atmosphere interactions.

1.4 Key scientific objectives

In the previous sections has been highlighted the importance of considering the air-sea coupling when dealing with the ISM and in particular with its variability. In this study a new tool, consisting of a fully coupled ocean-atmosphere-land-river system, has been developed and applied over the South Asia CORDEX domain to take into account the related coupled phenomena. As first goal the coupled system has to be able to simulate the mean state of the atmosphere, ocean and rivers and this will be verified and assessed. Since the major added values linked with the use of an air-sea coupled model are related to the varibility of the ISM, meticulous attention will be dedicated to its two main scales. In particular, the skills in simulating the intraseasonal and interannual variability of ISMR are expected to increase compared to the standalone atmospheric counterpart. This will make available a powerful tool to study more in detail the different scales of varibility of the monsoon. The implementation of a new more resoluted hydrological model is necessary to be able to simulate the correct hydrological cycle over BoB. Summarizing, the main objectives of this study are to:

1) Develop an instrument that is able to realistically reproduce the mean state of the ISM;

2) Emiliorate the simulation of the variability of the ISM on its two main scales: the intraseasonal and the interannual;

3) Use the developed instrument to study the external forcings that influence the variability of the ISM;

4) Emiliorate the hydrological cycle in the coupled system implementing a new ad-hoc developed hydrological model;

5) Study the potential influences of a more realistic freshwater discharge into the ocean over the BoB.

Chapter 2

Data and Metodology

2.1 The regional earth system models

In the last years it has been seen an increased effort toward the development of fully coupled regional Earth System Models (ESM) including coupled atmosphere, ocean-sea ice, chemistry-aerosol, land hydrology and biosphere components. The study of the interactions of the different components of an ESM is adeguate with the scale at which the RCMs operate (Giorgi [1995]). The RESM recently developed at the Earth System Physics section of the Abdus Salam International Centre for Theoretical Physics (ESP-ICTP), well fit in this effort (Sitz et al. [2017]).

2.2 RegCM-ES

First described by Sitz et al. [2017], the Earth System Regional Climate Model (RegCM-ES) was born by an effort of different european research institute whith the aim of improving the research activity on coupled regional climate modeling. In the last decades different Regional Climate Models (RCM) have been developed with the aim of obtaining regional scale information starting from global scale simulations. This informations are proved to be useful for impact assessment and climate change studies (Giorgi [2006]; Dash et al. [2013] ; Giorgi et al. [2004] ; Giorgi and Lionello [2008]). The main advantage of the using a RCM is related to the possibility of increasing the spatial resolution and of improving the simulation of land-atmosphere feedback processes that are really important at such small scales.

The Earth System Physics section of the Abdus Salam International Centre for Theoretical Physics (ESP-ICTP) develops and distributes, in collaboration with other research institutes (Instanbul Technical University, ITU ; Climate modelling and impacts Laboratory, ENEA), RegCM-ES under the GNU General Public License (version 3). RegCM-ES, in the current state of the art, implements the coupling between atmoshpere, ocean, fresh water, biogeochemistry and land surface componets.

The development path followed different steps. In a first phase, an early version of the model, has been adapted over the South Asia domain to simulate the Indian Summer Monsoon (Ratnam et al. [2009]). The coupling for this study is implemented using the Spherical Coordinate Remapping and Interpolation Package (SCRIP) (http://oceans11.lanl.gov/trac/SCRIP) following the conservative remapping method

by Jones [1999] to interpolate fluxes through the different grids of the version 2.2 of the ocean model ROMS (Shchpetkin and McWilliams [2005]) and version 3 of RegCM (RegCM3; Giorgi et al. [1993a] ; Giorgi et al. [1993b] ; Pal et al. [2007b]). In 2010 the PROTHEUS system, composed by RegCM3 and the ocean model MITgcm (Marshall et al. [1997]) and coupled through the version 3 of OASIS coupler (https://verc.enes.org/oasis), has been implemented over the Mediterranean region and, the capabilities of reproducing the SST, tested (Artale et al. [2010]). During the following years, a collaborative work between ITU, ENEA and ICTP, has led to the development of a new driver. This driver is currently implemented in the state of the art version of RegCM-ES and the source codes can be retrived through the public code repository GitHub (https://github.com/uturuncoglu/RegESM). First testing of this driver has been realized over the Caspian Sea (Turuncoglu et al. [2013]) and over the Mediterranean (Turuncoglu and Sannino [2016]). A schematic of the current version of the RegCM-ES can be found in Figure 2.1.

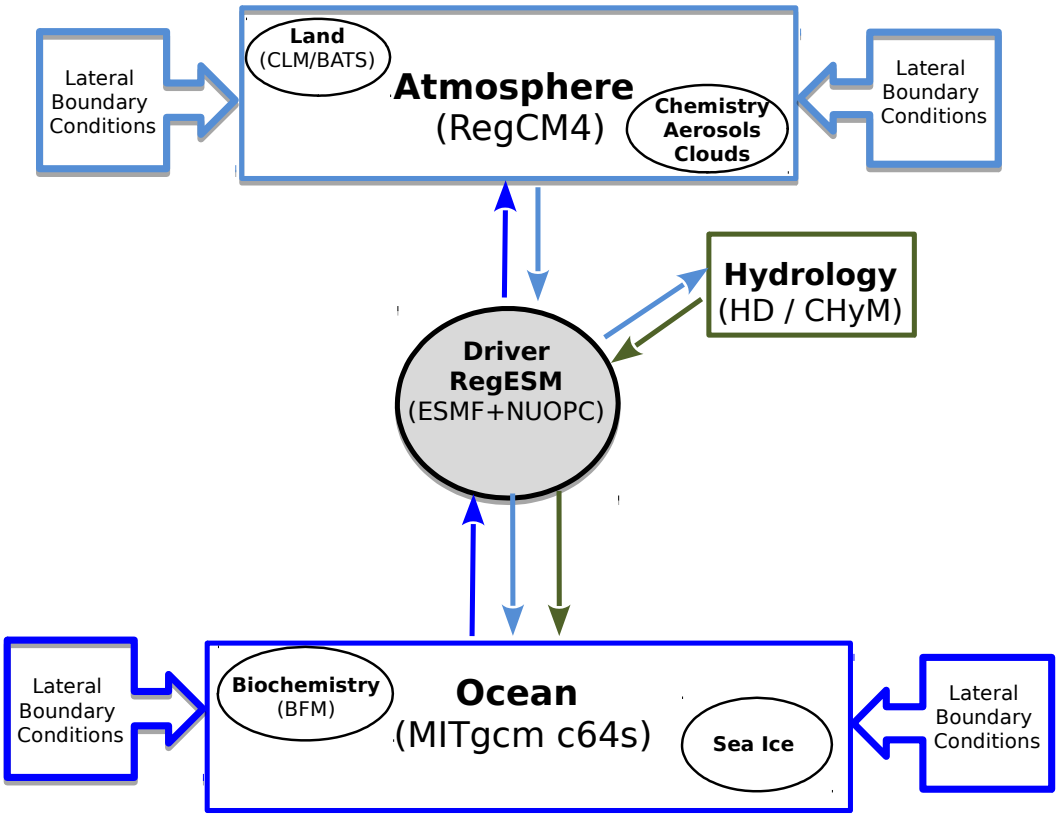

Figure 2.1. Schematic view of all RegCM-ES modelling components. The arrows indicate the interaction direction between individual components. Both atmosphere and ocean are forced by lateral boundary conditions. Figure taken from Sitz et al. [2017].

2.2.1 The Atmospheric component

The representation of the atmospheric physical and dynamical processes in the coupled system is taken care by the version 4 of RegCM (RegCM4; Giorgi et al. [2012]). RegCM4 has born as an evolution of the RegCM3 and, among others

updates, it has been adapted to be integrated easily in the RegCM-ES system through the compatibility adjustments to support the Earth System Modeling Framework (ESMF; Hill et al. [2004a] ; Hill et al. [2004b] ; Collins et al. [2005]). The model has an hydrostatic dynamical core based on Mesoscale Model version 4 (MM4; Anthes et al. [1987]), run in an Arakawa B-grid and terrain following sigma-p vertical coordinate and employs an explicit time splitting integration scheme. The development and maintenance of RegCM4 is under the coordination of the ICTP's Earth System Physics (ESP) section and the source code is freely distributed under the terms of the General Public License (GNU). The latest revision of the model is downloadable through the gforge repository accessible via the following link `http://gforge.ictp.it/gf/project/regcm/`. This version of the model has been applied in many region of the world and is greately used by a very large community involving universities and research centers mainly from developing countries. The non-hydrostatic version of the model is now available for testing (based on MM5 dynamical core; Grell et al. [1994]) and a new non-hydrostatic dynamical core is under development and is planned to be implemented in one of the future releases of the model (Tumolo and Bonaventura [2015]).

Different physical parametrization schemes for cumulus convection are available in RegCM4 and they can be applied over land and ocean in a mixed configuration. A description of them, together with the implemented parametrizations for planetary boudary layer and radiative transfer processes, can be found in Giorgi and Anyah [2012]. In this version of RegCM it has been implemented also a new accurate scheme for cloud microphysics (Nogherotto et al. [2016]). The "Zeng Ocean Air-Sea Parameterization scheme" (Zeng et al. [1998]), to date, is the only scheme that can be used to describe the exchanges with a coupled ocean component in RegCM-ES but RegCM includes different other schemes available if the standalone version of the model is used.

Two different land surface schemes are coupled and available in the model: the Biosphere-Atmosphere Transfer Scheme (BATS, Dickinson et al. [1993]) and the version 4.5 of the Community Land Model (CLM4.5; Oleson et al. [2010]). CLM4.5 is a comprehensive land model representing several aspects of the land surface biogeophysics, hydrology, biogeochemistry and ecological dynamics. This version of CLM calculates the parametrized surface and sub-surface runoff, used in the hydrological models that will be described later in this chapter, through the TOPMODEL-based (Beven and Kirkby [1979]) runoff model (SIMTOP) described by Niu et al. [2005]. In addition to these runoff, CLM calculates liquid runoff from glaciers, wetlands and lakes that togheter with the surface and sub-surface runoff constitute the total runoff available for each gridbox in the atmospheric component.

Geophysical Fluid Dynamics Laboratory (GFDL) flexible modeling system mixed layer (SOM) is also included in RegCM4, a 0-dimensional simplified SLAB ocean model that uses an approximation of the well-mixed ocean with fixed width (Solmon et al. [2015]).

2.2.2 The Oceanic component

RegCM-ES has two different ocean components: the Regional Ocean Modelling System (ROMS; Haidvogel et al. [2008]) and the Massachussets Institute of Technology General Circulation Model version 63 (MITgcm; Adcroft et al. [2008] ;

http://mitgcm.org) that has been chosen for this study. MITgcm has a non-hydrostatic kernel and supports horizontal orthogonal curvilinear coordinates with a finite volume treatement of topography. In its code are implemented a wide range of physical parametrizations, the nonlocal K-Profile Parameterization (KPP) scheme of Large et al. [1994] that is the most utilized by MITgcm community for vertical mixing. The model has been tailored to fit in the RegCM-ES. It allows in the present form to exchange a set of preselected fields with the atmospheric model through the driver that will be decribed in details in the following sections. The ocean component MITgcm needs a bathymetry in which all the singularities and bays are removed. The cleaning of the bathymetry has been done thanks to an ad-hoc application, written in R, that allow a visually interactive modification for all the points in the grid. The cleaning of the botton by spurious points has been automatically done using an ad-hoc application, that has been developed in fortran and that makes use of cellular automata methods to accomplish this task. The monthly boundary conditions coming from MOM have been interpolated over the two open boundaries and a fortran routine has been written to automatically restore the net mass fluxes to the original MOM values for each of the boundaries after the interpolation.

2.2.3 The Hydrological component HD

The Hydrological Discharge (HD) model is implemented in ReCM-ES to estimate the freshwater river discharge at the river mouths. The model is developed by the Max Planck Institute (Hagemann and Dümenil [1997] ; Hagemann and Gates [2001]) and run on a fixed global regular grid of 0.5° horizontal resolution with a daily time step. The model was designed with the intent of closing the hydrological budget in a coupled atmosphere/ocean GCM and computes the lateral waterflows from the continents into the ocean. Through the use of global land surface charasteristics globally available, HD calculates the retention time and the flow velocity for each grid cell. In RegCM-ES the HD simulated lateral waterflow derives from the sum of several contributions: the overland flow, the baseflow and the riverflow. The surface overland flow of HD gridbox is fed by the surface runoff available from the atmospheric component whereas the baseflow is fed by the remaining part of the total runoff calculated by CLM4.5 after that the surface part has been removed. The simulated lateral freshwater discharge in the river mouths is then spread over a predefined area of the ocean grid as a surface water flux. The river mouths have to be manually selected in the preprocessing phase of the simulation in two steps. In the first step it is needed to interpolate the HD grid over the ocean grid and to idetify the points of the river mouths, in the second step it has to be filled up the driver namelist with the latitude and longitude of the points identified in the first step and it has to be defined the radius that delimits the area where to spread the freshwater.

2.2.4 The Hydrological component CHyM

For this study a new hydrological model has been included in the RegCM-ES. The new hydrological model is neded to take into account also small river basins and finer scale spatial resolution of river network than what is available at the 0.5 degree global grid of the HD model. Cetemps Hydrological Model (CHyM; Coppola et al. [2007]) is

a spatially distributed hydrological model that uses a cellular automata algorithm to extract from a DEM (Digital Elevation Model) an eight flow direction map (D8). The model is able to simulate surface runoff, infiltration, evapotranspiration, percolation, melting and return flow.

CHyM model has been designated to provide a general purpose tool for flood alert mapping and can be used for any geographical domain with any resolution up to the resolution allowed by the DEM, namely about 30 meters in the current implementation Abrams [2000]. In previous applications, the model has been used coupled off line with two regional climate models for climate change impact studies on water resources in the Po river drainage basin Coppola et al. [2014].

An ad-hoc version of CHyM has been coupled with the Community Land Model 4.5 (CLM4.5) used in RegCM4. CLM4.5 provides the total runoff at each model grid point, which is then routed through each CHyM grid cell using a continuity and a momentum equation based on the kinematic wave approximation Lighthill and Whitham [1955] of the shallow water wave. In this approximation the water flow velocity is a function of the longitudinal bed slope of the flow element, the Manning's roughness coefficient (Manning et al. [1890]) and the hydraulic radius. In the preprocessing, CHyM builds the drainage networks at the selected domain and resolution (flow direction matrix, drained area, acclivity matrix and Land Use map derived from USGS products and scaled at the CHyM grid resolution). In the preprocessing phase using CHyM as the hyrological component is not necessary any more to individually identifying the river mouths using the latitude and longitude values but they are automatically identified at run time using an algorithm written specifically to carry out this task. At run time, a velocity matrix is calculated taking into account the overland and channel flow, and the routing equations are integrated using a time step that depends on the spatial resolution used. The discharge values calculated at the river mouths are then interpolated and passed to the ocean. Furthermore, it is possible to select a threshold (defined as the minimum drained area by a mouth point) to discriminate rivers that have a very small catchment.

In the previous applications CHyM was utilized successfully only over relatively small catchments and the routines were developed to build the drainage network mainly in single catchments. A meticulous work has been done to find the right way to reconstruct the drainage network in a such big domain with a very complex orography. The presence of endorheic basins in the Tibetan Plateau, Arabic Peninsula and over the Southeast Asia makes this task a more complicated work. The cellular automata based algorithms, that were developed to perform this job, find the right path towards the sea (or towards a point in the boudaries) following the topography, when it finds singularities, as for the endorheic basins, build a new path to connect the closest river point to drain the water towards the sea (or towards a point in the boundaries). This is uncorrect since the endhorheic basins are watersheds that do not drain to the sea and the connection of this basins with the non-endorheic one it is a possible source of errors in the simulation of the correct amount of river discharges.

2.2.5 The driver component

RegCM-ES incorporates a driver-based model coupling approach in which the driver plays a central role exchanging and interpolating the fields between all the coupled

components (Turuncoglu and Sannino, 2016). To achieve this task the driver uses the version 7.0.0 of the Earth System Modeling Framework (ESMF; Hill et al. [2004a] ; Hill et al. [2004b] ; Collins et al. [2005]) and The National Unified Operational Prediction Capability (NUOPC) layer. Different regriding methods are available in the ESMF and a two steps interpolation, integrated in the last version of the driver, allows to solve the problems arising from the unaligned land-sea masks between ocean and atmosphere components. In the driver, thanks to the introduction of the NUOPC layer, have become available explicit and semi-implicit type model interaction and the possibility to use different coupling time interval among the components. The driver has been modified to be able to interpolate and exchange the fields between the CHyM and the other components. The introduction of a finer grid allows the possibility to also consider small catchments. All the river mouths found with CHyM under a predefined threshold for the drained area, are interpolated on the oceanic grid with a new algorithm implemented in the driver that automatically find the closest ocean points.

2.3 Observational datasets

2.3.1 IMD high resolution daily gridded rainfall

We use an extended version (Unnikrishnan et al. [2013]) of gridded daily rainfall dataset at 0.5° of resolution initially prepared by Rajeevan et al. [2006] using 1803 stations over India. The original version of IMD (Indian Meteorological Department daily gridded rainfall) was available for the period 1951-2003 interpolated on a grids of 1° x 1° degree resolution. The new version has been extended to 2007 using an icreased number of stations (from 1803 to 2140) and standard quality controls were made on the data before been interpolated using a weighted sum of observations.

2.3.2 GPCP precipitation data

The Global Precipitation Climatology Project One-Degree-Daily (GPCP-1DD; Huffman et al. [2001]) has a daily temporal and 1° degree resolution for the period 1996-present. This dataset is computed by the GPCP Global Merge Development Centre in the NASA/GSFC Mesoscale Atmospheric Processes Laboratory and uses different methods to estimates precipitations: microwave, infrared and sounder data observed by the international precipitation-related satellites, and precipitation from rain gauge analyses.

2.3.3 TRMM: Tropical Rainfall Measuring Mission

Born as a joint mission between NASA and the Japan Aerospace Exploration Agency (JAXA), the Tropical Rainfall Measuring Mission (TRMM; Huffman et al. [2007]) is available for the period spanning from 1998 to 2014. The product utilizes two different types of satellite sensors, namely microwave and IR and is available with a three-hourly time step on a grid of 0.25° x 0.25° degree resolution.

2.3.4 Hadley Centre SST (HadISST)

A global monthly mean dataset for sea surface temperatures with a spatial resolution of 1degree (Rayner et al. [2003]) distributed by the Hadley Centre for Climate Research and available from 1870 to date. The data comes from the Met Office Marine Data Bank (MDB) and from 1982 onwards also includes data from the Global Telecommunications System (GTS) and the International Comprehensive Ocean-Atmosphere Data Set (ICOADS) where MDB data are not available. To reconstruct the temperature dataset is used a two stage reduced space optimal interpolation method to data from the different sources.

2.3.5 World Ocean Atlas 2013 (WOA13)

To validate the subsurface temperature and salinity has been used the version 2 of World Ocean Atlas 2013 (WOA13 v2; Boyer et al. [2014]) that consists on 1° gridded objectively analyzed climatologies of salinity, temperature and others physical and chemical variables. Produced by the National Oceanographic Data Center - Ocean Climate Laboratory at National Oceanic and Atmospheric Administration (NOAA), this Ocean Atlas extends the previous versions with an higher vertical resolution that consists on 102 level from the surface to sea floor (5500 m depth). The long-term set of monthly climatologies from 1955 to 2012 are also available on 0.25° latitude/longitude grid for temperature and salinity.

Chapter 3

Analysis and discussion of the experimental results

3.1 Experimental design

In this section the results of the RegCM-ES simulations will be analysed and discussed together with the corresponding stand alone RegCM simulations. The analysis will be mainly focused on the monsoon season and it will examine the model capability in representing the monsoon mean state, the intraseasonal and interannual monsoon variability and a particular attention will be given to the ENSO-monsoon relation.

RegCM-ES has been integrated over the South Asia Coordinated Regional Climate Downscaling Experiment (CORDEX; www.cordex.org; Giorgi et al. [2009]) domain, at 50km of spatial resolution (170 x 216 grid-points) using 18 vertical sigma levels for the atmospheric component. For the ocean, the revision c63s of MITgcm has been used with a spatial resolution of about 18km (276 x 408 grid-points) with 45 vertical levels, spacing from 1 meter on the surface to 200 meters at the ocean bottom and with a bathymetry derived by Smith and Sandwell [1997] (Fig. 3.1). The spatial resolutions for the hydrological models are 55 and 12 km respectively in the HD and CHYM grids and the time step is one day in all the experiments.

In the ocean grid, we have two open boudaryes in the south and east edges where monthly boundary conditions are prescribed coming from two different datasets, the remaining two are bounded by land. We have choosen two different kinds of dataset to force the ocean over the two open boudaries that have been interpolated linearly in time and over the MITgcm grid, the first one comes from a simulation of a global ocean model MOM run under the CORE II experiment (Danabasoglu et al. [2014]) whereas the second one is a global ocean reanalysis (ORAP) coming from the ECMWF center (Zuo et al. [2015]). In the two active open boundaries have been taken care of the conservation of mass in the basin. MITgcm uses KPP to parametrize upper ocean processes and no mesoscale eddy parametrizations are used since the 18 km in the horizontal grid spacing it solves most of their features. No relaxation to observed SST is used in any of our model runs.

In HD model configuration, due to the manual selection of the river mouth, all the rivers with a mean annual discharge greater than 500 m^3/s have been choosen whereas in the CHyM configuration a threshold of 500km^2 drainage area has been used to include only the major river catchments. Three different coupled simulations

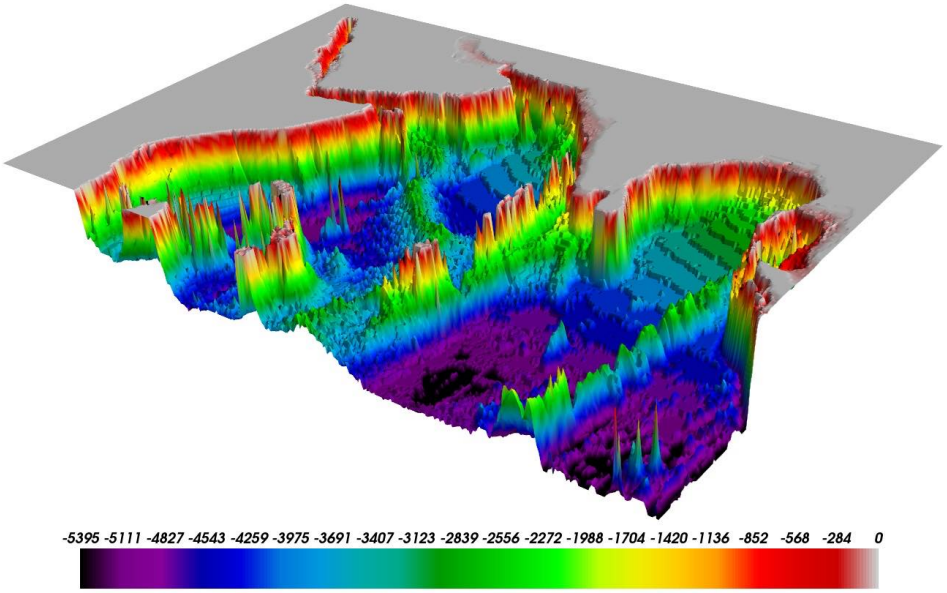

Figure 3.1. Bathymetry used to run MITgcm model and derived from Smith and Sandwell [1997].

have been completed. The first simulation, to which we will refer to by the acronym ESM-Em, uses Emanuel cumulous convection scheme, the HD model and boundary conditions from MOM during the period 1979-2007 (the restriction to 2007 is due to the unavailability of a longer MOM simulation); the second one, to which we will refer to by the acronym ESM-TkHD, uses the Tiedtke cumulous convection scheme, the HD model and ORAP during the period 1979-2013 and finally the third one, to which we will refer to by the acronym ESM-TkCH, uses Tidtke cumulous convection scheme, the CHyM model and ORAP during the period 1979-2013. Furthermore, two simulations have been completed with the stand-alone version of the RegCM model using the same model setting of the corresponding coupled simulation and for the same period. For the two stand-alone simulations we will use the acronym RCM-Em for the simulation that uses Emanuel as cumulous convection scheme and RCM-Tk for the one that uses Tiedtke. In the Table 3.1 all the simulations are summarized and the relative main features and the acronims that will be used in the rest of this text. We will refer to the two small ensembles of coupled and uncoupled simulations with the ESMs and RCMs acronims respectively.

All the simulations, coupled and stand alone, are forced at the lateral atmospheric boundaries by the European ECMWF reanalysis at 1.5 degree (EIN15) horizontal resolution and make use of CLM4.5 (Oleson et al. [2010]) as land surface model. Prescribed SSTs from EIN15 are also used to force, at the underlying ocean boundary, the standalone simulations and in that area of the ocean where, in the RegCM-ES, is missing the dynamic ocean domain as shown in the Figure 3.2. Here the domains for the three different model components used to perform the coupled simulations are illustrated. For the simulations driven at the open boundaries by ORAP, the minimum depth in the bathymetry has been increased from 5 to 20 meters to solve

Simulation Acronym	Convective schemes	Ocean model ICBC	Hydrological model
RCM-Em	Emanuel		
RCM-Tk	Tiedtke		
ESM-Em	Emanuel	MOM (GCM)	HD
ESM-TkHD	Tiedtke	ORAP5 (Reanalysis)	HD
ESM-TkCH	Tiedtke	ORAP5 (Reanalysis)	CHyM

Table 3.1. Simulations performed and relative main characteristics.

problems arised over shallow costal areas. The analysis has been carried out for the simulted period from 1980 to 2007 removing the first simulated year considered as speen up for the models.

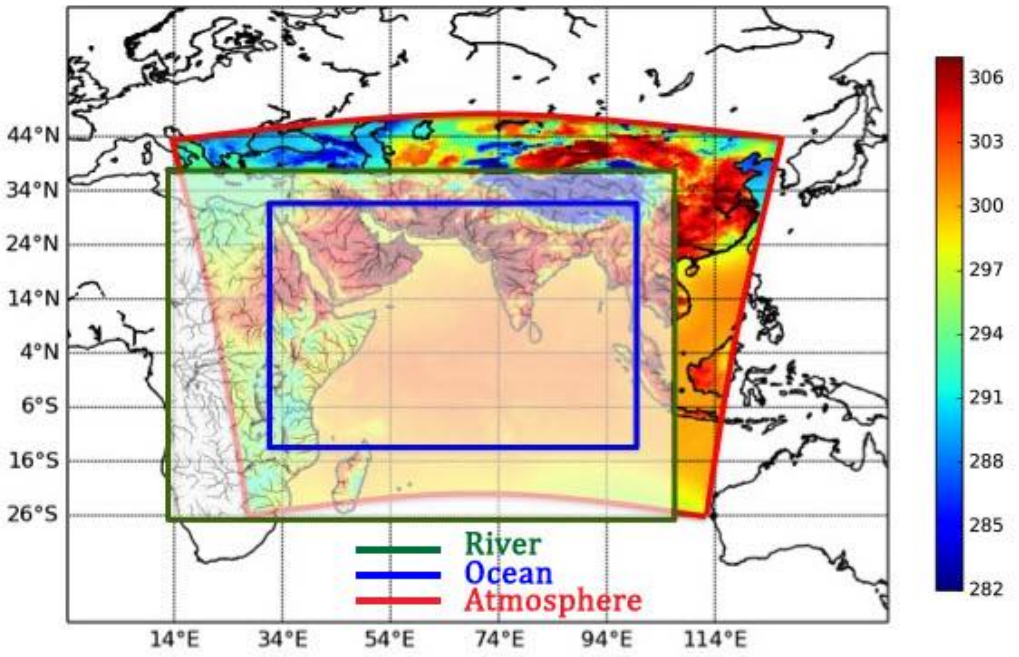

Figure 3.2. Surface temperature (°K) over the South Asia Cordex domain for the RegCM-MITgcm-CHyM (RegCM-ES) coupled model. The solid red box indicates full atmospheric model domain (RegCM4). The blue solid box shows ocean model domain (MITgcm). The solid green box indicates hydrological domain and drainage networks (CHyM).

3.2 Ocean validation

The main goal of this study is to evaluate the role of the air-sea interaction in modulating the ISM and the major focus has been directed to the atmospheric component of this complex system. Nevertheless a brief validation of the ocean is needed for the sake of completeness, in particular we will evaluate the quality of the different experiments in reproducing the main oceanic features in the IO basin. For all the three experiments neither relaxation nor restoring to observed Sea Surface

Temperature and Sea Surface Salinity has been used.

3.2.1 Sea surface temperature

In this section we will discuss the simulated seasonal climatology of sea surface temperature (SST) for the analized period from 1980 to 2007 by the coupled experiments and the related biases with observations. Figure 3.3 shows the simulated SST for the monsoon season by ESM-Em (a), ESM-TkHD(b) and ESM-TkCH(c). The HadISST observational dataset, reported in the subplot (d) of this figure, shows the three main feature that we will analize in the three experiments: the upwelling of cold waters over western coastal areas of IO and the two main warm pools, one over the equatorial belt and the other, very important for monsoon ISO, situated over the BoB. The equatorial warm pool is slightly clockwise inclinated under the effect of the southwesterlies moonsoon winds and shows its maximum off Indonesian coasts. The BoB warm pool has a comparable temperature and a shape that resembles that of the east India coastlines. The model in all the three experiments reproduces

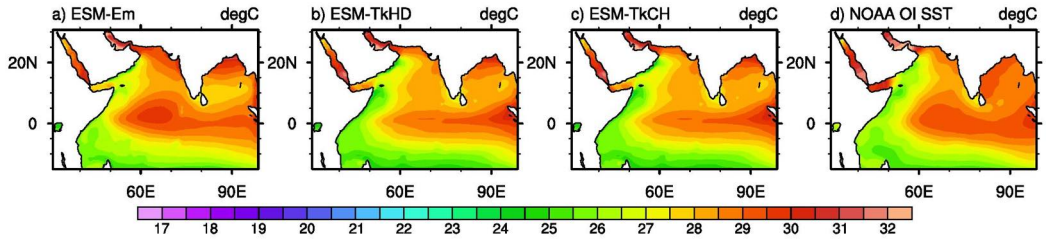

Figure 3.3. Seasonal JJAS climatology of sea surface temperature (°C) as simulated by (a) ESM-Em, (b) ESM-TkHD, (c) ESM-TkCH and of (d) the observational dataset HadISST.

the main patterns although the BoB warm pool does not extend southward as in observations. The shape of the western equatorial warm pool is better reproduced by the ESM-Em (Fig. 3.3(a)). In the ESM-TkHD and ESM-TkCH (Fig. 3.3(b-c)) the equatorial warm pool is more thin and flattened along the equator assuming an unrealistic shape. The cold pattern associated with the upwelling over the western IO coastal areas seems instead better simulated by the ESM-TkHD and ESM-TkCH (Fig. 3.3(b-c)), at least in its magnitude and extension. For what concern the BoB warm pool, any of the experiments is able to reproduce its shape with the higher temperatures that are pushed towards the north part of the BoB in all the three experiments.

From the biases maps of SST (Fig. 3.4) we can observe a general warm bias in the ESM-Em (Fig. 3.4(a)) and of opposite sign for the ESM-TkHD and ESM-TkCH (Fig. 3.4(b-c)) related to the upwelling region. In particular, a cold bias of the order of 0.5°C - 1°C is observed over south BoB in all the experiments and a warm one with maximum values of the order of 2°C over the Oman-Somalia upwelling area (Fig. 3.4(a)) for the ESM-Em.

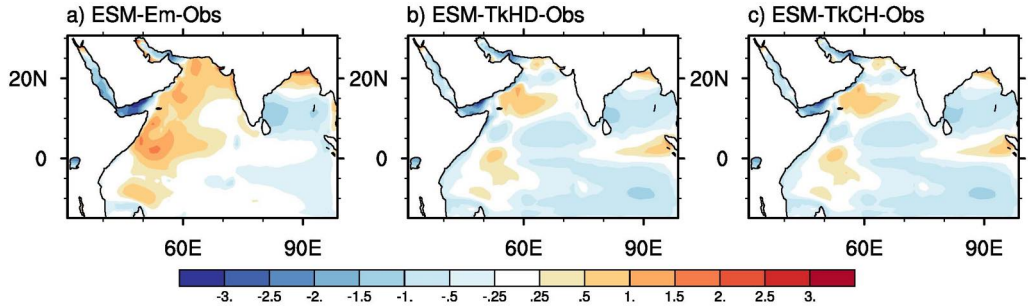

Figure 3.4. JJAS differencies of averaged sea surface temperature (°C) between (a) ESM-Em, (b) ESM-TkHD, (c) ESM-TkCH and the observational dataset HadISST.

3.2.2 Sea Surface Salinity

The IO shows a dipole in the distribution of the Sea Surface Salinity during the JJAS season. The highest values are observed in the western part, over the Arabian Sea (AS), which, beeing bounded in the north, west and east side can be defined as an evaporative sub-basin. The lowest values are instead observed over BoB, where there is a great contribution of freshwater from riverine discharge and from the Indonesian throughflow (Fig. 3.5(d)). The lower values observed for the ESM-Em

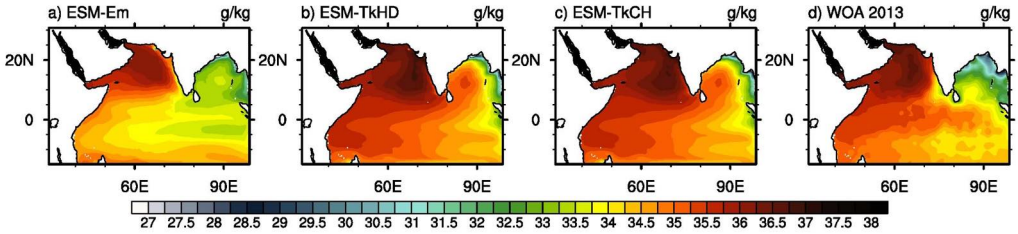

Figure 3.5. Seasonal JJAS climatology of sea surface salinity (g/Kg) (SSS) as simulated by (a) ESM-Em, (b) ESM-TkHD, (c) ESM-TkCH and of (d) the observational dataset WOA.

(Fig. 3.5(a)) are probably linked to the large bias in precipitation observed for this experiment over Equatorial Indian Ocean (EIO ; Fig. 3.17(a)). Looking at the biases maps reported in Figure 3.6 it is evident that simulated conditions over BoB are saltier in all experiments. In particular, biases of more than 3 g/kg are observed for ESM-TkHD (Fig. 3.6(b)) and ESM-TkCH (Fig. 3.6(c)). Weaker biases are observed over BoB by ESM-Em (Fig. 3.6(c)) although ESM-Em is freshest almost in all the IO basin. The differences in SSS between ESM-TkHD, ESM-TkCH are very small and limited to the coastal areas of north BoB (not shown). The differences among the experiments will appear more clear when we will investigate the vertical structure in the BoB.

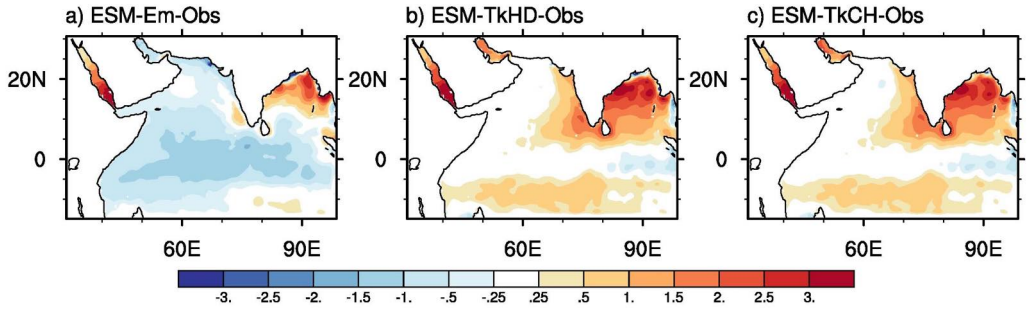

Figure 3.6. JJAS differencies of averaged sea surface salinity (g/Kg) between (a) ESM-Em, (b) ESM-TkHD, (c) ESM-TkCH and the observational dataset WOA, and between (d) ESM-TkHD and ESM-TkCH.

3.2.3 Interannual variability of SST

The seasonal climatologies of SST has been averaged over three main area of Indian Ocean, AS (between 8°N-24°N and between 55°E-77°E), the BoB (between 8°N-24°N and between 80°E-93°E) and the EIO (between 5°S-5°N and between 52°E-93°E) for the coupled simulations, and compared with that of the HadISST dataset. The cross correlation coefficient (CC) and the root-mean-square difference (RMSD) values are presented for each region, season and simulation respectively in the top-right and top-left edges of each plot. The CC and RMSD values are also summarized in table 3.2 for a comparison.

	SEAS	ESM-Em		ESM-TkHD		ESM-TkCH	
		CC	RMSD	CC	RMSD	CC	RMSD
Arabian Sea	JF	0.57	0.27	0.69	0.17	0.63	0.19
	MAM	0.62	0.63	0.55	0.73	0.54	0.72
	JJAS	0.69	0.30	0.72	0.48	0.72	0.48
	OND	0.66	0.24	0.63	0.67	0.55	0.66
Bay of Bengal	JF	0.32	0.68	0.38	0.32	0.4	0.32
	MAM	0.49	0.69	0.52	0.32	0.51	0.32
	JJAS	0.74	0.81	0.81	0.95	0.78	0.97
	OND	0.64	0.68	0.48	0.35	0.52	0.34
Tropical Indian Ocean	JF	0.78	1.02	-0.03	0.88	0.01	0.89
	MAM	0.54	0.97	0.56	1.05	0.56	1.06
	JJAS	0.54	0.35	0.50	0.36	0.49	0.36
	OND	0.16	1.01	-0.28	0.44	-0.28	0.44

Table 3.2. Tabular representation of the correlation coefficient (CC) and root-mean-square difference (RMSD) values of the ESM simulations over the three main area of Indian Ocean (Arabian Sea, Bay of Bengal and Tropical Indian Ocean) for all seasons

The AS is the region that seems better simulated by all the experiments with the highest CC values (greater than 0.54) and the lowest RMSD values observed. The ISM season, in AS, is well represented with a small cold bias in the ESM-TkHD and ESM-TkCH, whereas the ESM-Em is slightly warmer than observation. A systematic cold bias, in AS, is observed in MAM season for all the simulations,

whereas in OND this systematic bias is present only in the two simulation that use ORAP.

Over the BoB, the CC for the monsoon season is the highest founded among all seasons and regions considered (values of about 0.8), but with a cold bias of about 1 degree. This cold bias is reduced in the other seasons for ESM-TkHD and ESM-TkCH, along with smaller CC.

The worst results can be observed over EIO, in particular for ESM-TkHD and ESM-TkCH. Over this region a sistematic cold bias of about one degree is observed for ESM-Em in JF, MAM and OND. The same bias is observed in the two other simulations in JF and MAM, but not in OND, where these two simulations result negatively correlated with observations. Moreover, correlation around zero is observed in JF for them. In contrast, the monsoon season, over EIO, shows CC values of about 0.5 for all the simulation along with small RMSD values.

3.2.4 Surface currents

Figure 3.10 shows the surface currents for the three experiments and the SODA reanalysis for the ISM season. The Somali current can be easily recognized with two main branches, one reaches the coasts of Oman on the north and the other extends eastward along the equator reaching 60°E (Fig. 3.10(d)). An easterlies current can be also observed along 10°S throughout the longitudinal extent of the considered domain (Fig. 3.10(d)). The experiments simulate an anomalous easterlies current along the equator with the equatorial branch of the Somali current that is not reproduced in all the experiments ((Fig. 3.10(a,b and c)). The north branch of the Somali current is well reproduced by the ESM-Em (Fig. 3.10(a)), in shape and magnitude as well as the easterlies current along 10°S. In contrast, a stronger north branch of Somali current is simulated by ESM-TkHD (Fig. 3.10(b)) and ESM-TkCH (Fig. 3.10(c)) along with strong anomalous easterlies current along the equatorial IO.

3.2.5 Salinity and Thermal vertical structures over Bay of Bengal

The BoB has a strong haline stratification in its upper 50m that extends for the whole BoB latitudinal extension. The simulation of the shallow and highly stratificated haline layer is a challenge for most of the state-of-the-art coupled models (Goswami et al. [2016]). The shallow haline layer has a big role in permitting to correctly simulate the thermal vertical structure and SST over BoB that, in turn, strongly affect the ability of the model in reproducing the Low Pressure Systems and the associated ISO of monsoon. In Figure 3.11 is reported a latitude/depth plot for salinity along 90°E, in the middle of BoB. The strong haline stratification can be observed in the subplot (Fig. 3.11(d)) from WOA13 and seems to be reproduced partially only by the ESM-Em experiment (Fig. 3.11(c) and Fig. 3.5(a)). The other two experiments show pratically no haline stratification over BoB (Fig. 3.11(a,b)) probably due to stronger northwesterly currents observed for this two simulations over BoB (Fig. 3.10(b,c)). Freshest waters are simulated, in the coastal area, by ESM-TkCH (Fig. 3.10(b)) thanks to the better simulated annual cycle of riverine discharge, that will be treated in the section dedicated to the hidrological model validation.

The biases between the simulated sea salinity sections over BoB and the WOA13

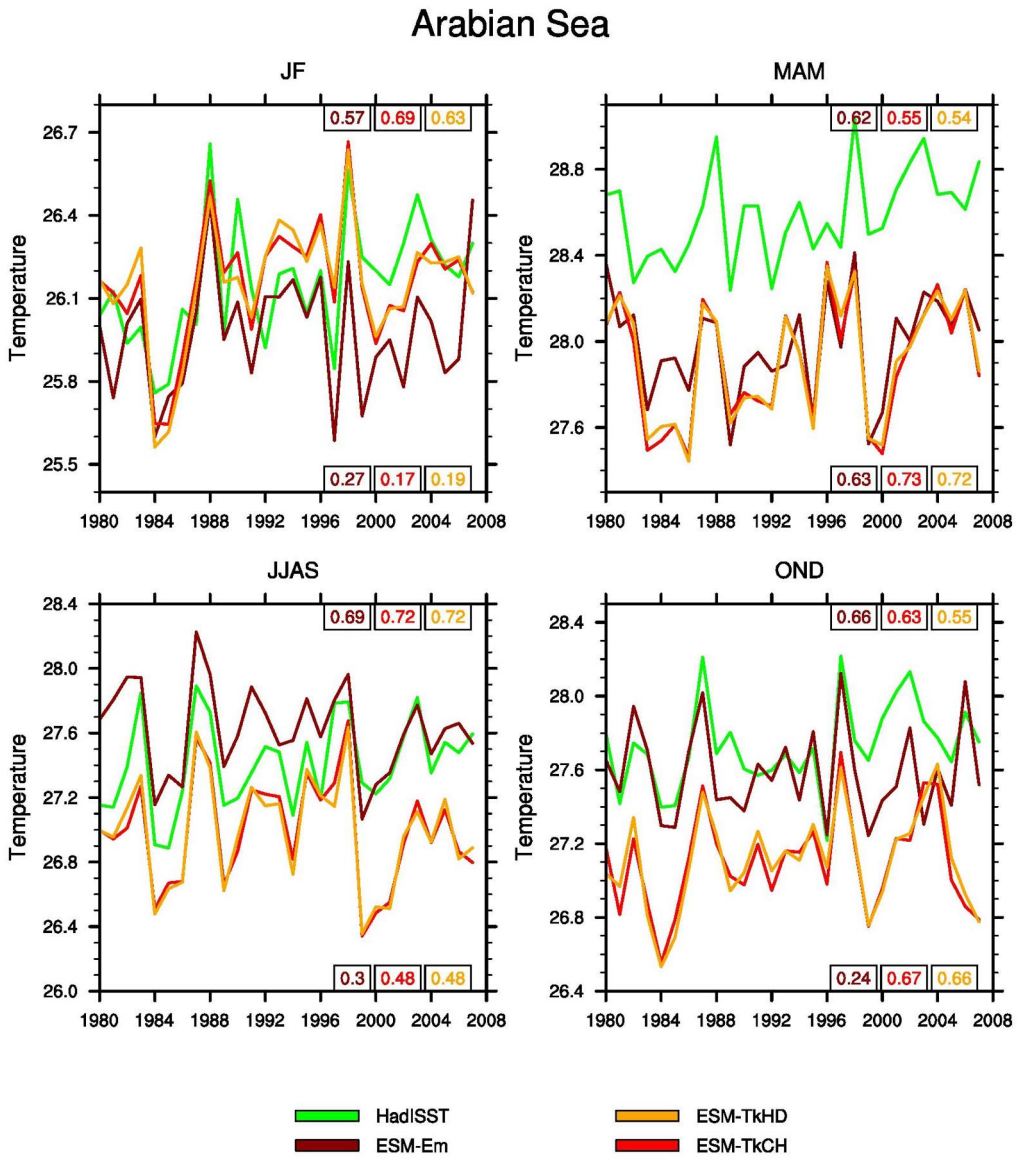

Figure 3.7. Seasonal sea surface temperature (SST; °C) interannual variability over Arabian Sea as simulated by ESM-Em (dark-red), ESM-TkHD (red), ESM-TkCH (orange) and of the observational dataset HadISST (green) between 1980 and 2007. The correlation coefficienties and the root mean square differencies (between each experiment and HadISST) are reported respectively in the top right and bottom right corners of the plot using the same colors used to depict the lines.

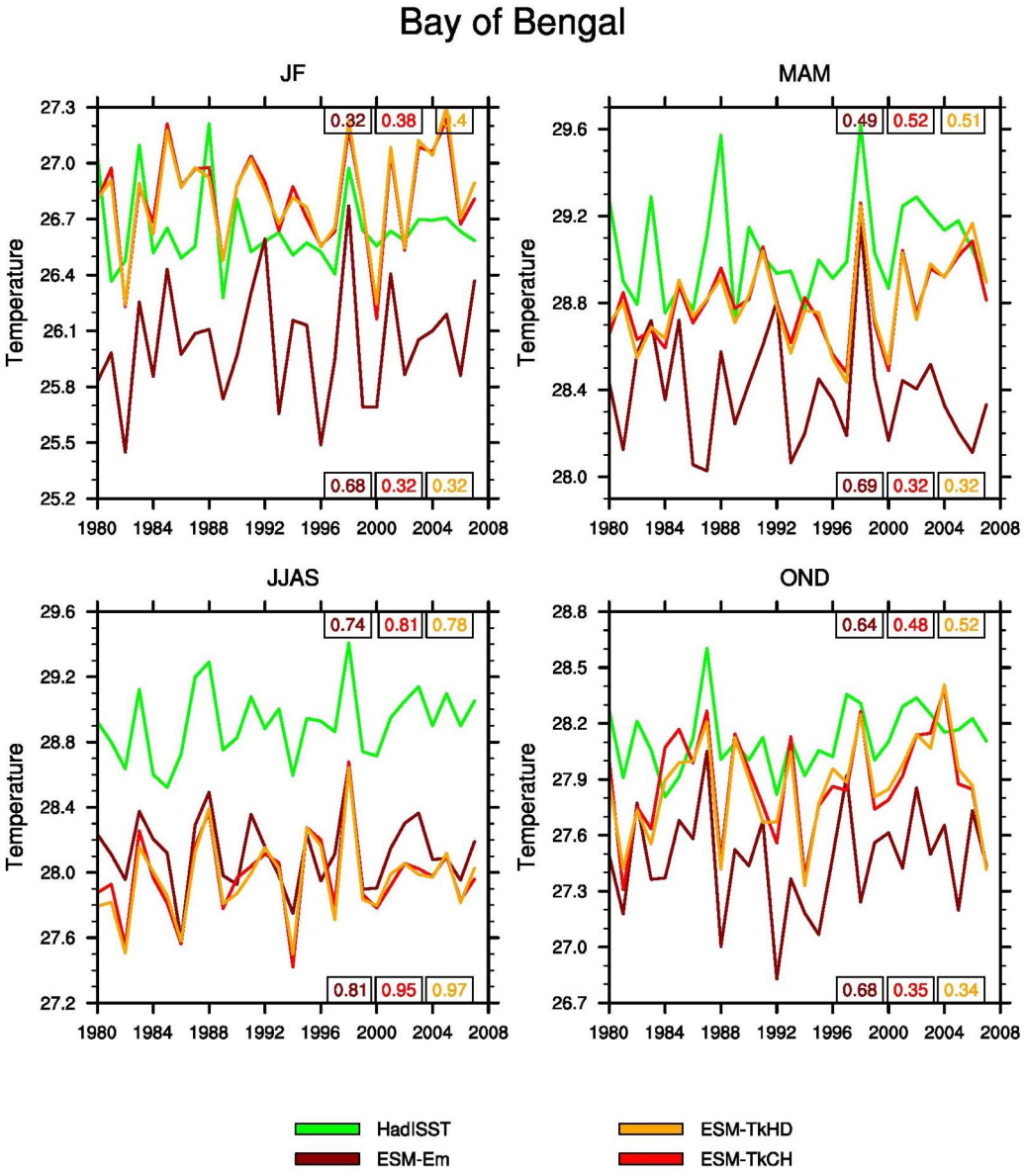

Figure 3.8. Seasonal sea surface temperature (SST; °C) interannual variability over Bay of Bengal as simulated by ESM-Em (dark-red), ESM-TkHD (red), ESM-TkCH (orange) and of the observational dataset HadISST (green) between 1980 and 2007. The correlation coefficienties and the root mean square differencies (between each experiment and HadISST) are reported respectively in the top right and bottom right corners of the plot using the same colors used to depict the lines.

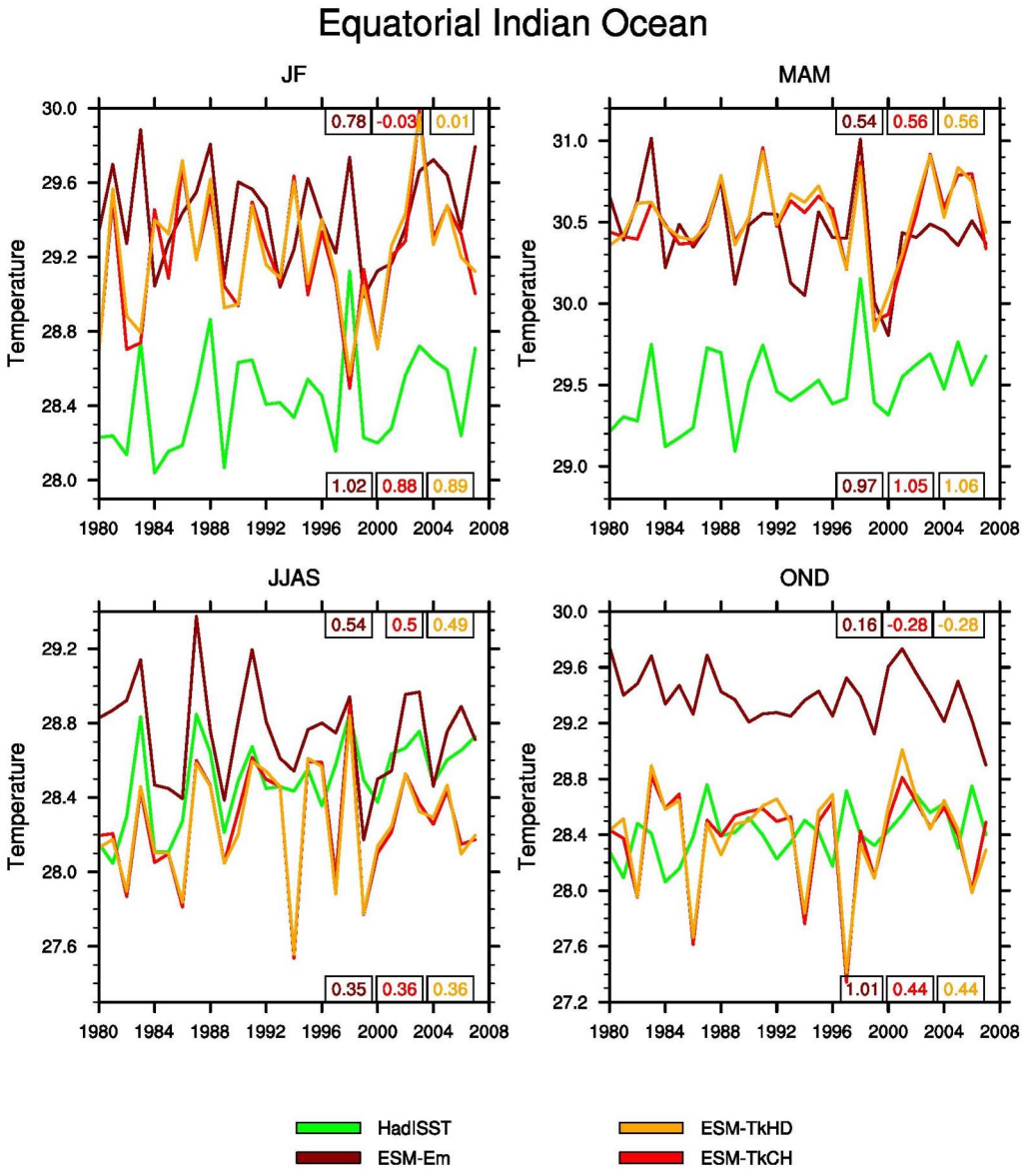

Figure 3.9. Seasonal sea surface temperature (SST; °C) interannual variability over Equatorial Indian Ocean as simulated by ESM-Em (dark-red), ESM-TkHD (red), ESM-TkCH (orange) and of the observational dataset HadISST (green) between 1980 and 2007. The correlation coefficienties and the root mean square differencies (between each experiment and HadISST) are reported respectively in the top right and bottom right corners of the plot using the same colors used to depict the lines.

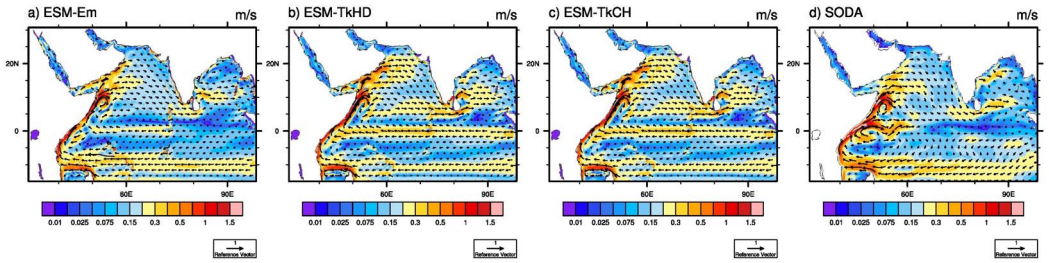

Figure 3.10. Seasonal JJAS climatology of surface ocean currents (m/s) as simulated by (a) ESM-Em, (b) ESM-TkHD, (c) ESM-TkCH and (d) the SODA reanalysis.

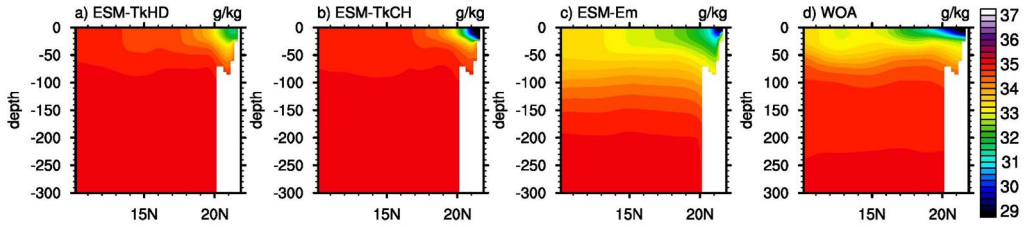

Figure 3.11. Depth-latitude diagrams of salinity (g/Kg) along 90°E for (a) ESM-Em, (b) ESM-TkHD, (c) ESM-TkCH and (d) the WOA13 observations.

are depicted in Figure 3.12(a,b and c), the bias between ESM-TkHD and ESM-TkCH in Figure 3.12(d) and the bias between ESM-TkHD and ESM-Em in Figure 3.12(e). The higher salinity biases can be observed in the first layers of ESM-TkHD (Fig. 3.12(a)) and ESM-TkCH (Fig. 3.12(b)) with a strong overestimation of salinity values close to the surface. Smaller biases but still positive can be observed also in the ESM-Em (Fig. 3.12(c)) over the same superficial layers and close to the coastal areas, morover can be observed also a deeper mixing with a more deep haline stratification (up to 150 meters depth). Smaller differences between ESM-TkHD and ESM-TkCH (Fig. 3.12(d)) are observed in the central and north vertical structure of the BoB and significant differences between the two are limited only to the coastal areas.

The missing salinity stratification is probably the missing feature that doesn't allow a realistic representation of the SST and of the thermal structure over the Bay of Bengal. The shallow mixed layer and the large SST anomalies observed over this basin are thought to significantly affect the convective activity that has a significant role in modulating the intraseasonal and interannual variabilty of the Indian Summer Monsoon rainfall (Rahman et al. [2009] ; Bhat et al. [2001]). As it as been done for the salinity we show the different biases between the experiments and WOA, between ESM-TkHD and ESM-TkCH and between ESM-Em and ESM-TkHD (Fig. 3.13(from a to e)). An underestimation of the temperatures in the shallow layer (of the order of 1°C) can be observed in all the three experiments together with an overestimation under 50 meter deep in ESM-TkHD and ESM-TkCH (Fig. 3.13(a,b)) and under 120 meter depth in ESM-Em (Fig. 3.13(c)) both at south of 17°S. These biases represent an indication of a stronger mixing in the central and north part

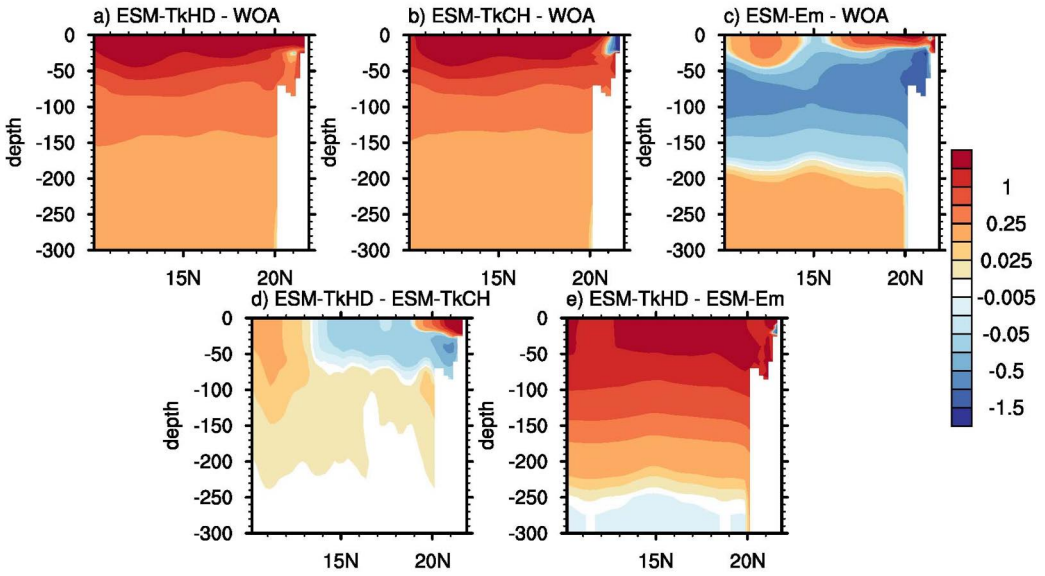

Figure 3.12. Depth-latitude diagrams of salinity (g/Kg) biases along 90°E between (a) ESM-Em, (b) ESM-TkHD, (c) ESM-TkCH and the WOA13 observations, between (d) ESM-TkHD and ESM-TkCH, and between (e) ESM-TkHD and ESM-Em.

of BoB. The differences between ESM-TkHD and ESM-TkCH (Fig. 3.13(d)) are not significant probably due to the effect of the better representation of the riverine discharge annual cycle be limited to the coastal areas (Fig. 3.12(d)).

More sensitivity tests are needed to assess the role of the different components, boundary conditions and of the cumulus convection scheme in inducing the biases seen above. Moreover, the increase of the upper veritical resolution in the ocean component could increase the skills on simulate the barrier layer over BoB and the extensions of the southern boundary towards south is needed to include the Indian Ocean subduction zone.

3.2.6 The Indian Ocean Dipole

The Indian Ocean Dipole (IOD) has been recognized as a source of interannual variability for the ISMR and an index has been proposed in the 1999 by Saji et al. [1999]. The IOD mode Index (DMI) is defined as the the difference between the SST anomalies (C) of Western (10°S-10°N and 50°E 70°E) and Eastern (10°S-0°N and 90°E-110°E) Equatorial Indian Ocean regions. Our domain doesn't extent enough to the east to calculate the proposed DMI but we have calculated a similar index considering the difference between the SST anomalies (C) of Western (10°S-10°N and 50°E 70°E) and Eastern (10°S-0°N and 90°E-100°E), with the Eastern box extending only up to 100°E. The index has been calculated for the three experiments and for the HadISST observation dataset and the monthly time series are reported in Figure 3.14. The four curves look in good agreements and the correlation coefficients between ESM-Em, ESM-TkHD, ESM-TkCH and HadISST are respectively 0.61, 0.53 and 0.55 proving the ability of the coupled model in reproducing this phenomenon.

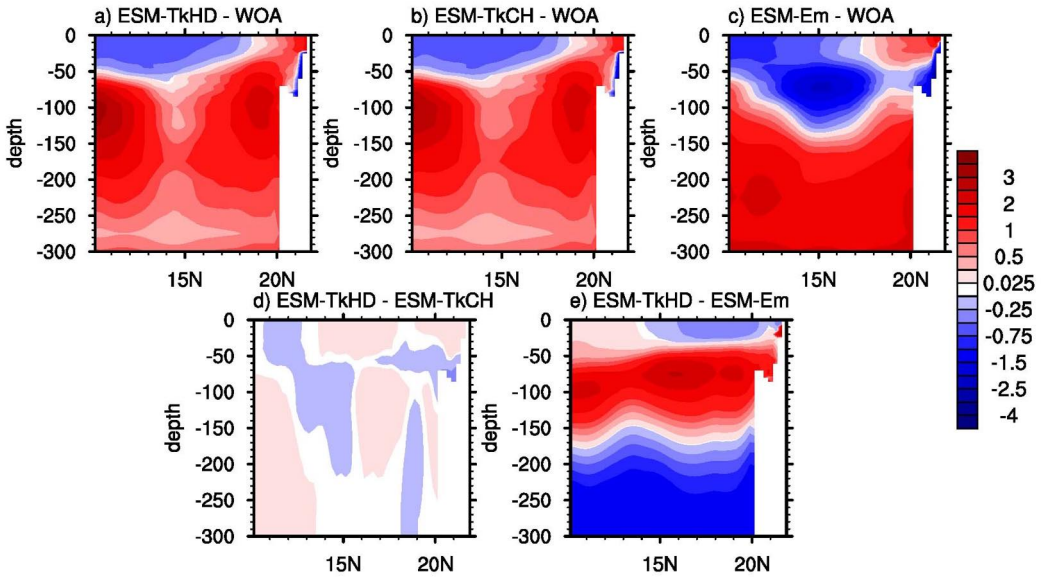

Figure 3.13. Depth-latitude diagrams of temperature (°C) biases along 90°E between (a) ESM-Em, (b) ESM-TkHD, (c) ESM-TkCH and the WOA13 observations, between (d) ESM-TkHD and ESM-TkCH, and between (e) ESM-TkHD and ESM-Em.

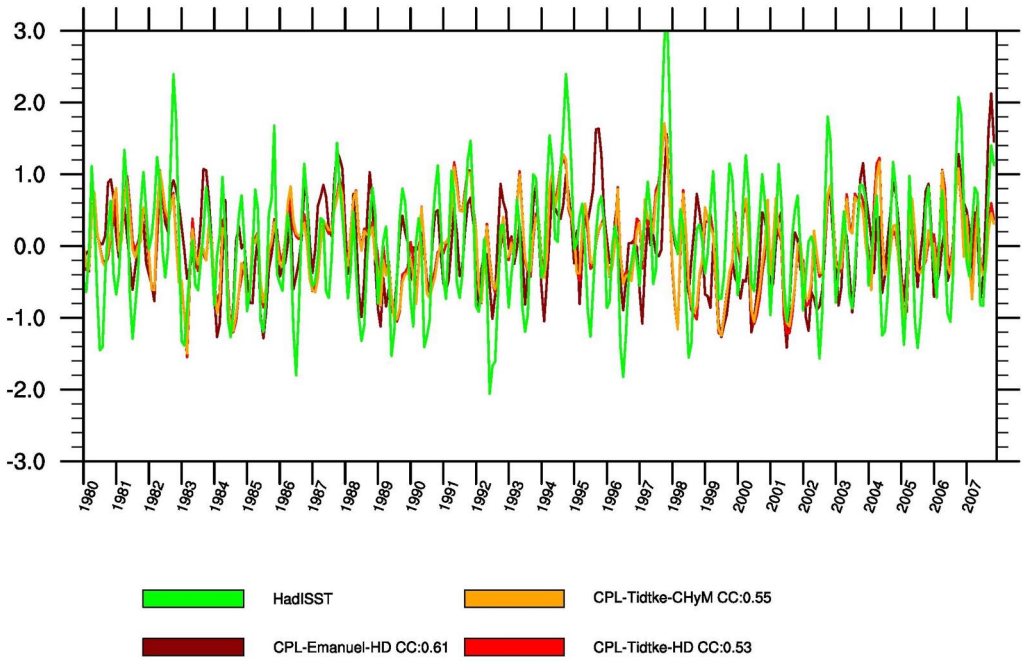

Figure 3.14. The IOD mode Index (DMI) calculated considering the differences between the SST anomalies of Western (10°S-10°N and 50°E 70°E) and Eastern (10°S-0°N and 90°E-100°E) as simulated by ESM-Em (dark-red), ESM-TkHD (red), ESM-TkCH (orange) and HadISST (green).

3.3 The hydrological models validation

Since one of the new features of this work is the implementation, inside the RegCM-ES system, of a new hydrological model, the validation for the freshwater discharges at river mouths is needed. The BoB is one of the freshest area of the Indian ocean basin receiving very large amount of fresh water discharge during the ISMR (Thadathil et al. [2002] ; Varkey et al. [1996]). The effect of the freshwater forcing on the oceanic vertical structure has a big role in manteining a shallow mixed layer, through the establishment of a barrier layer acting against the oceanic vertical density stratification (Seo et al. [2009]) and hence on SST. The convection over this basin is strengthened by high SST values resulting from the shallow mixed layer (Shenoi et al. [2002]) and in turn, the convection acts on SST trough variation in air-sea heat fluxes (Krishnamurti et al. [1988] ; Mujumdar et al. [2011]) This complex system is essential in modulating the spatial and temporal variability of the monsoon intraseasonal oscillation (MISO; Goswami et al. [2016]) and a correct representation of the freshwater discharge in this basin is needed.

The scarsity of a continuos temporal availability of observations for the Bangladesh river discharge observations and the restricted access to them all over the India region makes the validation a difficult task for the BoB area. For this brief validation we have utilized data that were collected from the Bangladesh Water Development Board (BWDB) for the well-known Hardinge Bridge gauge station on the Gange river. The available observation for this station spans from 1970 to 1998 and we selected the period that overlapps to our experimental window (from 1980 to 2007) to compare with our simulations. Figure 3.15 shows the comparison of the river discharge annual cycle for the BWDB observation and for the ESM-TkHD and ESM-TkCH averaged from 1980 to 2007.

The magnitude and the timing of the annual cycle for the Gange River discharge is very well captured by the CHyM model compared to the HD model. The last one has an understimation and a shift in the peak during the monsoon season and an overestimation for the dry period. The root mean square error and correlation coefficient are 11000 m^3/s and 0.71, between HD and observations and 3000 m^3/s and 0.98 between CHyM and observations. These differences in magnitude are due to the finer model resolution used in CHyM and the more realist surface description of the drainage network. Moreover the HD model has parametrised two different routing velocities, one for the surface flow and one for the subsurface flow, being the last one a function of the landuse. Probably the latter one is the responsible of the shift of the annual cycle. This doesn't happen for the CHyM model that treats the two flows together because they are coming out of the CLM land surface model as a total runoff ready to be routed in the surface and subsurface channels.

3.4 Atmospheric mean state validation

In this section we evaluate the simulated climatological mean state of the atmosphere against the observations and reanalysis. We highlight the major differences between the stand alone RCM and the coupled RegCM-ES experiments, as well as that arising from the different parameterization schemes used to perform the simulations. The ensemble mean of the RCMs and ESMs is also analysed.

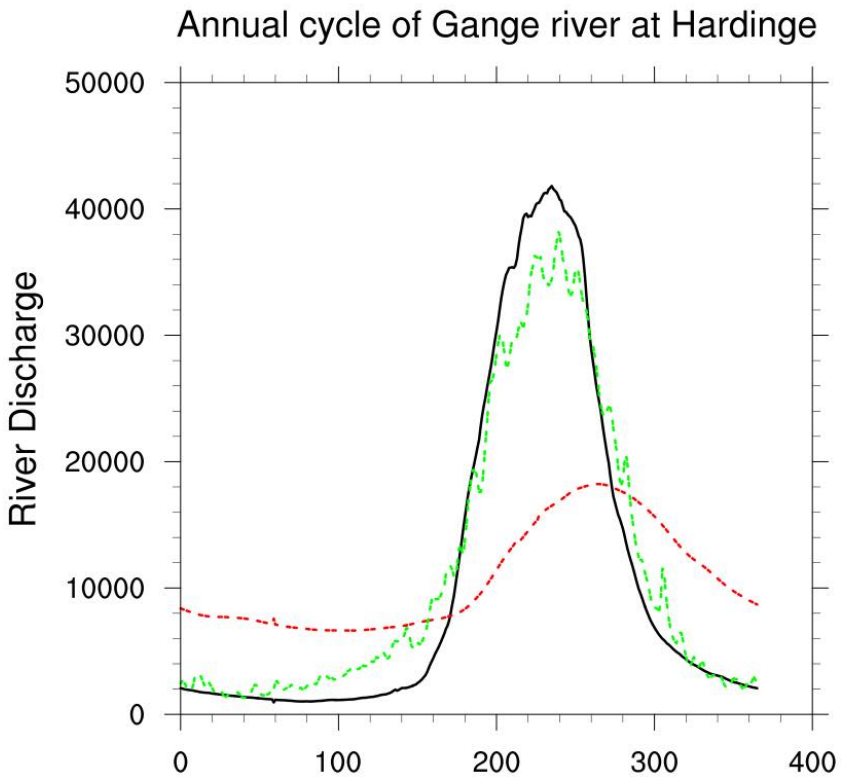

Figure 3.15. Annual river discharge (m^3/s) for Gange River, at Hardinge Bridge gauge station, from Bangladesh Water Development Board (BWDB ; black line), ESM-TkHD (red dashed line) and ESM-TkCH (green dashed line), averaged for the period from 1980 to 2007.

Figure 3.16 depicts the comparison of climatological ISMR simulated by RCMs and ESMs compared with the observation datasets (IMD over India and TRMM elsewhere). All the simulations are able to capture the main precipitation patterns although with some substantial differences. The shape of the mean precipitation over land is clearly dictated by the two different cloud parameterization schemes. The differencies with the climatological observed values are reported in Figure 3.17. RCM-Em (Fig. 3.17(a)) and ESM-Em (Fig. 3.17(a)) overestimates the precipitation over the Indian Western Ghats, peninsula and north-west India whereas a pronounced underestimation is observed over the north east. RCM-Tk (Fig. 3.17(f)), ESM-TkHD (Fig. 3.17(b)) and ESM-TkCH (Fig. 3.17(c)) on the other hand underestimates the precipitation over the monsoon trough, the north part of Western Ghats and Himalayas mountain chain while overestimates over the foothills. A common feature is the overestimation observed over the Kerala region, the region that is usually used to assess the monsoon onset and this is more evident in case of the RCM-Em and ESM-Em and in the coupled simulations. The role of the coupling over the Indian subcontinent doesn't seem to play a major role except for producing a small decrease of precipitation over the monsoon trough and an increase over the extreme south of the peninsula.

Over the ocean instead, beside the still predominating role of the cloud parameterization schemes, the role of the coupling seems to be significant. The positive bias in RCMs (Fig. 3.17(g)) over the south BoB appears reduced in the ESMs (Fig. 3.17(d)). A general increase of precipitation is generally observed over the Tropical Indian Ocean (TIO) in the Esm-Em simulation compared to its standalone version Rcm-Em with the exception of BoB (Fig. 3.16(a) against Fig. 3.17(e)) while a general decrease is observed in the ESM-TkHD and ESM-TkCH compared to its stand alone version Rcm-Tk (Fig. 3.16(b-c) against Fig. 3.16(f)).

The increases of precipitation over the western TIO is supposed to be partially linked with the positive bias of the SST observed for the ESM-Em (Fig. 3.4(h)). Over these areas, the SSTs have a relevant role in maintining clear sky conditions as elucitaded in section 1 of chapter 1. The treshold of 27.5^{o}C, above which deep convection is induced, can be observed in the overlapped contours in Figure. 3.16. This threshold is reached by the ESM-Em during JJAS allowing convection to start over Arabian Sea.

Overall, the use of the new CHyM model doesnâĂŹt seem to influence the seasonal average distribution of precipitation. Threfore, as explained in the previous section the correct simulation of the freshwater discharge in the BoB is essential, but on the other hand not sufficient, to correctly simulate the MISO and the spatial and temporal distribution of monsoon precipitations associated with them, in fact, we think that the missing representation of the barrier layer forming in this basin is also caused by other factors. One of those factors cames from the parameterization of the vertical mixing used in the ocean model (the KPP scheme). The KPP in fact, used for this experiment and that is largely used by a wide ocean modeler community (not only in the MITgcm), seems to be inadequate to reproduce the physical processes involved in the mixing in such a low-salinity basins like the BoB (Goswami et al. [2016]).

The mean JJAS temperature patterns appear quite similar among the models and the small differencies observed by comparing the simulated temperatures with the observations are mainly linked with the precipitations bias commented above.

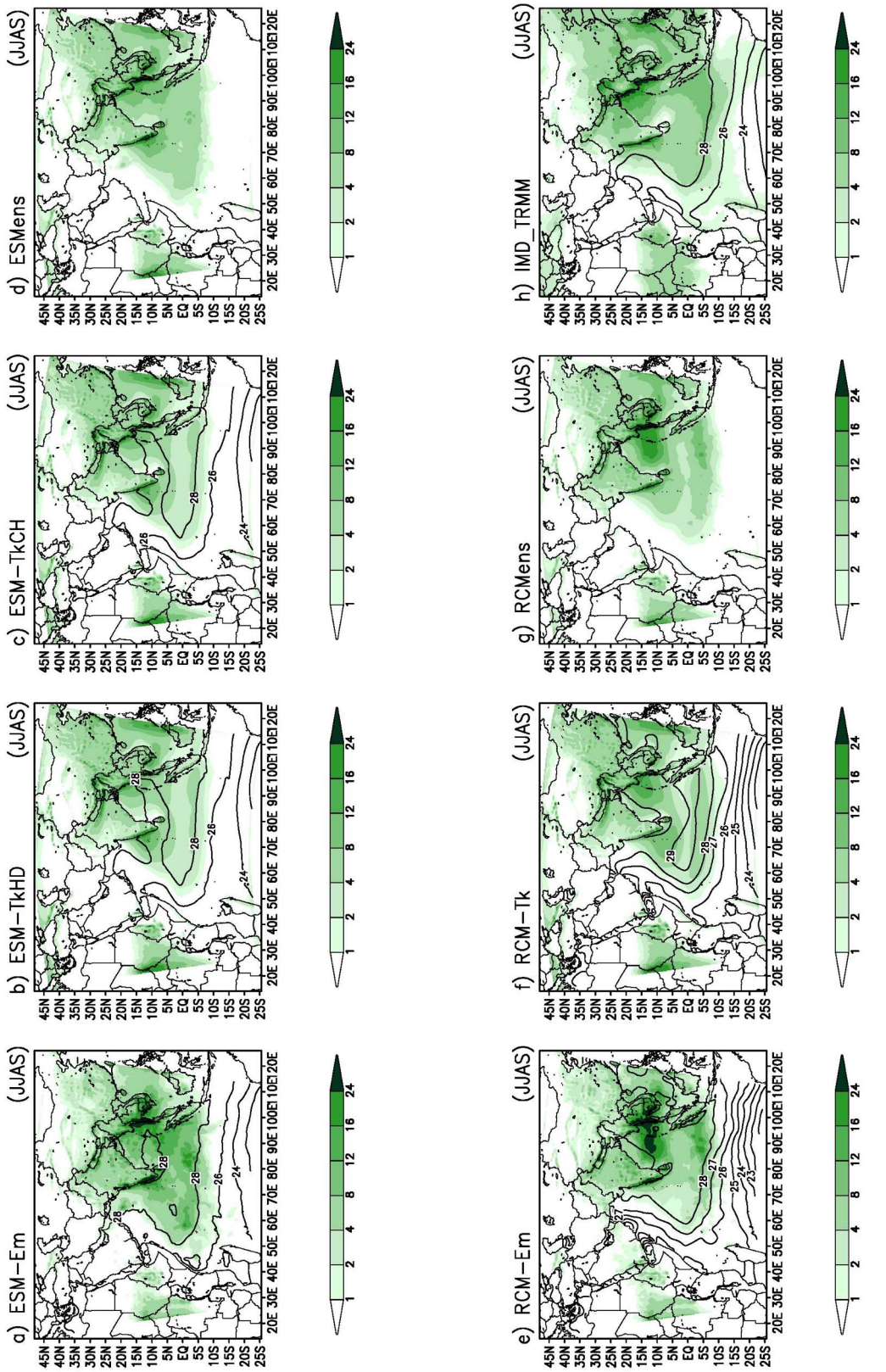

Figure 3.16. Climatology of JJAS mean precipitation (mm/day) for the period 1980-2007 in (a) ESM-Em, (b) ESM-TkHD, (c) ESM-TkCH, (d) ESMs, (e) RCM-Em, (f) RCM-Tk, (g) RCMs and (h) the observations IMD over India and TRMM elsewhere. Solid contours idicate the Climatology of JJAS mean simulated SST (°C) for each ESMs and HadISST for TRMM-IMD.

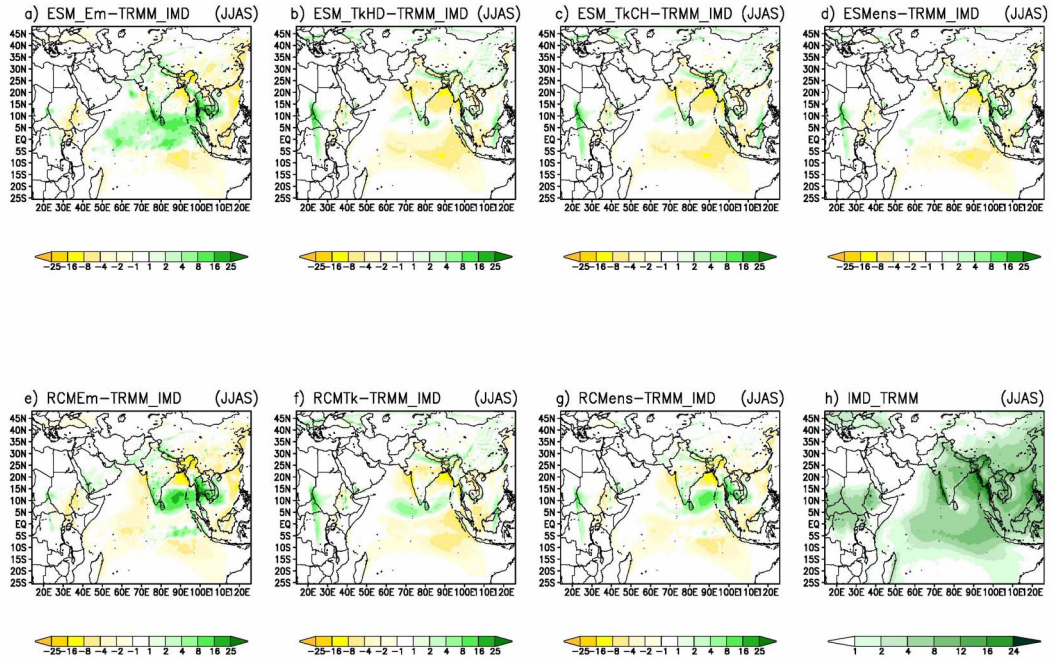

Figure 3.17. Precipitation biases of JJAS mean precipitation (mm/day) for the period 1980-2007 between (a) ESM-Em, (b) ESM-TkHD, (c) ESM-TkCH, (d) ESMs, (e)RCM-Em, (f) RCM-Tk, (g) RCMs and the IMD observations over India and TRMM elsewhere.

Colder(warmer) simulated temperatures (Fig. 3.18) are observed over the regions with positive(negative) biases in the precipitations (Fig. 3.16). In particular, sistematic colder temperatures are observed over the Himalayas in all the experiments (Fig. 3.19). Moreover, slightly warmer temperatures produced by RCM-Tk, ESM-TkHD and ESM-TkCH (Fig. 3.19(b,c,f)) respect to RCM-Em and ESM-Em (Fig. 3.19(a,e)), can be observed over the arabian peninsula.

The annual cycle for the precipitation has been calculated over the five Indian Homogeneous Rainfall Zones (IHRZ). IHRZ are identified by the Indian Institute of Tropical Meteorology (IITM; `www.tropmet.res.in`) on the basis of the temporal and spatial variations of rainfall over India. They are named refering to their geographical location such as Central Northeast (CNE), Northwest (NW), Northeast (NE), West Central (WC) and Peninsular (PS), and they are shown in Figure 3.20. The period considered to calculate the monthly means to plot the annual cycles span from 1980 to 2007 for the IMD observations and for the five experiments whereas for the TRMM observations data are available only from 1998.

The observational datasets, showed in Figure 3.21 using a dashed green line for IMD and a dashed black line for TRMM, are in good agreement in all zones except over the NE. The fact that for NE it has been observed an important increasing trend of the number of heavy rain days during the last fifthy years (Dash et al. [2009]) may provide an explanation to this discrepancy between the two set of observations, since the TRMM dataset is available only for the last ten analized years.

Since, the cumulus convection scheme is resulted to be the main source of the differencies among the experiments, the analysis will be divided in two parts. In the

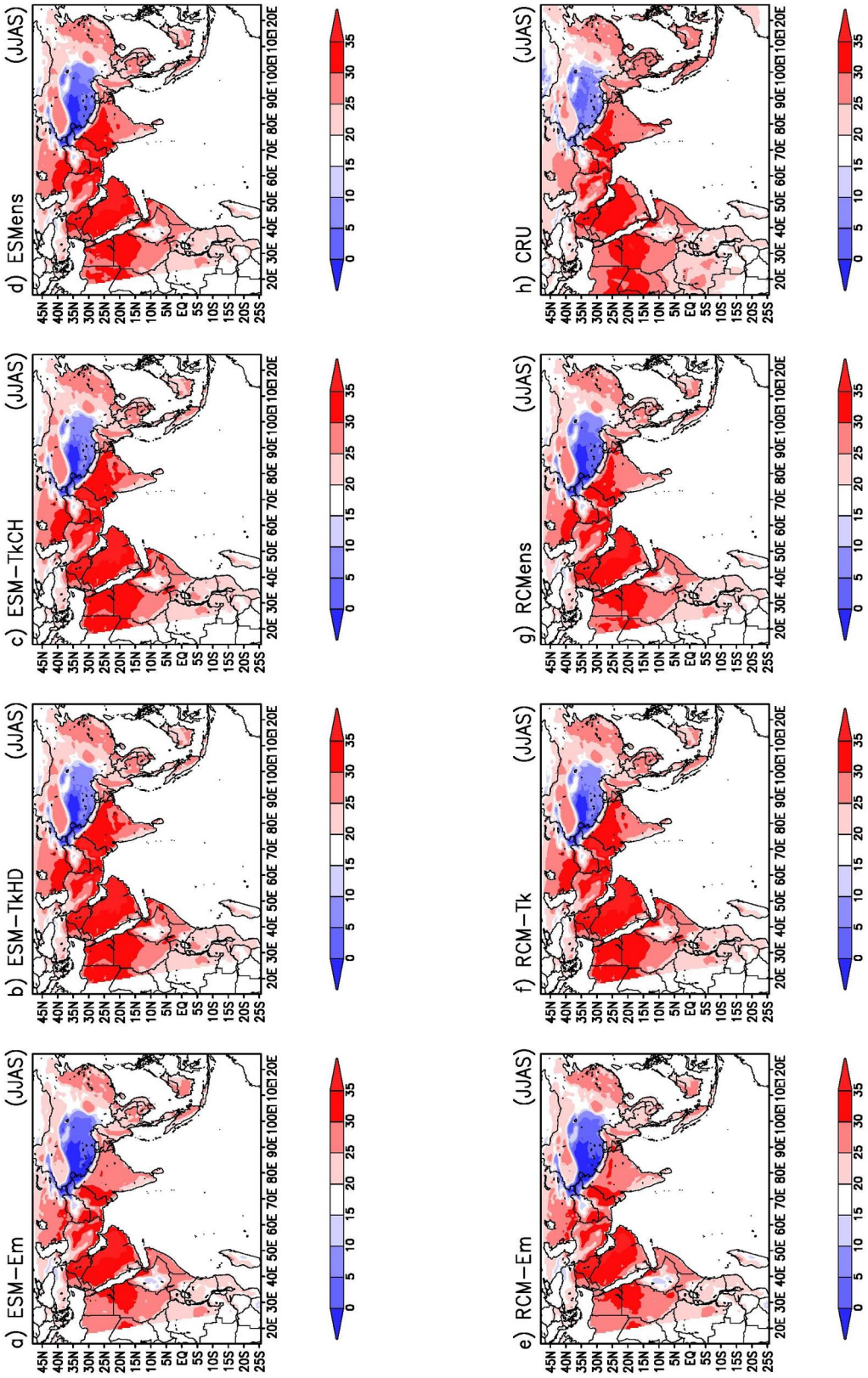

Figure 3.18. Climatology of JJAS mean temperature (°C) for the period 1980-2007 in (a) ESM-Em, (b) ESM-TkHD, (c) ESM-TkCH, (d) ESMs, (e) RCM-Em, (f) RCM-Tk, (g) RCMs and (h) the CRU observations.

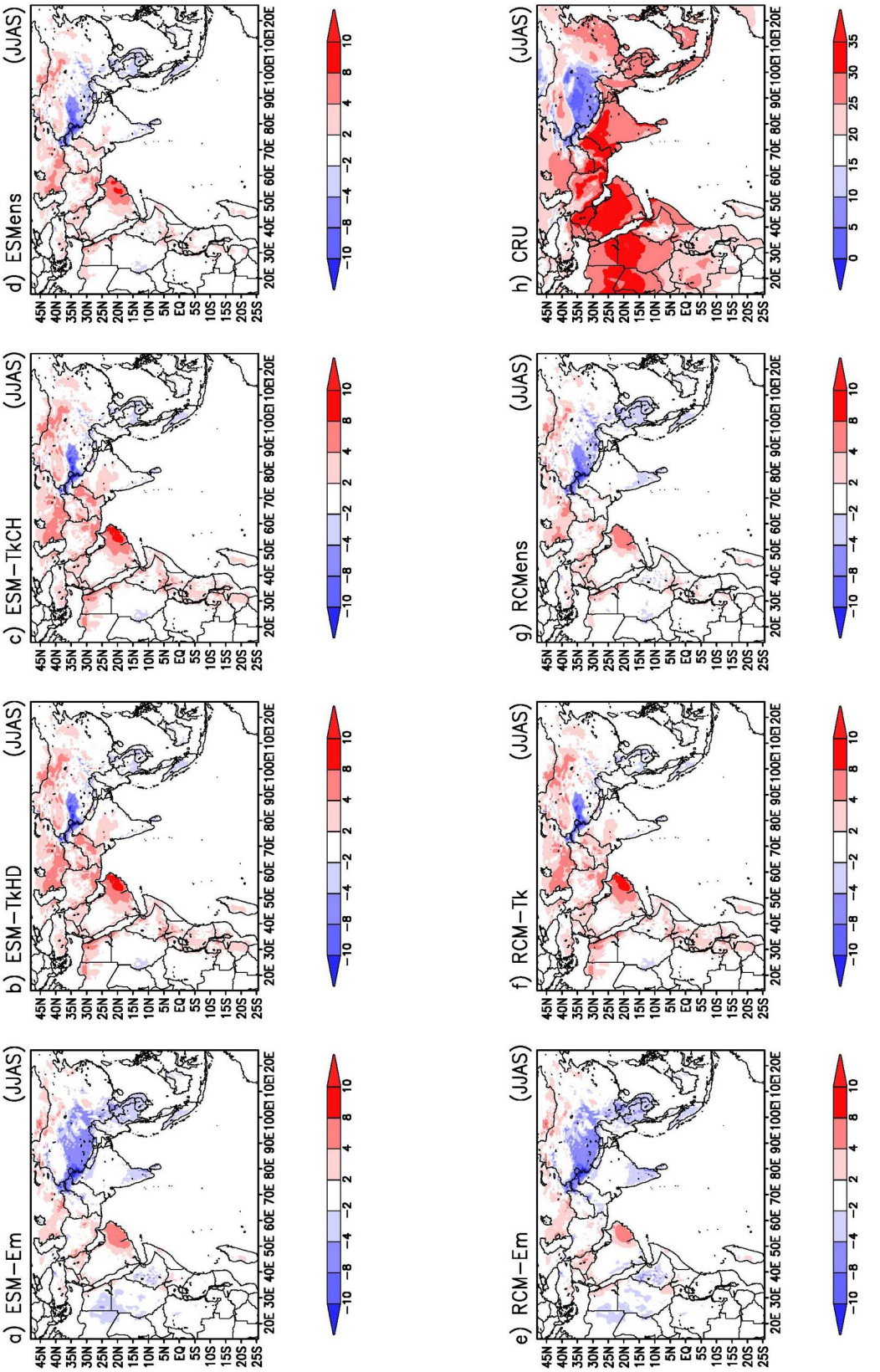

Figure 3.19. Temperature biases of JJAS mean precipitation (°C) for the period 1980-2007 between (a) ESM-Em, (b) ESM-TkHD, (c) ESM-TkCH, (d) ESMs, (e)RCM-Em, (f) RCM-Tk, (g) RCMs and the CRU observations.

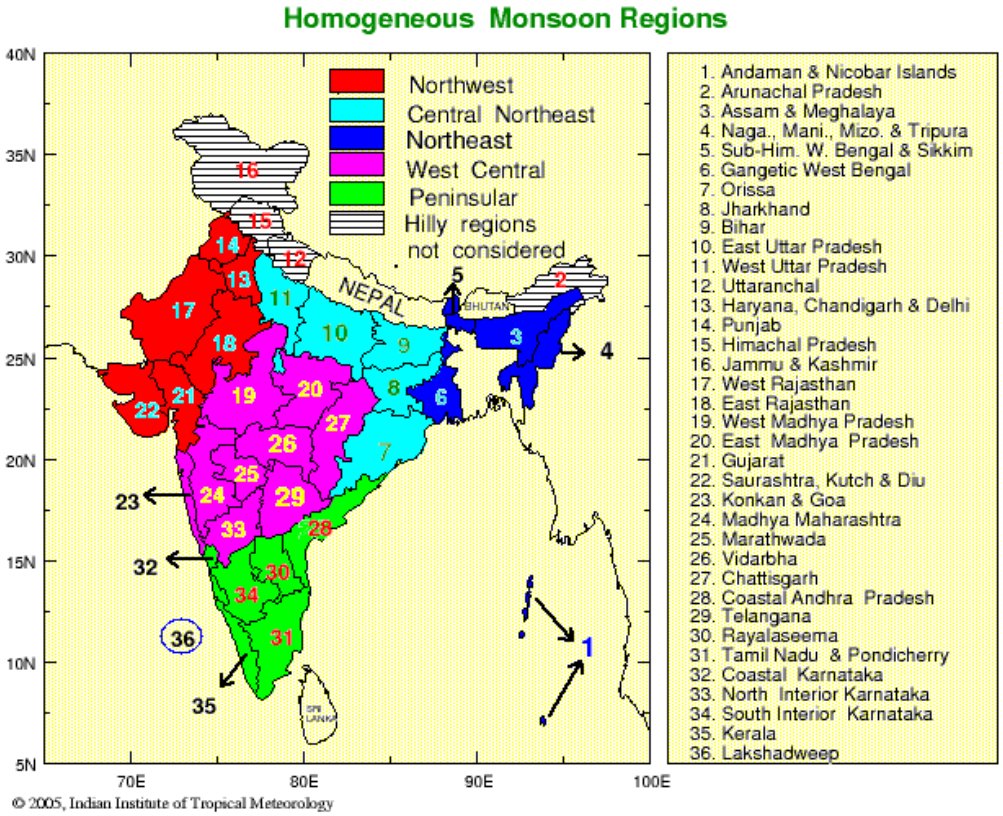

Figure 3.20. Indian Homogeneous Rainfall Zones (IHRZ). Northwest (NW), Central Northwest (CNE), Northeast (NE), West Central (WC) and Peninsular (PS). Picture taken from: `www.tropmet.res.in`

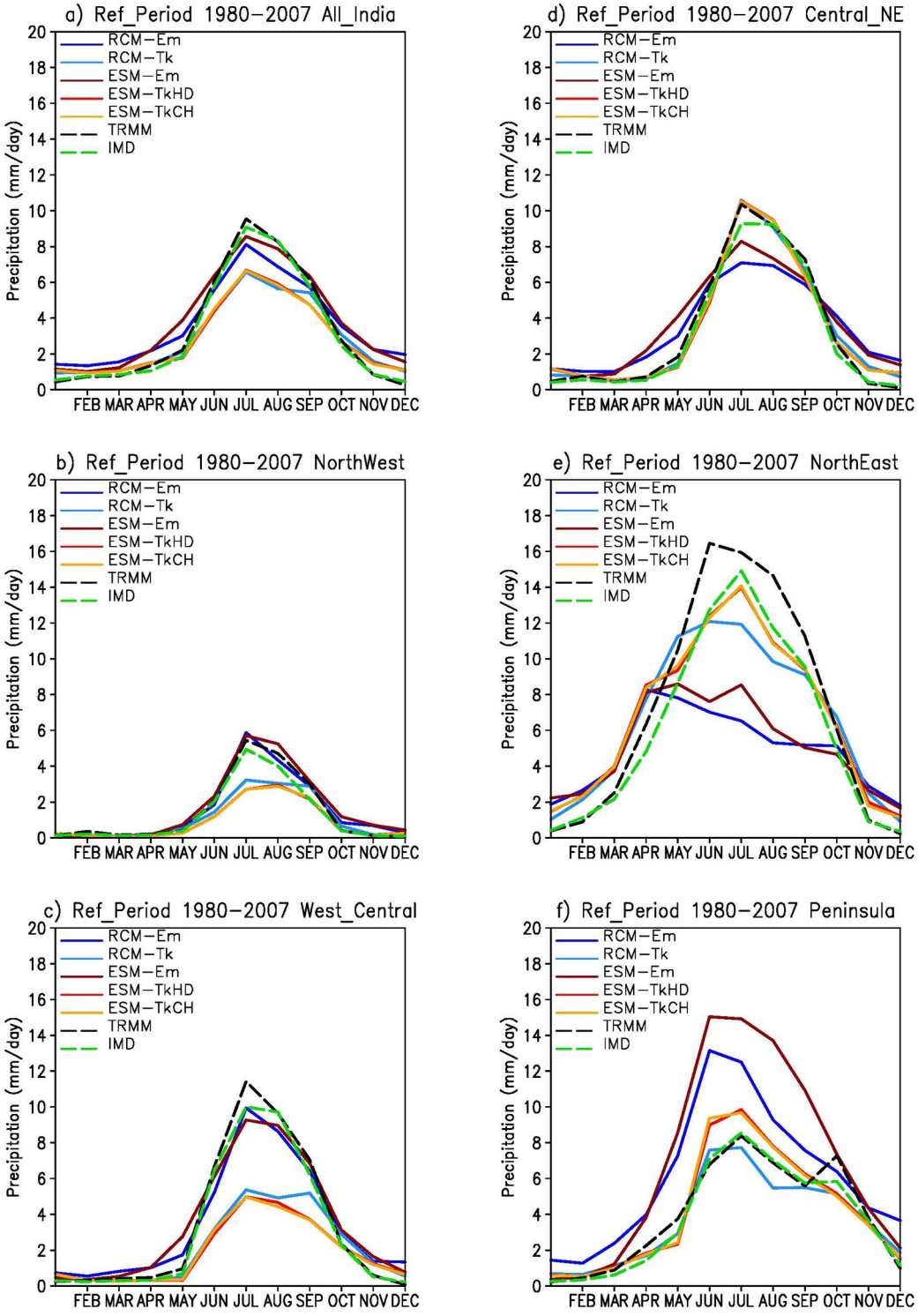

Figure 3.21. Annual cycle of monthly averaged rainfall (mm/day) for all the ESM experiments (ESM-Em, ESM-TkHD, ESM-TkCH) in reddish colors, all the RCM experiments (RCM-Em and RCM-Tk) in bluish colors, and for two set of observations, namely TRMM and IMD (dashed lines).

first part it will be analyzed separately the results on the basis of the convection scheme utilized and in the second part we will highlight the differences that arises in using the two different schemes.

We remember that the two experiments that have Emanuel as cumulus convection scheme are RCM-Em and ESM-Em, and they are depicted in Figure 3.21 rispectively with the dark blue and dark red solid lines. The observed results for "Emanuel experiments" present an overestimation of rainfall during the pre-monsoon season (MAM) over all the IHRZ with the exception of NW and during the post-monsoon season (OND) over all the five IHRZ. A well representation of the peak of ISMR (JA) is observed over NW and WC but a marked overestimation(underestimation) over PS(NE) can be also noted. With the Emanuel convection scheme, in general, the coupled experiment (ESM-Em) seems to increase rainfall over all IHRZ, especially during MJJAS months and over PS.

The three experiments that have Tiedtke as cumulus convection scheme are RCM-Tk, ESM-TkHD and ESM-TkCH, and their are depicted in Figure 3.21 rispectively with the light blue, light red and orange solid lines. The "Tiedtke experiments" present good performances on simulating the shape of the annual cycle over most of the zones. To highlight in these simulations is an underestimation during the peak of ISMR (JA) over NW and WC but along with a very good representation of the peak over the remaining IHRZ. The effect of the coupling for "Tiedtke simulations" has an opposite sign, positive over NW and WC zones and negative over NE and PS, whereas is absent in the CNE (overlapped lines in Figure 3.21). The simulated annual cycles for ESM-TkHD and ESM-TkCH over NW and WC zones are dryer compared to that of RCM-Tk but with a shape more similar to the observed one. In the NE whe have observed the best improvements with the coupled models. The annual cycles for ESM-TkHD and ESM-TkCH are wetter than that for RCM-Tk and shape, and values in JA, are very close to IMD. The annual cycles of the twin experiments with the different hydrological model (ESM-TkHD and ESM-TkCH) are overlapped for the most of the months confirming the little impact for these experiments on the mean state of the moonsoon.

If we consider the annual cycle over all India (Fig. 3.21(a)) for the simulations that make use of Emanuel (RCM-Em and ESM-Em), the curve is close to the observational datasets during ISM although overestimating the pre and post-monsoon phases. On the contrary, for the simulations that make use of Tiedtke (RCM-Tk, ESM-TkHD and ESM-TkCH), is observed an underestimation during ISM and a smaller overestimation, compared to the Emanuel one, during the post-monsoon phase. This is partly misleading because, as it has been seen, the Emanuel scheme totally fails to reproduce the peak over NE and produces a strong overestimation during all the months over PS. The shape of the annual cycles produced by Tiedtke, expecially in the coupled version of the experiments, better resemble the observations and, even though with the underestimation over WC and NW, this scheme seems most suitable in reproducing the annual cycle over India.

3.4.1 The Summer Monsoon Low Level Jet

The ability of the models to simulate the summer monsoon Low Level Jet (LLJ) is crucial to correctly reproduce the patterns of precipitation during ISM over South Asia region and in particular over India. The cross of the equator line off to the

Somali coasts and the increasing of its speed over the Arabian Sea is one of the main characteristics of the LLJ and give rise to the well-known Somali current. Moreover, as will be shown in the section dedicated to the relation of the ISMR with ENSO, the Somali Current with the associated upwelling over the eastern coasts of equatorial Africa, plays an important role in modulating the interannual variability of the ISMR over India.

Figure 3.22 shows the LLJ at 850hPa hight simulated by the experiments (subplot a and e) and by the reanalysis of ERA-Interim (EIN75) (subplot f). The shape of the Jet is captured by all the experiments but a general overestimation of its intensity is observed for RCM-Em and ESM-Em. The experiments RCM-Tk, ESM-TkHD and ESM-TkCH produce a weaker jet over the Arabian Sea and a less pronunced wave over the India peninsula compared to RCM-Em and ESM-Em. The stronger Jet over the Arabian Sea for RCM-Em and ESM-Em experiments is supposed to be the cause of the overestimation of rainfall over the Penisula (Fig. 3.21(f)) during ISM, probably due to the increased moisture advection towards Western Ghats. In addiction, a cyclonic circulation is observed over the monsoon trough in RCM-Em and ESM-Em making this area more prone to convection during ISM as can be clearly observed in the annual cycle of the NW and WC (Fig. 3.21(b-c)) and in the mean seasonal precipitation map (Fig. 3.17(a-e)).

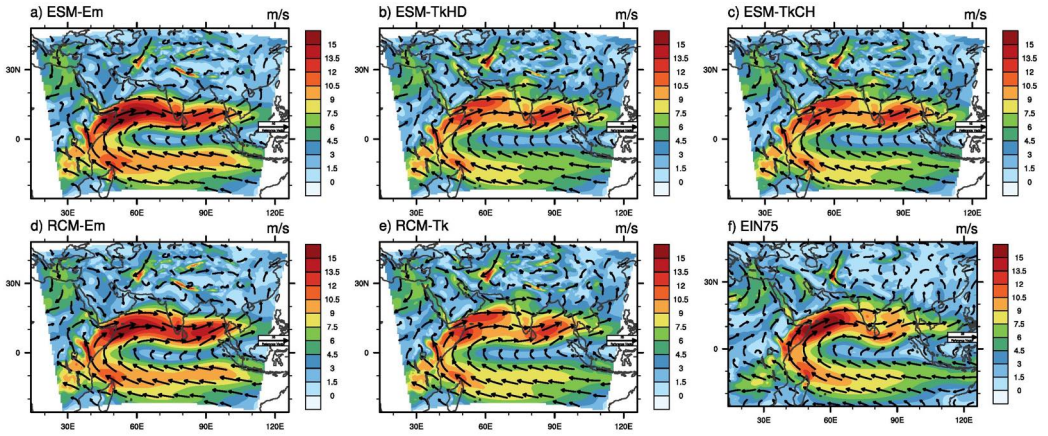

Figure 3.22. Climatology (1980-2007) of JJAS mean wind (m/s) at 850 hPa in (a) ESM-Em, (b) ESM-TkHD, (c) ESM-TkCH, (d) RCM-Em, (e) RCM-Tk and (f) Era-Interim reanalysis (EIN75). The shaded colours indicate the magnitude of the winds.

Over BoB the Jet is overestimated by all the experiments, but a reduction of the overestimation over this basin is observed in the coupled ESM-Em respect to its stand alone version RCM-Em (Fig. 3.22 subplot (a) respect to subplot(d)) along with a strengthening of the jet over the Arabian Sea. The same signal but weaker, can be observed also in the RCM-Tk compared to ESM-TkHD and ESM-TkCH. This response of the Jet to the coupling could be an explation for the increased precipitation over the Western Ghats (increased moisture advected against Western Ghats) and the reduction of precipitation over the BoB (Fig. 3.16 (e) against (a) and fig (f) against (b-c)) of the coupled experiments respect to its stand alone counterpart. This highlights the major role of the ocean in modulate the intensity of the Jet and a quite strong sensitivity to the coupling.

3.5 Variability of the ISM

As discussed in the introduction, beside the monsoon mean state, another important feature of the monsoon is the intraseasonal and intereannual variability and its close relationship with ENSO. A special attention will be given to the response of ISMR to ENSO due to the main role that this close relationship seems to have in the last decades as shown in many studies (Kucharski et al. [2011] ; Wang et al. [2003] ; Clark et al. [2000] ; Krishnamurthy and Shukla [2000] ; Murtugudde et al. [2000] ; Ashok et al. [2004] ; Ashok and Saji [2007] ; Bracco et al. [2005] ; Bracco et al. [2007] ; Cherchi et al. [2007] ; Cherchi and Navarra [2013] ; Yang et al. [2007] ; Xie et al. [2009] ; Izumo et al. [2008]). Furthermore, one of the major finding of this study is related to a source of predictability of the ISMR linked to ENSO and this will be better explained in a dedicated section.

3.5.1 Simulated break and active spells

From section 1.2.2 we have learned that one of the important intraseasonal monsoon characteristic is the succession of alternating break and active phases. To investigate the model ability in reproducing this feature we focus now our attention on the monsoon core zone. The chosen area is identical to the one used by Rajeevan et al. [2010] to define the two phases of the monsoon. This irregular box extends over central part of India, from the Rajasthan to the northwest coast of BoB. The monsoon core zone doesn't include the foothills of Himalaya where strong precipitations are observed also during the break phases. The Figure 3.23 represents the composite of precipitation for the RCMs, ESMs and ERA-Interim reanalysis, for the break and active spells. According to the definition of Rajeevan et al. [2010] the active(break) composite is obtained by selecting the daily mean precipitation for the days in which there is a positive(negative) standardized anomaly greater(less) then 1(-1) standard deviation from the relative daily climatology during the monsoon peak months (JA) (Rajeevan et al. [2010]). The number of break and active days during the peak of monsoon season make the difference between a dry and a wet year. The migration of the TCZ from the monsoon trough to the foothills of Himalaya leads to dry conditions over India and is associated with the break days. This can be observed in the composite maps (Figure 3.23(g,o)) of the break and active days for the observational dataset TRMM and the difference between the two (Figure 3.23(v)). During the active days a band of strong precipitation is observed over the monsoon trough whereas, during the break days, the strongest precipitation can be observed over the ocean, the NE and PS. The simulated precipitation patterns for the active phases over India are better reproduced by RCM-Em and ESM-Em (Fig. 3.23 (a,b)). The strongest precipitations are simulated correctly over the trough with the maximum over WC. In contrast, RCM-Tk, ESM-TkHD and ESM-TkCH (Fig. 3.23 (c,d,e)) experiments simulate an unrealistic maximum precipitation zone over CNE.

To better understand these differences we examine the maps of Sea Level Pressure for the active and break phases of monsoon obtained by following the same criteria used for the composite break/active phases of precipitation. Figure(Fig. 3.24) indicates that the RCM-Em and ESM-Em simulations (subplots a, b, f, g, k and l) better represent the low-pressure regimes over the monsoon trough with the migration of the low center above the NE during the break phases. The RCM-Tk

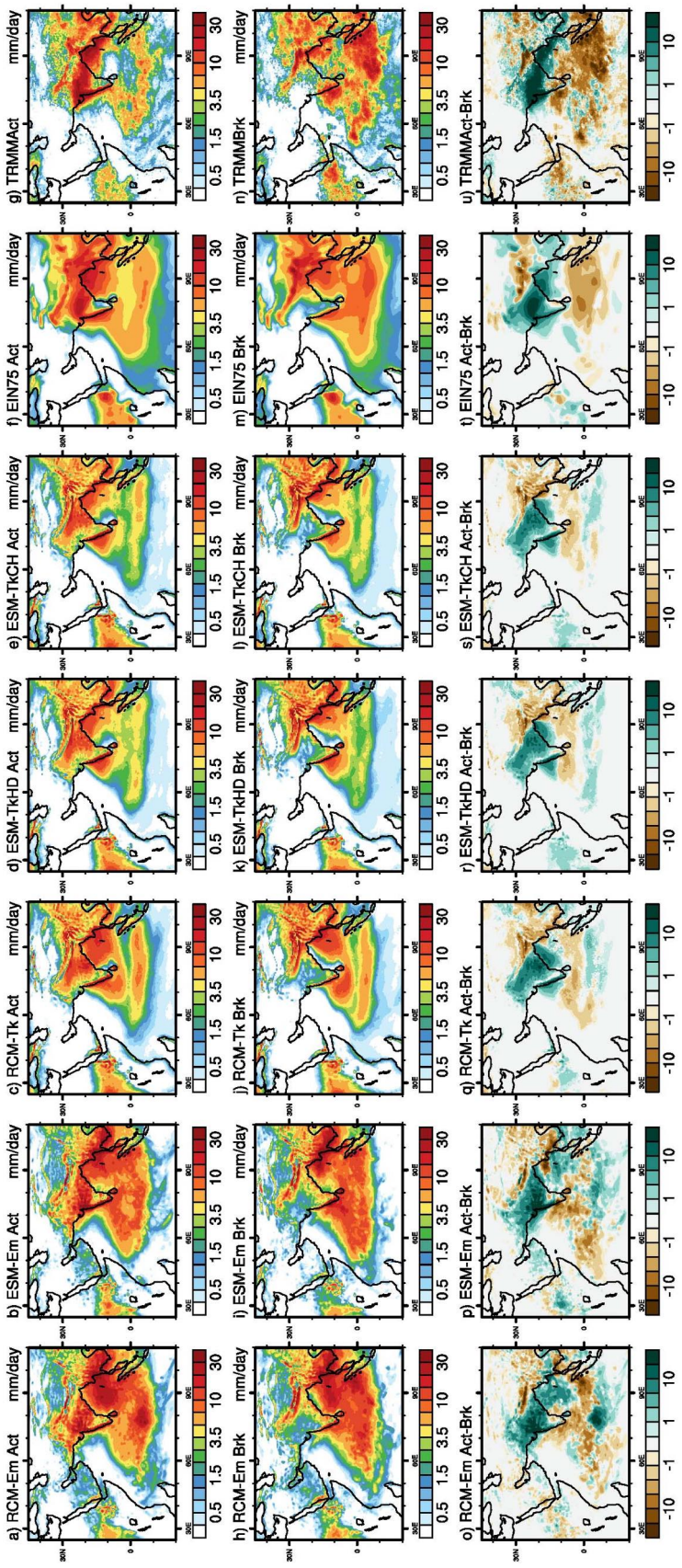

Figure 3.23. Composite of precipitation (mm/day) for break and active spells during JA for ESMs (b, i, d, k, e, l), RCMs (a, h, c, j), ERA-Iterim Reanalysis (f, m) and TRMM (g, n). The differences (mm/day) between the two spells for each of them are also reported (o, p, q, r, s, t, u).

and ESM-TkHD simulations produce instead an unrealistic low-pressure regime over the Tibetan plateau in both active and break, altought it is able to capture the differences between the two phases. This explains why the precipitation are displaced in CNE using the Tiedtke scheme during the active phases. The coupling doesn't seem to be relevant in the patterns of low-pressure regime and in the associated precipitation over India.

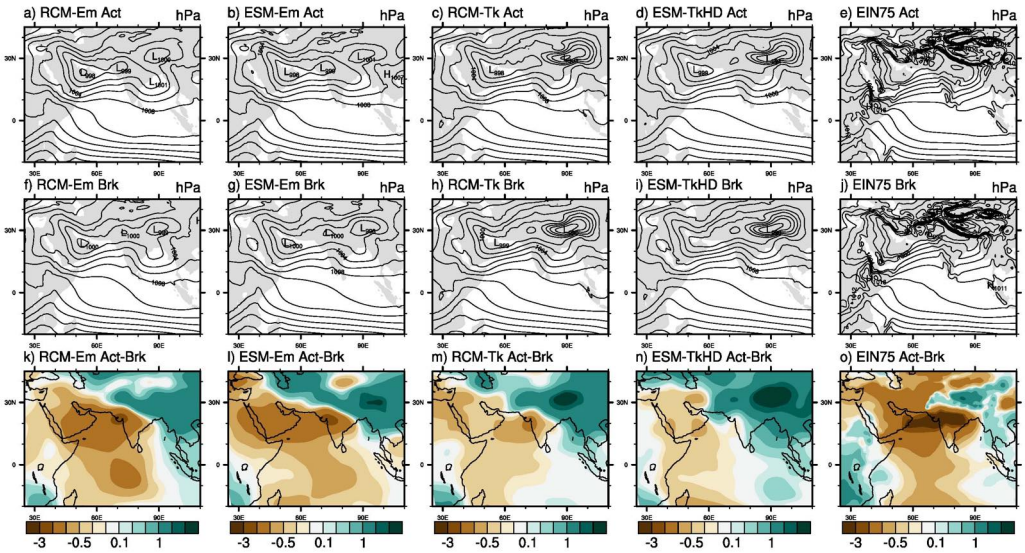

Figure 3.24. Composite of mean sea level pressure (hPa) for break and active spells during JA for ESMs (b, g, d, i), RCMs (a, f, c, h) and ERA-Iterim Reanalysis (e, j). The differences (hPa) between the two spells are also reported (k, l, m, n, o).

3.5.2 Simulated Intraseasonal Variability

As seen in the chapter 1, during the boreal summer, concurrently with the ISM, the Intraseasonal Oscillations (ISO) of the ISMR show two different propagation features over the Indian ocean. The first is related to eastward propagating convective anomalies over the equatorial belt associated with the Madden-Julian Oscillation (MJO ; Wang and Xie [1997] ; Lawrence and Webster [2002] ; Sperber and Annamalai [2008]) and it is responsible for relevant anomalies over Indian subcontinent as breaks with duration of more than 10 days (Joseph and Sabin [2008]). The second kind of propagation is related to northward propagating convective anomalies from equatorial latitudes towards the Indian domain (Yasunari [1979] ; Yasunari [1980] ; Sikka and Gadgil [1980] ; Webster et al. [1998] and is responsible of smaller scale anomalies in the ISMR. To examine the ability of the models to simulate the propagations responsible for the ISO during the monsoon season (JJAS) we follow the methodology proposed by Sabeerali et al. [2013]. We have performed the regression on the 20-100 day band pass filtered precipitation anomalies for the period JJAS against a reference time series for each point on the grid. The reference time series is obtained averaging the precipitation over the west Tropical Indian Ocean (TIO) (between 10°S-5°N and between 75°E-100°E) for the eastward propagating mode and over the monsoon

trough (between 12°N-22°N and between 70°E-90°E) for the northward propagating mode. The lag-longitude diagrams have been obtained averaging the regressed precipitation anomalies between 5°S and 5°N while the lag-latitude diagrams have been obtained averaging the regressed precipitation anomalies between 70°E and 95°E (Fig. 3.25 ; Fig. 3.26).

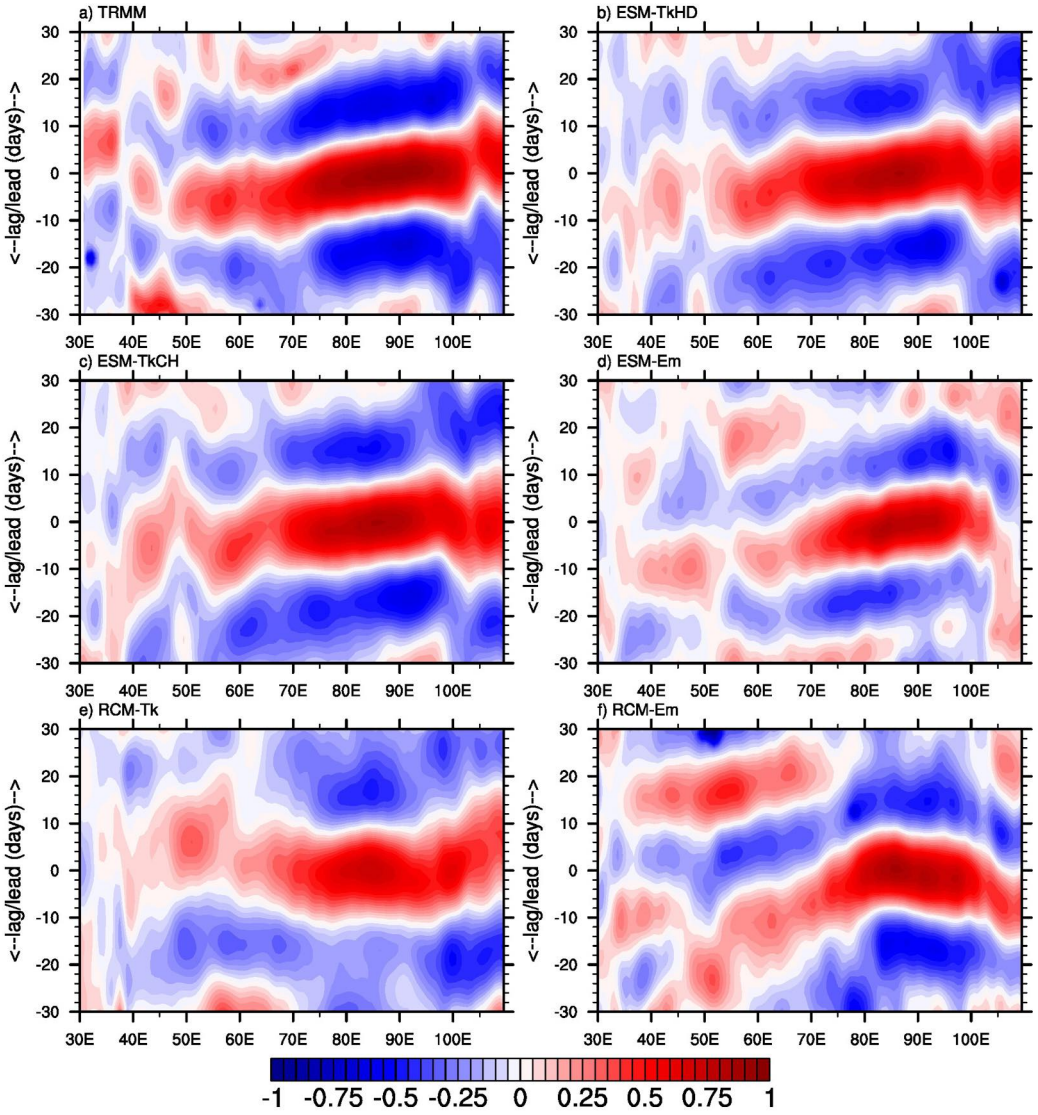

Figure 3.25. Eastward propagation diagrams of the 20-100 day band-pass filtered precipitation (mm/day) anomalies for 5°S and 5°N averaged band with reference time series averaged for a box over TIO (10°S-5°N - 75°E-100°E). The maps for (a) TRMM, (b-d) ESMs and (e-f) RCMs are showed.

The eastward propagating mode is shown in Figure 3.25 for the observational dataset TRMM, the coupled ESMs and uncoupled RCMs simulations. The eastward propagating signal in the ECMs ensemble (Fig. 3.25 (b,c,d)) is consisten with that of the TRMM observations (Fig. 3.25 (a)) with convection starting around 50°E

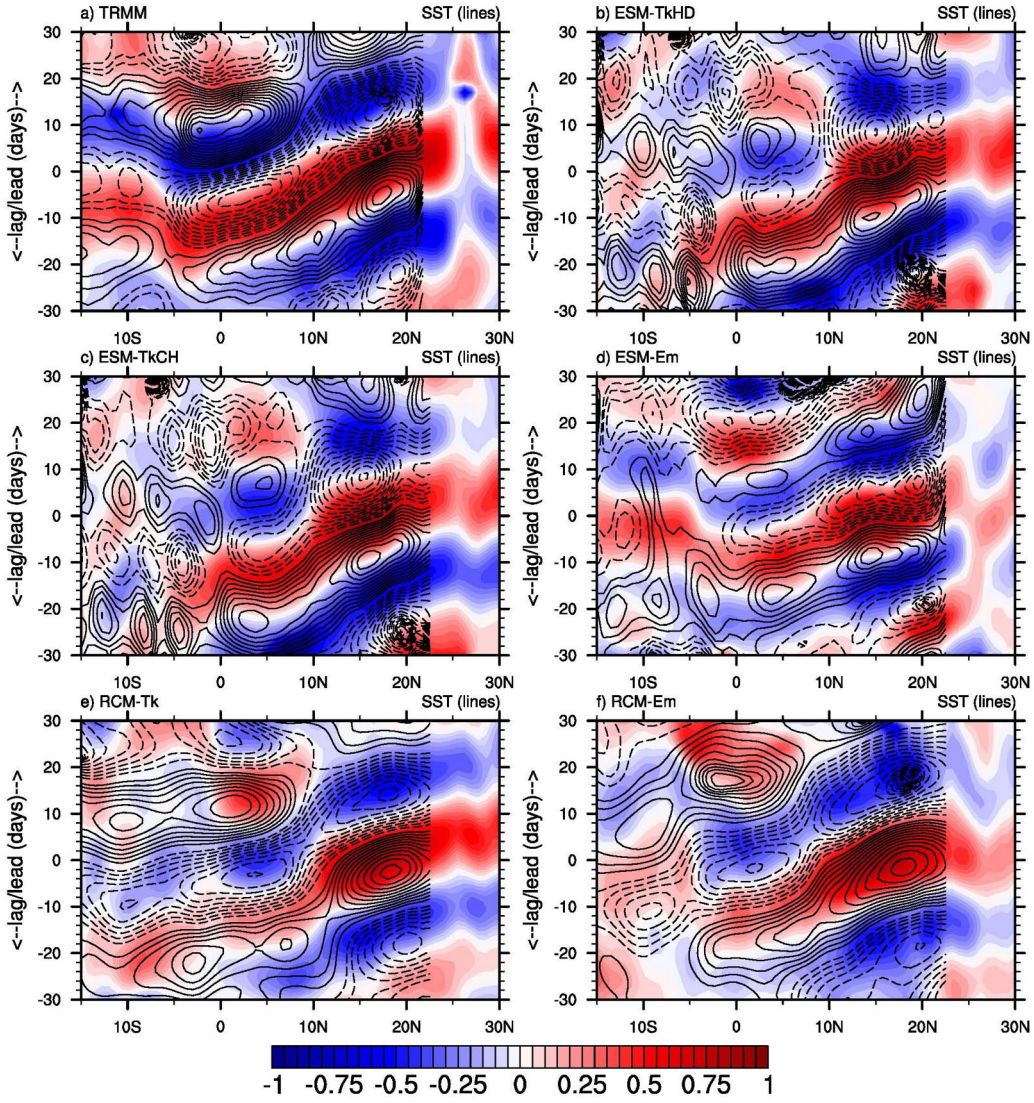

Figure 3.26. Northward propagation diagrams of the 20-100 day band-pass filtered precipitation (mm/day) and SST (contour lines ; °C) anomalies for 70°E and 95°E averaged band with reference time series averaged for a box over monsoon zone (12°N-22°N - 70°E-90°E). The maps for (a) TRMM, (b-d) ESMs and (e-f) RCMs are showed. The dashed contour lines are for negative values and the interval is 0.01 degree Celsius.

increasing around 70°E and decreasing around 90°E. In particular, ESM-TkHD and ESM-TkCH show an eastward propagating mode closer to the observations. The two standalone simulations totally fail in reproducing the eastward propagating mode, with an unrealistic propagation in the RCM-Tk simulation (Fig. 3.25 (e)) and in the RCM-Em one(Fig. 3.25(f)).

Also in the case of the northward propagating anomalies the better results come from the coupled models that use Tidke as convection parametrization (Fig. 3.26 (b,c)), at least at latitudes northern than 5°S. In the plot of the northward propagation are shown with countour lines also the anomalies for the SST (Fig. 3.26). In Figure 3.26(a) it is possible to observe how the SST anomalies lead the convection of about ten days, feature that it has been reproduced by the ESMs over north Indian Ocean (Fig. 3.26(b,c,d)). In contrast, this feature is not reproduced by the RCMs that show an almost overlapped SST to the convection anomalies (Fig. 3.26(e,f)). In general, both the eastward and northward propagation convection and SST anomalies are more realistics in the coupled experiments that have the Tiedtke scheme (ESM-TkHD and ESM-TkCH) although the pattern of the averaged break and active days over India are more realistics in the experiments with the Emanuel scheme as shown in the previous section. The better results of the coupled experiments compared with that of the stand alone experiments, are in agreement with the previous studies that showed how the air-sea interactions have a main role in influencing the ISO of the Indian monsoon (Sabeerali et al. [2013] ; Singh et al. [2016]).

3.5.3 Simulated Interannual Variability

The large oscillations in the intensity of the ISMR observed from one year to the next are the result of two main source of variability including the atmospheric internal ISO, that has a very small predictability (Syed et al. [2012] ; Kang et al. [2004] ; Ajaya Mohan and Goswami [2003]) and the influences from external forcings as the El Niño Southern Oscillations (ENSO ; Rasmusson and Carpenter [1983] ; Ju and Slingo [1995] ; Webster and Yang [1992]) that is the first mode of the interannual varibility of the ISMR as described in the first chapter of this thesis. Figure 3.27 depicts the departure, expressed in standard deviations from respective mean values of JJAS, of masked land precipitation over India.

From Figure 3.27 is clear the added value of the coupled Regional Earth System model when compared to the atmosphere only component. The signs of the simulated anomalies by ESM runs are in better agreement with the observations for most of the years. To quantify this we computed the temporal correlation between all the simulation and the IMD observed standardized anomalies over India and showed in Figure 3.27 and reported in the following table 3.3.

It is clear from the correlation coefficients shown in table 3.3 how the RCMs anomalies are totally uncorrelated with the observations weather the ESMs runs have all a correlation of the order of 0.35. This is a clear example of the importance of the sea-air interaction in modulating the interannual evolution of the monsoon system in agreement with Bracco et al. [2007], Kucharski et al. [2007], Samson et al. [2014] and Saha et al. [2016].

In support to this thesis we performed the analysis of the wet and dry composite years for JJAS season. The Figure 3.28(Figure 3.29) for wet(dry) composite have been obtained averaging the JJAS precipitation of RCMs and ESMs for the years in

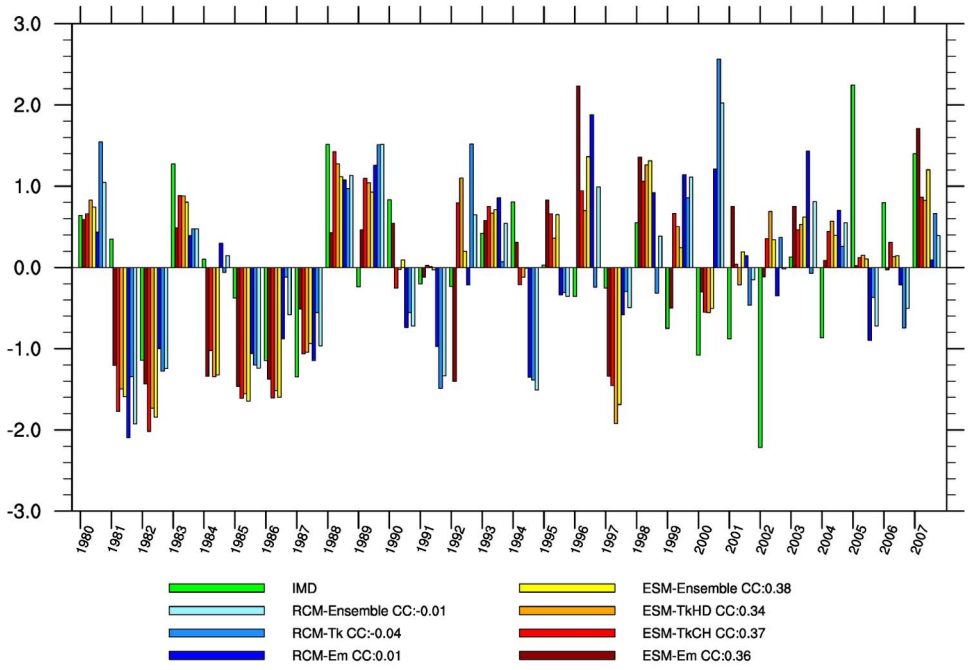

Figure 3.27. JJAS Precipitation Anomaly over India expressed in standard deviation units for the analized whole simulation period for observational dataset (IMD ; green color), RCM uncoupled simulations (bluish colors), ESM coupled simulations (reddish colors) and relative ensembles. The cross correlation coefficients (CCs) between the simulated departure anomalies obtained with each ESMs, RCM and IMD are presented.

Simulation Acronym	Correlation Coefficient
RCM-Em	0.01
RCM-Tk	-0.04
ESM-Em	0.36
ESM-TkHD	0.34
ESM-TkCH	0.37

Table 3.3. Tabular representation of the Correlation Coefficienties calculated between the time series of the standardized observed annual anomalies from IMD and the time series of the standardized observed annual anomalies for all the experiments performed in this study

which the precipitation of IMD, for the all India, are great(less) than 1(-1) standard deviations. During the wet years it is observed an increase of precipitation along the west coast, over the PS and over the North (Fig. 3.28(f)). The dry composite shows generally reduced precipitation over the same areas (Fig. 3.29(f)). The plot of wet composites for the coupled experiments (Figure 3.28(a,b,c)) shows how the ESMs are able to reproduce the positive signal over the west coast and PS, more uniform in ESM-TkHD and ESM-TkCH respect to ESM-Em. A signal of opposite sign is observed for their stand alone couterparts, over the west coast (Figure 3.28(d,e)). The same signal but with opposite sign is also catched by the ESMs for the dry composite maps (Figure 3.29(a,b,c)) and also for the dry composites it can be observed that the signal is better captured by the ESMs compared to the stand alone simulations (Figure 3.29(d,e)). These large differencies in the two set of experiments (ESMs against RCMs) will be partially elucidated in the next section where the relationship between ENSO and the ISMR will be treated. In fact, the big role of the coupled ocean in driving the ISMR response to ENSO will come up from the next analysis showing the strongest signal expecially over the regions just mentioned in this section.

3.5.4 The ISM anomalies related to ENSO

As discussed in section 1.2.3 the ENSO is the first mode of climate variability in the tropical regions. In this section we will focus on its effects over the IO, in particular on the ISMR, and the skills that the experiments have in representing it. Particular attention it will be given to the possible relationship between the ISMR with the ENSO index Niño-3.4 and the one year delayed ENSO impact to ISMR.

The maximum El Niño SST anomalies are reached during the boreal winter season and the greatest related effects on climate are observed concurrently with them through atmospheric teleconnections. In the 80s and 90s a weakening has been observed of its concurrently effects over the IO (as seen in section 1.2.3) and a major focus has been redirected to a possible late response of IO to this phenomenon. In fact, in the last ten years more attention has been dedicated to the delayed effect of ENSO on the SSTs over the IO and Northwest Pacific (NWP) and the related influence on ISMR. The Indo-western Pacific ocean capacitor (IPOC) (Xie et al. [2009] ; Xie et al. [2016]), the decrease of Western Arabian Sea Upwelling (WASU ; Izumo et al. [2008]) and the Indo-Tropical NorthWest Pacific ocean-atmosphere

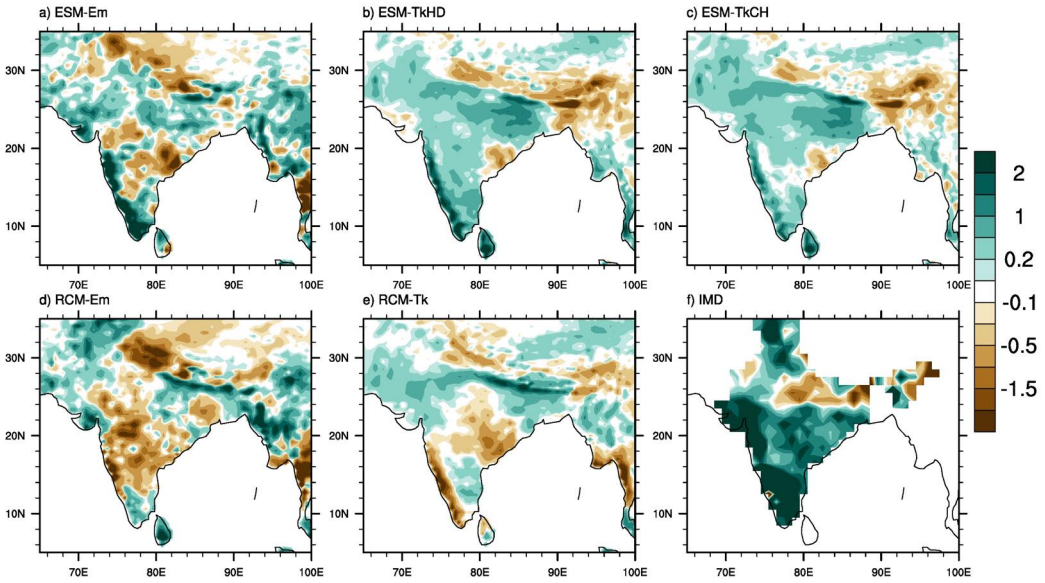

Figure 3.28. Composite of the wet IMD years in (a) ESM-Em, (b) ESM-TkHD, (c) ESM-TkCH, (d) RCM-Em, (e) RCM-Tk and (f) IMD.

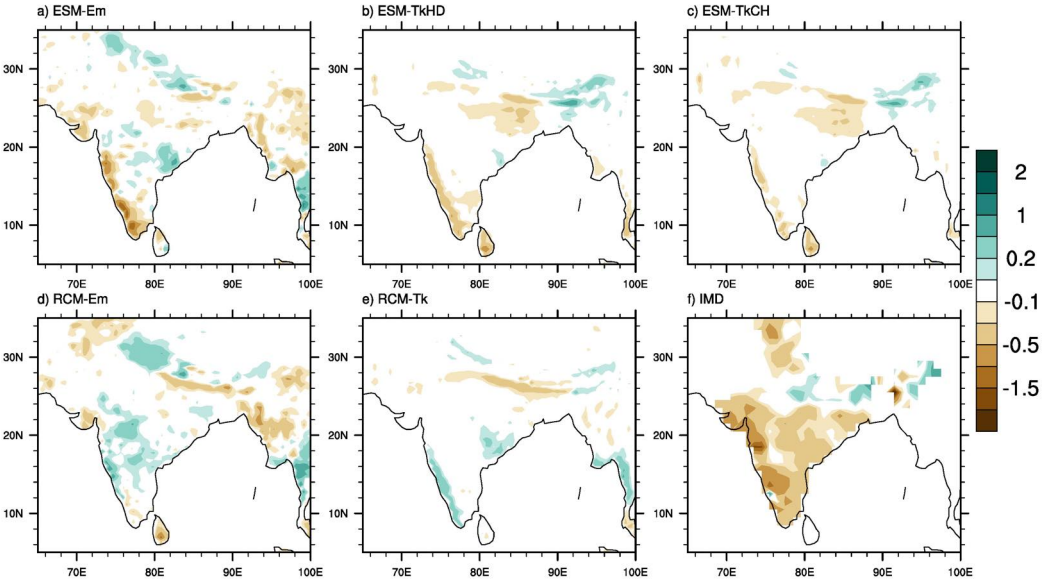

Figure 3.29. Composite of the dry IMD years in (a) ESM-Em, (b) ESM-TkHD, (c) ESM-TkCH, (d) RCM-Em, (e) RCM-Tk and (f) IMD.

interaction (Du et al. [2009] ; Kosaka et al. [2013] ; Wang et al. [2013]) are supposed to be the main phenomena that contribute to a delayed and prolonged response of the ISM to ENSO. We propose, in the following, a possible chronological sequence of events that lead to a strengthening of ISMR following a positive phase of El Niño involving the previously listed phenomena. A coupled effect of anomalies forming over the IO and the NWP (Indo-western Pacific ocean Capacitor; IPOC) leads to a longer duration of a large-scale anomalous anticyclone (AAC) forming during active phase of El Niño over the NWP and north IO. Through the effect of anomalous winds developing in its southern side, the AAC has an active role in inducing downwelling Rossby waves in the south tropical IO. This Rossby waves slowly propagate toward western IO during the following spring inducing anomalous northeasterly winds at the beginning of summer. The resulting effect on the Somali current reduces the upwelling over western Arabic Sea leading to warmer SST lasting until the ISM. The enhanced evaporation and moisture transport concurrently with the onset of the monsoon finally lead to an increase of precipitation over west India. Since the ocean plays an active role, the study of this phenomena and their response on the climate is possible only thanks to the develop of full ocean-atmosphere coupled models.

Our findings have confirmed and extended previous findings and we discovered the possibility that the relationship between ENSO and ISMR may have a longer feedback time, in fact, significant correlation coefficients have been found between the ISMR and the lagged 4-month running averages of Niño-3.4 index (Fig. 3.30) surprisingly with a lead-time of more than one year. Here after, the numerical in parenthesis refer to the phases of ENSO, 0 for the developing and 1 for the decay, so that the concurrent correlation between Niño-3.4 index and ISMR is represented by the JJAS(1) season, whereas the one-year lead correlation between Niño-3.4 index and ISMR is represented by the JJAS(0) season. For the IMD observation, the maximum values of correlation coefficients, greater than 0.5, have been found in the AMJJ(0), MJJA(0) and JJAS(0) four-month averages of Niño-3.4 index. This high values of correlations can be found considering the last 30 years (namely from 1979 to 2008 to be consistent with our analysis) in contrast to what can be found in the previous three decades (from 1950 to 1979) where we can observe maximum values of negative correlation in JJAS(1) and much smaller for JJAS(0) (respectively -0.62 and 0.15). The negative correlation that was found looking at the concurrent ENSO during 1950s, 1960s and 1970s, is lower during the 80s and 90s (Kucharski et al. [2007]) in agreement with our analysis.

The SST anomalies observed during an El Niño/La Niña event induce a modification in the Walker circulation along the western Pacific Ocean that with its descending branch leads to positive MSLP anomalies over the Tropical Northwest Pacific (TNWP ; Wang et al. [2003]). To explain the simulated process in the ESMs we will use the regressed maps of relevant fields onto the Niño-3.4 index for JJAS(0). The large-scale anomalous anticyclone (AAC) extending all over North India Ocean associated with the descending branch of the anomalous Walker circulation is clearly observed in the MSLP ERA-Interim reanalysis regression map against the JJAS(0) Niño-3.4 index (Fig. 3.31(a-m)) as well as in that one of ESM-TkCH simulation (Fig. 3.32(a-m)).

The positive anomalies observed over TNWP extends to the Indian Ocean starting from the JJAS(0), (developing phase of ENSO ; (Fig. 3.32(a-c))). The peak is reached during the boreal winter reaching values of about +2hPa over the south-

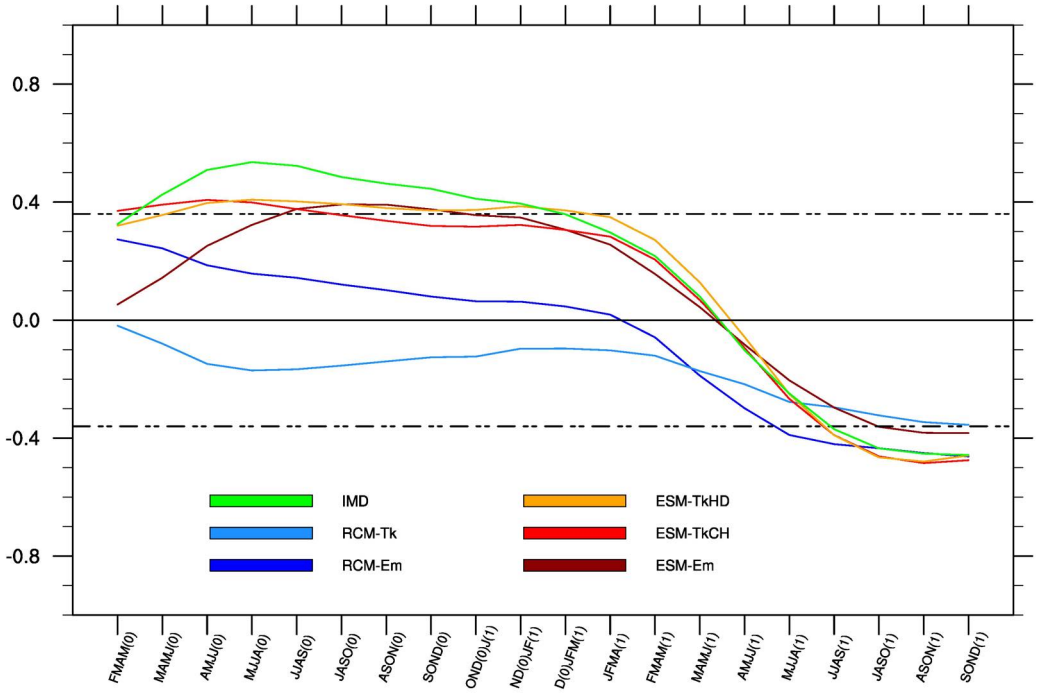

Figure 3.30. Plot of the lagged/leaded correlation between ISMR and 4-month averaged Niño-3.4 index for IMD, RMSs and ESMs. The horizontal dashed lines refer to a level of 95% of confidence. The numerical in parenthesis refer to the phases of ENSO, 0 for the developing and 1 for the decay, so that the concurrent correlation between Niño-3.4 index and ISMR is represented by the JJAS(1) season.

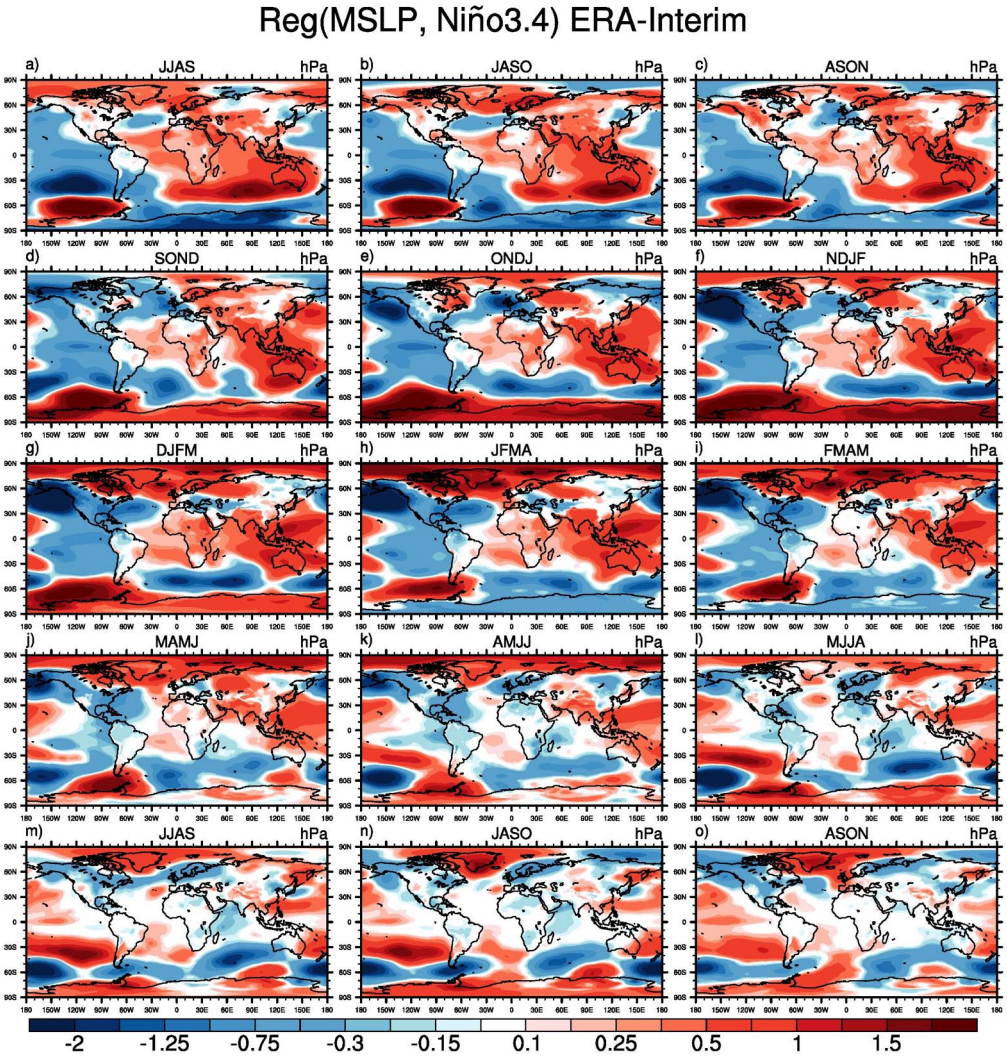

Figure 3.31. Regressed MSLP anomalies onto the Niño-3.4 index (calculated for JJAS(0)) for Era-Interim reanalysis

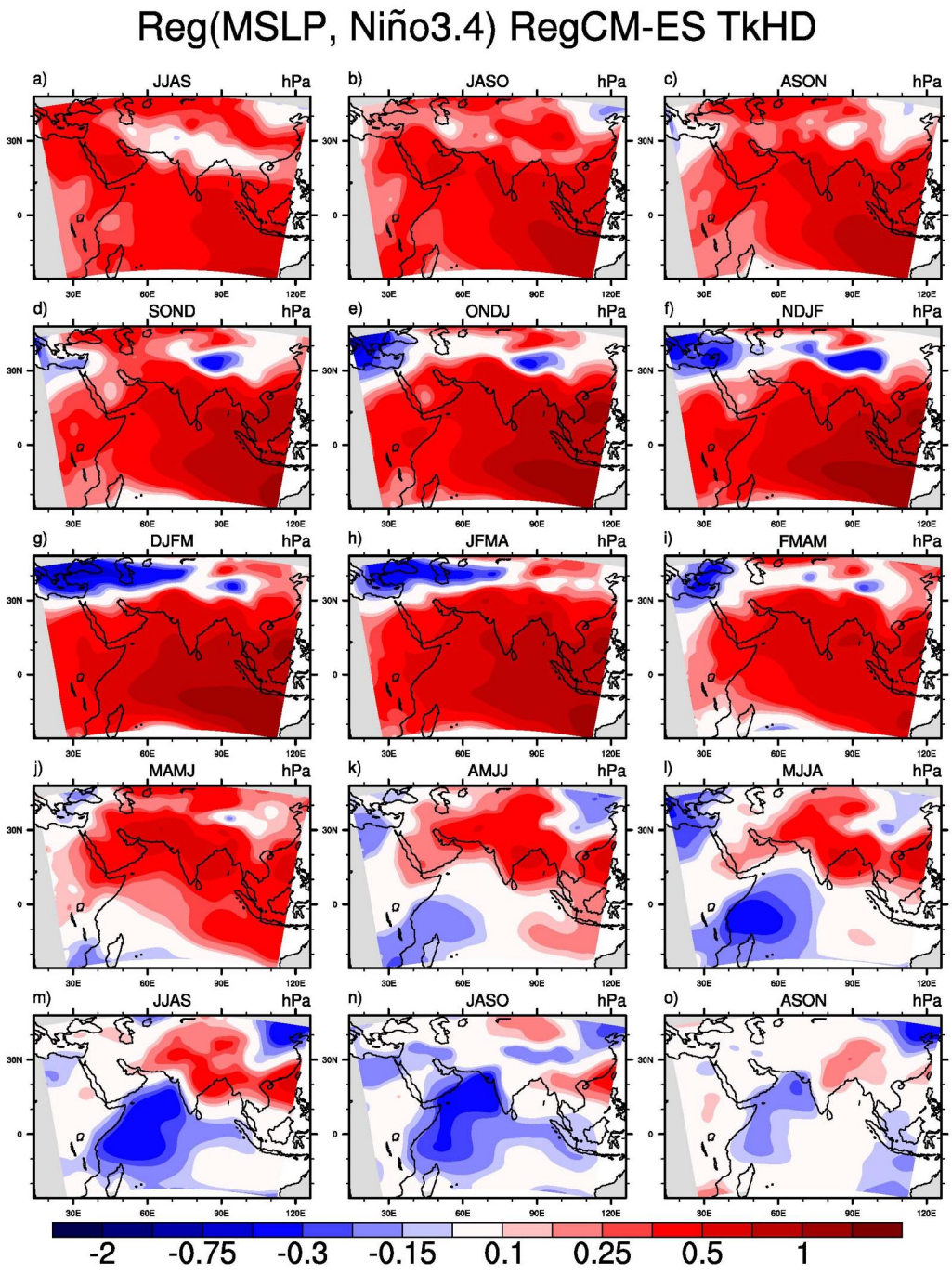

Figure 3.32. Regressed MSLP anomalies onto the Niño-3.4 index (calculated for JJAS(0)) for ESM-TkCH

east Indian Ocean (Fig. 3.32(d-g)) and start to decrease with the decaying phase of ENSO (Fig. 3.32Fig.(h-k)). The MSLP positive anomalies over the western part of Indian basin induce anomalies on the wind stress curl and generate an anomalous Ekman transport over equatorial and south-equatorial central IO (Fig. 3.33(c-k)). The anomalous Ekman transport leads to eastward propagating downwelling Rossby waves that propagates towards the west IO in about 4-5 months sustained by a positive feedback (Xie et al. [2002] ; Izumo et al. [2008]). The shallow termocline observed in the pre-monsoon season over the coastal area of west Arabian Sea is sensitive to upwelling changes and is warmed up by the Rossby waves (Fig. 3.34(j-m)). Positive SST anomalies are associated with positive precipitation anomalies that slow down the northward ITCZ migration with a delay in the onset of ISM (Fig. 3.35(k,l)). The LLJ over the Peninsula and North western Indian ocean shows a weakening in magnitude and a slight rotation to the north over India(Fig. 3.33Fig.(k-n)). The weakened LLJ undermines the establishment of a strong Somali current that leads to an increase of SST off the coastal areas of Arabian peninsula and Somalia (Fig. 3.34(k-n)). As final step, the warmed Arabian sea is now able to release more energy in form of latent heat through enhanced evaporation in the following months (Fig. 3.36(n-p)). The development of an anomalous low pressure regime in the Arabian Sea (Fig. 3.35(l,m)) induce anomalies in the LLJ wich increase moisture trasport into India (Fig. 3.33(k-n)). The model is able to reproduce the phenomenon with good fidelity and the regressed map of one-year lead-time precipitation against the Niño-3.4 index (Fig. 3.35 looks similar to the one regressed for IMD (Fig. 3.37(m)). From IMD observations, the one-year delayed response of ISMR to ENSO shows a dipole with dry anomalies over the Gangetic plain and a marked wet anomalies in particular over Peninsular and Himalaya regions (Fig. 3.37(m,p)). The dipolar distribution of precipitation over India is less obvious in the regression maps simulated by the model (Fig. 3.35(m,p)) that spreads the precipitation anomalies over the Gangetic plain still showing a marked increase over western part of India, expecially in the last months of ISM.

In this last section the mechanisms based on the major findings of the last ten years has been illustrated but a deep investigation is needed. More work is necessary to undestand the phenomena and to find the correct answer to the following questions:

- Why the late response to ENSO is so increased in the last forty years?
- How the IOD and ENSO modes are concurrently implicate in this response?
- Why ENSO in its developing phase show the large delayed impact on ISMR?

We believe that this arduous task can be accomplished through the use of the earth system models togheter with the extension of the domain over the NWP (to consider the coupled air-sea interaction involved in mantain alive the AAC) and with the increase of the spatial and vertical resolutions in both atmospheric and ocean components.

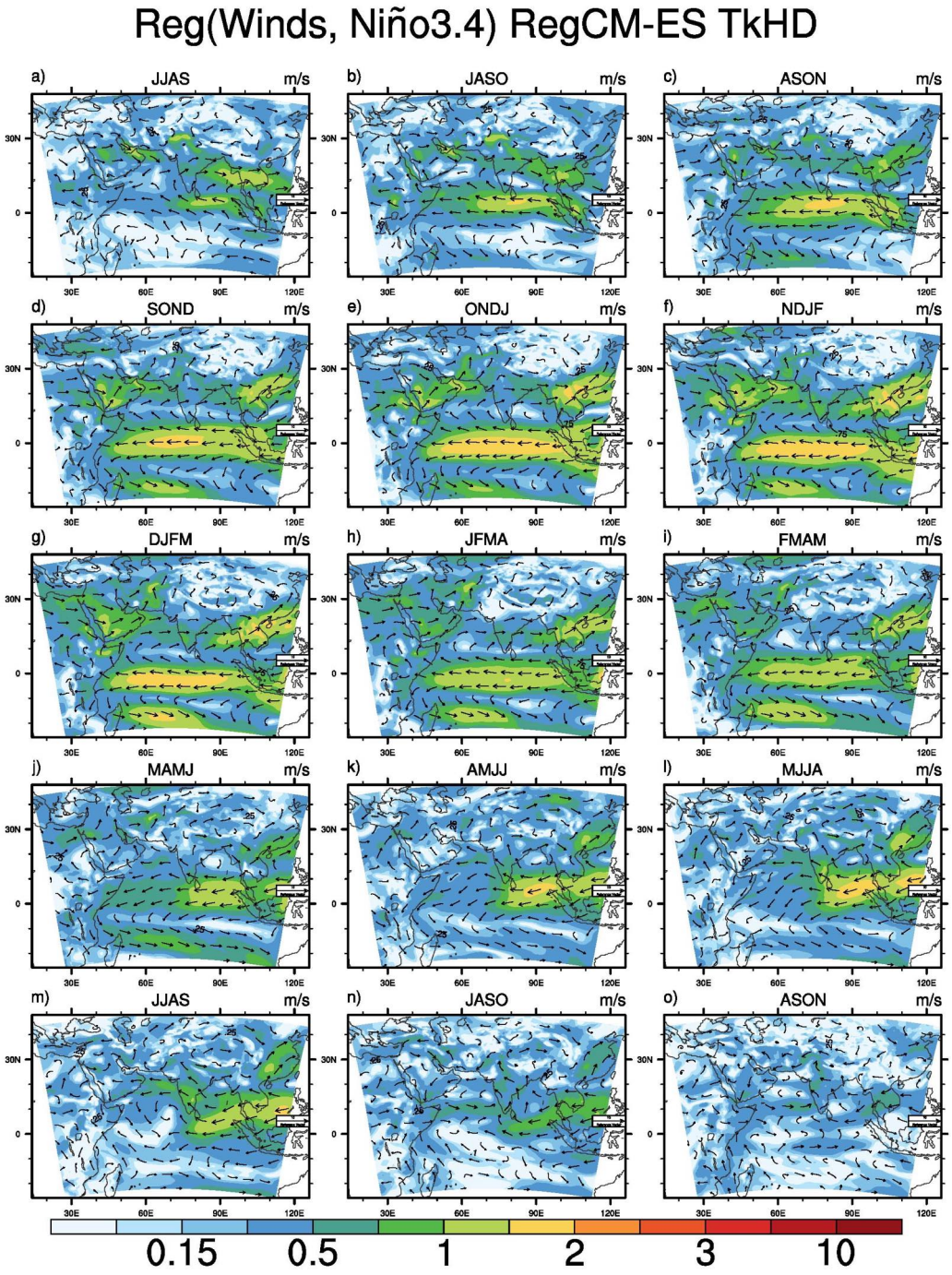

Figure 3.33. Regressed WIND anomalies onto the Niño-3.4 index (calculated for JJAS(0)) for ESM-TkCH

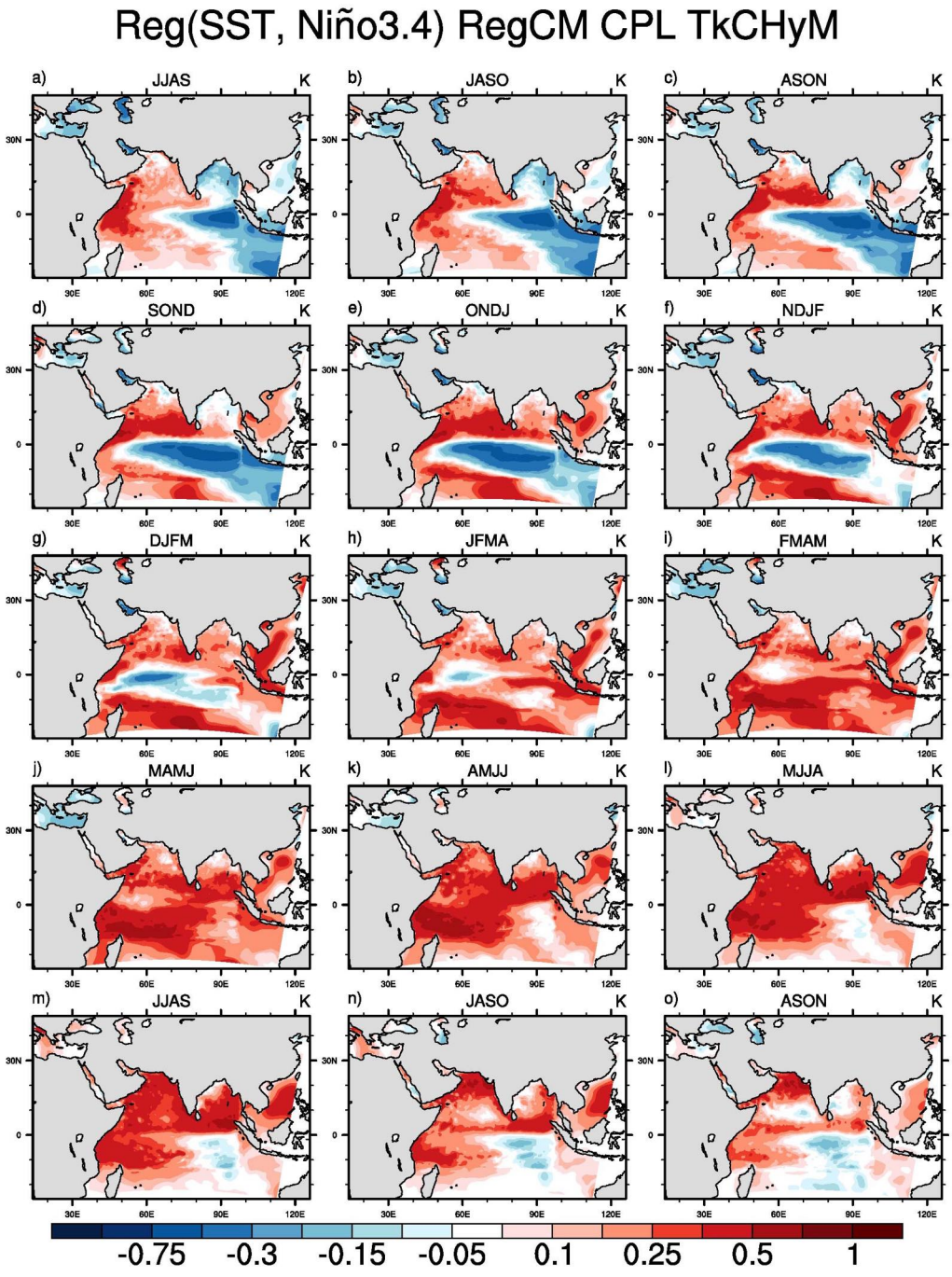

Figure 3.34. Regressed SST anomalies onto the Niño-3.4 index (calculated for JJAS(0)) for ESM-TkCH

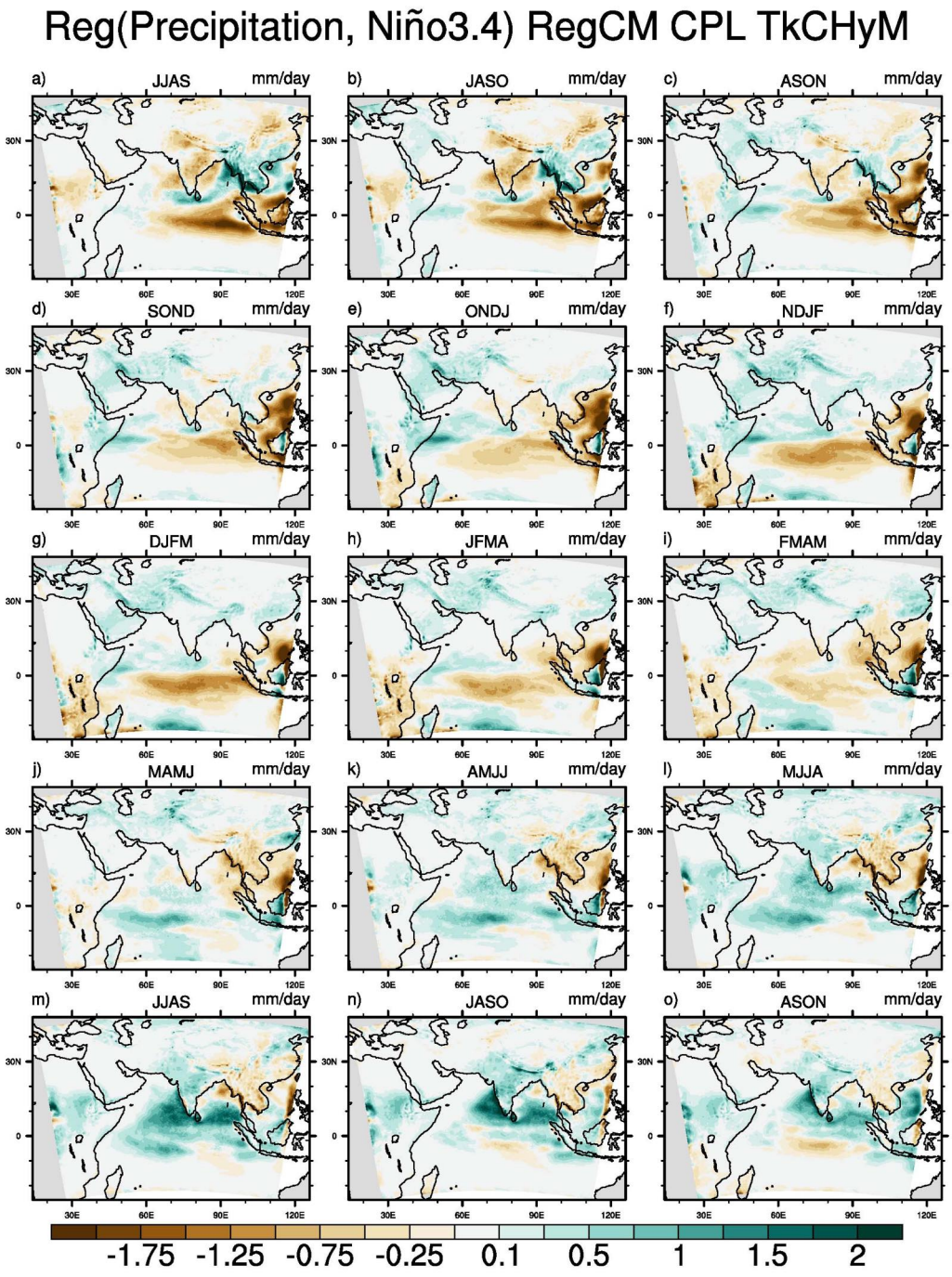

Figure 3.35. Regressed precipitation anomalies onto the Niño-3.4 index (calculated for JJAS(0)) for ESM-TkCH

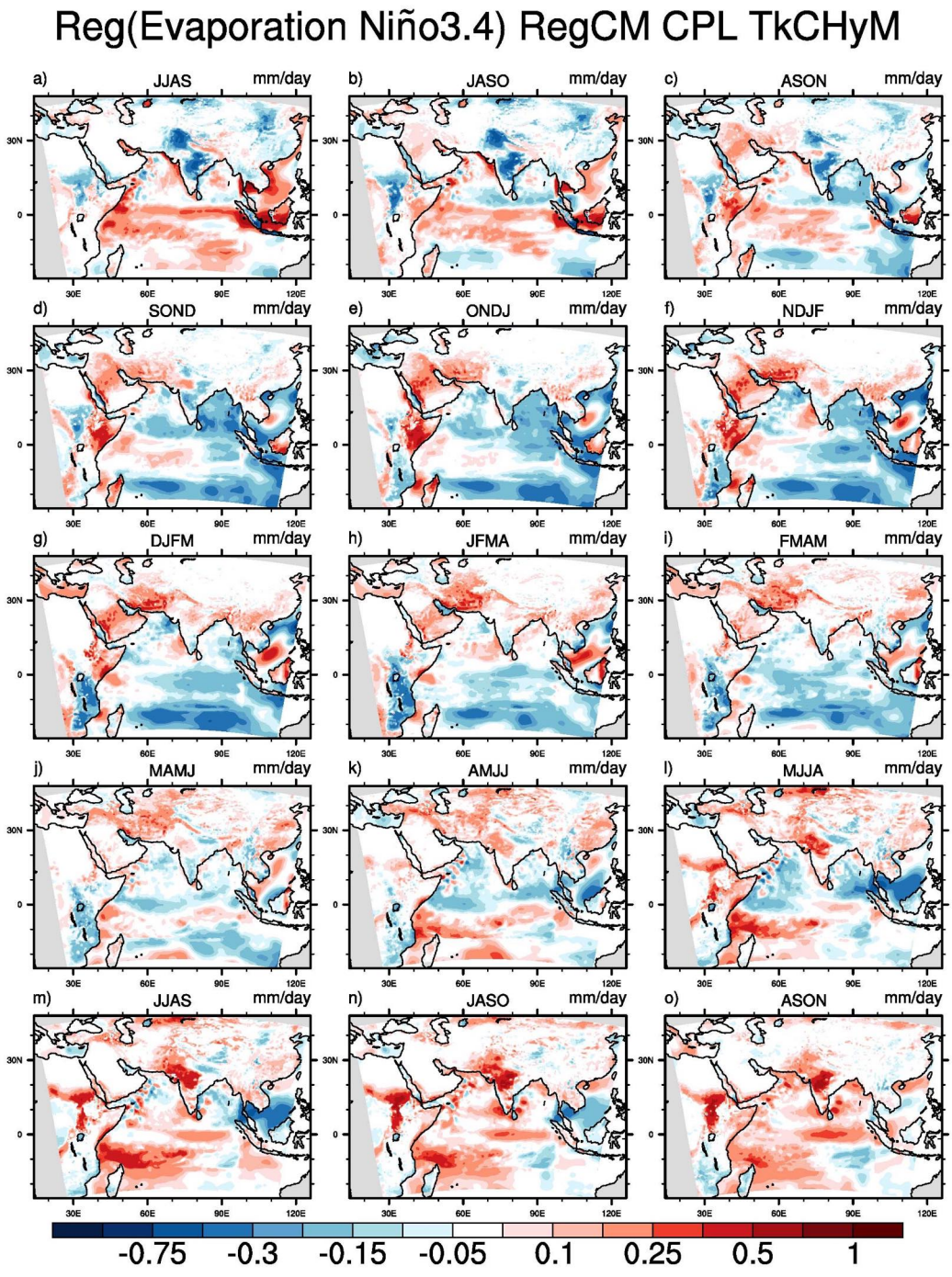

Figure 3.36. Regressed evaporation anomalies onto the Niño-3.4 index (calculated for JJAS(0)) for ESM-TkCH

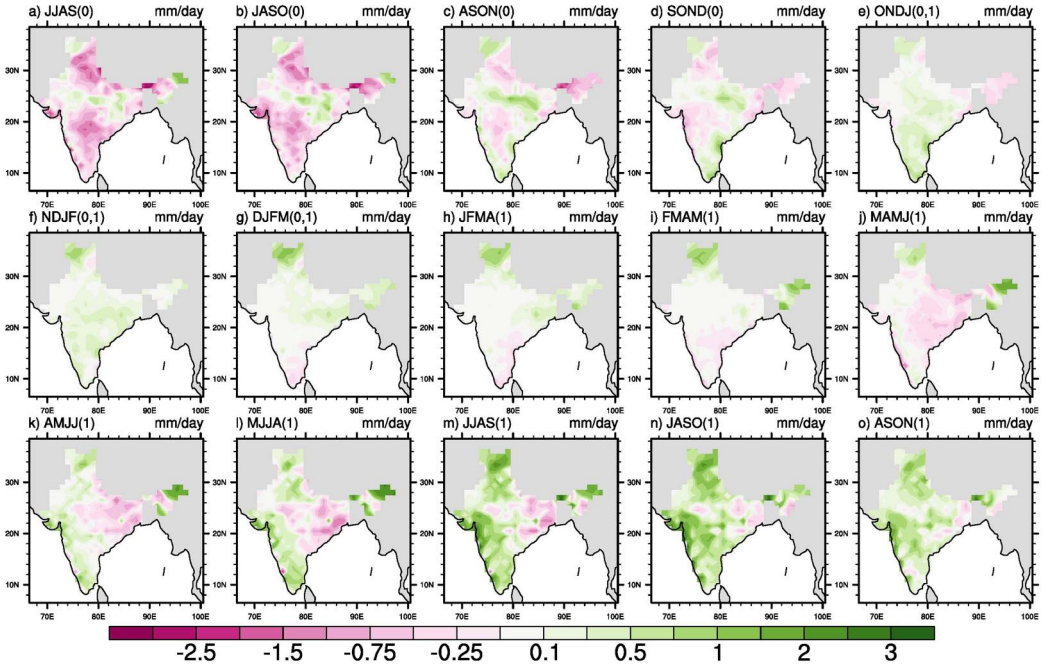

Figure 3.37. Regressed precipitation anomalies onto the Niño-3.4 index (calculated for JJAS(0)) for IMD

Chapter 4

Summary and conclusions

In this thesis the fully coupled regional Earth System Model RegCM-ES (Sitz et al. [2017]) has been applied over the new South Asia domain. Main development work has been done in the oceanic and hydrological components to allow the portability of the system. Furthermore, a new hydrological model has been introduced in the fully coupled system. This modification, needed to better simulate the hydrological cycle, resulted in major modifications in the driver and a total restyling of the new hydrological model (CHyM).

The new RegCM-ES is able to reproduce the main characteristics of the complex climate system over South Asia in all the three components analized.

The SST warm pools over the EIO and BoB are realistically reproduced by RegCM-ES with some differencies among the experiments. The experiments that make use of the Tiedtke cumulous convection scheme and ORAP ocean reanalysis as boundary conditions in the ocean (ESM-TkHD and ESM-TkCH) have better skills on the representation of the warm pools, however showing a negative bias over the central and south part of BoB, probably due to an improper representation of the shallow mixed layer observed in this region.

The IO has a dipole distribution of SSS with its highest values over AS and lowest over BoB. The freshest water observed in the BoB allows the formation of a shallow mixed layer depth on the surface that sustains the warm pool during ISM in BoB. All the model simulations show saltier conditions for the JJAS season with biases that are reduced in the ESM-Em experiment. The KPP scheme (Goswami et al. [2016]) and the too strong wind stirring may result in a deeper mixing ocean over BoB that could mask the added value of the new hydrological model CHyM.

The interannual varibility of SST is directly linked with the ISMR. Over the three main areas of the IO (AS, BoB and EIO) the SST is well simulated for the summer monsoon season as well as the DMI (a modified IOD index since the domain is not extending far enough towards east to calculate the one proposed by Saji in 1999) that shows good CCs for all the ESMs. Further investigations are needed in the ocean to assess the role of the two different settings in the atmosphere (namely between the two different convective schemes) and of the two different forcing utilized to drive the ocean model on the lateral open boundaries (ORAP and MOM).

The annual mean ISMR result from different scales of variability that show

its effects at seasonal and interannual time scales. The simulated climatology of precipitations over India has been compared using IMD and TRMM observations and with a major focus towards the ISMR over the Indian Homogeneous Rainfall Zones (IHRZ).

The two cumulous convection schemes (Emanuel and Tiedtke) show two different responses in the spatial distribution of the ISMR. The Emanuel scheme tends to underestimate the rainfall over the NE whereas the Tiedke one underestimate the precipitation over WC and NW. The air-sea coupling shows improvements in simulating pattern of precipitation over south BoB reducing the biases observed in the RCMs. The shape of the simulated LLJ is catched by all the experiments and their main differences are dictated by the two cumulous convection schemes. An overestimation of the jet by the ESM-Em and RCM-Em can be observed over the AS inducing the precipitation biases observed over PS. All the experiments show an overestimation of the jet over BoB, reduced in the coupled ESM-Em compared to the relative stand alone RCM-Em.

The two most important scales of variabilities of the ISMR are the intraseasonal and the interannual. The intraseasonal variability is dominated by the succession of alternating break and active phases of the monsoon. This is related to the two propagating modes that can be observed over the Indian region: the eastward and northward fluctuations that have respectively time scales of the order of 10-20 and 30-60 days. Contrary to RCMs, the ESMs esperiments are able to reproduce the two mods of propagation. To confirm the role of SST on driving the northward propagation, as can be observed, in the ESMs the SST anomalies lead the precipitation anomalies of about ten days whereas they are mainly overlapped in the RCMs. The patterns of active and break phases of the monsoon are better reproduced by the Emanuel scheme (ESM-Em and RCM-Em) with the rainfall concentrated over the WC during the active phases. Moreover, the migration of the "Low" over the foothills of Hymalayas during the breaks is reproduced by all the experiments.

The most interesting results are related with the interannual varibility of the ISMR. The interannual variability of ISMR is the result of the chaotic internal variability that are difficult to predict and of the external forcings (ENSO) that are instead more predictable. The external forcings in some circumstances lead the ISMR of one or two season or, as it has been investigated in the last part of the analysis chapter, one year.

The simulated JJAS standardized anomalies of ISMR appear not correlated with IMD in the RCMs whereas positive CCs can be observed in ESMs. This is a clear added value of the ESM when compared to the stand-alone counterparts. The added value can be observed also in the composite maps of the wet(dry) years based on IMD. The ESMs simulated spatial pattern of precipitation anomalies is better represented in both wet and dry years respect to the RCMs that fails to reproduce these features. All these results seen so far will be submitted in a paper, in preparation, to Climate Dynamics (Di Sante et al. [2017]). The new major findings of this thesis are related to the one-year lead-time predictability of ISMR to the delayed ENSO impact (Di Sante and et al. [2017]).

As seen in previous findings, the response of the ISMR to ENSO can be delayed of two seasons through the contribution of different air-sea coupled mechanisms as the

decrease of Western Arabian Sea Upwelling (Izumo et al. [2008]), the Indo-western Pacific ocean capacitor (Xie et al. [2009]) and the Indo-Tropical northwest Pacific ocean-atmosphere interaction (Du et al. [2009]). Our findings extend and confirm the possibility that this response may have a longer feedback time, a year or so. To perform this analysis we have make use of the Niño3.4 index and correlate its four-month running average with the ISMR. The results have been quite surprising, with the maximum CCs found with ENSO one-year lead-time on ISMR. We have tried to explain the involved mechanisms in this late response using the mechanisms previously proposed and the regression anomalies maps of the most interesting fields (observed and simulated by ESM-TkHD) built basing on the ElNiño3.4 index for the JJAS season with one-year lead-time. The mechanisms appear quite similar to those proposed in the previous studies but further investigations are needed to understand more in deep the phenomena involved. Because of the relevance of these findings, these last results will be submitted to the high impact rank journal Nature Geoscience (Di Sante and et al. [2017]).

4.0.1 New perspectives on predicting the Indian Summer Monsoon and on the use of RegCM-ES

The important results that came out during this work open the doors to the possibility of study the Indian Summer Monsoon through the powerful instrument that has been implemented to simulate the South Asia Climate. The development of the atmosphere-ocean-river coupled model and its implementation over the Indian region allow to better simulate the intraseasonal and interannual variability of the ISM compared to a standalone regional climate model. That capability is really relevant when the involved phenomena that modulate the intensity of the monsoon exhibit mechanisms that can be reproduced only when the mutual interaction between atmosphere and ocean is considered and makes this a necessary tool to study them. How showed in the last section of the analysis chapter, related to the delayed response of the ISMR to the ENSO forcing, the possibility of taking into account that phenomena could add a source of predictability of the ISM that would allow to plan measures act to mitigate the possible effects on the affected populations. The implementation of this instrument over regions where we have similar coupled mechanisms (as for example eastern tropical Africa and south-east Asia) will be of great interest, moreover if we consider the possible impact of the climate warming on that mechanisms, the coupled model is absolutely necessary to perform climate projections over that regions.

List of Acronyms

AAC Anomalous Anticyclone

AGCM Atmospheric General Circulation Models

AMIP Atmospheric Model Intercomparison Project

AOGCMs Atmosphere Ocean Land Cryosphere Climate Models

AORCM coupled Atmospheric Ocean Regional Climate Models

AR4 Fourth Assessment Report

AR5 Fifth Assessment Report

AS Arabian Sea

BATS Biosphere-Atmosphere Transfer Scheme

BL Barrier Layer

BoB Bay of Bengal

BSISO Boreal Summer Intraseasonal Oscillation

BWDB Bangladesh Water Development Board

CC Correlation Coefficient

CHyM Cetemps Hydrological Model

CLM Community Land Model

CMIP Coupled Model Intercomparison Project

CMIP3 Third Coupled Model Intercomparison Project

CMIP5 Fifth Coupled Model Intercomparison Project

CNE Central Northeast

CORDEX Coordinated Regional Climate Downscaling Experiment

CTCZ Continental Tropical Convergence Zone

DEM Digital Elevation Model

DMI Indian Ocean Dipole mode Index

ECMWF European Centre for Medium-Range Weather Forecasts

EEIO East Equatorial Indian Ocean

EIN15 ERA-Interim atmospheric reanalysis at 1.5 degree

EIN75 ERA-Interim atmospheric reanalysis at 0.75 degree

EIO Equatorial Indian Ocean

ENEA Climate Modelling and Impacts Laboratory

ENSO El Nino Southern Oscillation

EOF Empirical Orthogonal Functions

EQUIN Equatorial Indian Ocean Oscillation Index

EQUINOO Equatorial Indian Ocean Oscillation

ESM Earth System Model

ESM-Em Earth System Model experiment using Emanuel as convectvive scheme

ESM-TkCH Earth System Model experiment using Tiedtke as convectvive scheme and CHyM hydrological model

ESM-TkHD Earth System Model experiment using Tiedtke as convectvive scheme and HD hydrological model

ESMF Earth System Modeling Framework

ESP-ICTP Earth System Physics Section of the Abdus Salam International Centre for Theoretical Physics

GCM Global Climate Models

GFDL Geophysical Fluid Dynamics Laboratory

GNU General Public License

GPCP-1DD Global Precipitation Climatology Project One-Degree-Daily

GTS Global Telecommunications System

HadISST Hadley Centre Sea Surface Temperature

HD Hydrological Discharge

IAV Interannual Variability

ICOADS International Comprehensive Ocean-Atmosphere Data Set

IHRZ Indian Homogeneous Rainfall Zones

IMD Indian Meteorological Department

IOBM Indian Ocean Basin Mode

IO Indian Ocean

IOD Indian Ocean Dipole

IO-TNWP AAC Indian Ocean Tropical North Western Pacific Anomalous Anticyclone

IPCC Intergovernmental Panel On Climate Change

IPOC Indo-Western Pacific Ocean Capacitor

IR Infrared

ISM Indian Summer Monsoon

ISMR Indian Summer Monsoon Rainfall

ISO Intraseasonal Oscillation

ISV Intraseasonal Variability

ITCZ Intertropical Converge Zone

ITU Instanbul Technical University

JAXA Japan Aerospace Exploration Agency

JF January February (Winter Season)

JJAS June July August September (Indian Summer Monsoon Season)

KPP K-Profile Parameterization

LLJ Low Level Jet

LPS Low Pressure System

MAM March April May (Pre-monsoon season)

MCZ Maximum Cloud Zone

MDB Met Office Marine Data Bank

MISO Monsoon Intraseasonal Oscillations

MIT Massachussets Institute of Technology

MITgcm Massachussets Institute of Technology General Circulation Model

MJO Madden-Julian Oscillation

MM4 atmospheric Mesoscale Model version 4

MM5 atmospheric Mesoscale Model version 5

MMM Multy-Model Means

MOK Monsoon Onset Over Kerala

MOM Modular Ocean Model

MSLP Mean Sea Level Pressure

NCAR National Center for Atmospheric Research

NCEP National Center for Environmental Prediction

NE Northeast

NEMO Nucleos for European Modelling of the Ocean

NINO3 El Nino Southern Oscillation Index

NOAA National Oceanic and Atmospheric Administration

NUOPC National Unified Operational Prediction Capability

NWP Northwest Pacific Ocean

OASIS3 OASIS coupler version 3

OND October November December (Post-monsoon season)

ORAP Ocean ReAnalysis Pilot 5

PS Peninsular

RCM Regional Climate Model

RCM-Em Regional Climate Model using Emanuel as cumulus convection scheme

RCM-Tk Regional Climate Model using Tiedtke as cumulus convection scheme

RESM Regional Earth System Models

RMSD Root-Mean-Square Defference

ROMS Regional Ocean Modelling System

SCRIP Spherical Coordinate Remapping and Interpolation Package

SIMTOP TOPMODEL-based runoff parameterization

SODA Simple Ocean Data Assimilation (ocean reanalysis)

SOM Geophysical Fluid Dynamics Laboratory (GFDL) flexible modeling system mixed layer

SSH Sea Surface Height

SSS Sea Surface Salinity

SST Sea Surface Temperature

TCZ Tropical Convergence Zone

TIO Tropical Indian Ocean

TNWP Tropical Northwestern Pacific Ocean

TRMM Tropical Rainfall Measuring Mission

USGS United States Geological Survey

WAS West Arabian Sea

WASU Western Arabian Sea Upwelling

WC West Central

WCRP World Climate Research Programme

WEIO West Equatorial Indian Ocean

WIO Western Indian Ocean

WOA World Ocean Atlas

WOA13 v2 Version 2 of World Ocean Atlas 2013

WRF Weather Research and Forecasting

Bibliography

Abrams, M. (2000). The advanced spaceborne thermal emission and reflection radiometer (aster): data products for the high spatial resolution imager on nasa's terra platform. *international Journal of Remote sensing*, 21(5):847–859.

Adcroft, A., Campin, J., Dutkiewicz, S., Evangelinos, C., Ferreira, D., Forget, G., Fox-Kemper, B., Heimbach, P., Hill, C., Hill, E., et al. (2008). Mitgcm user manual.

Ajaya Mohan, R. and Goswami, B. (2003). Potential predictability of the asian summer monsoon on monthly and seasonal time scales. *Meteorology and Atmospheric Physics*, 84(1-2):83–100.

Ananthakrishnan, R., Pathan, J., and Aralikatti, S. (1983). The onset phase of the southwest monsoon. *Current Science*, 52:755–764.

Ananthakrishnan, R. and Soman, M. (1988). The onset of the southwest monsoon over kerala: 1901–1980. *Journal of Climatology*, 8(3):283–296.

Ananthakrishnan, R. and Thiruvengadathan, A. (1968). Thermal changes in troposphere associated with seasonal transitions over india. *Current Science*, 37(7):184–186.

Annamalai, H., Hamilton, K., and Sperber, K. R. (2007). The south asian summer monsoon and its relationship with enso in the ipcc ar4 simulations. *Journal of Climate*, 20(6):1071–1092.

Anthes, R. A., Hsie, E.-Y., Kuo, Y.-H., et al. (1987). *Description of the Penn State/NCAR mesoscale model version 4 (MM4)*. NCAR Boulder, CO.

Artale, V., Calmanti, S., Carillo, A., DellâĂŹAquila, A., Herrmann, M., Pisacane, G., Ruti, P. M., Sannino, G., Struglia, M. V., Giorgi, F., et al. (2010). An atmosphere–ocean regional climate model for the mediterranean area: assessment of a present climate simulation. *Climate Dynamics*, 35(5):721–740.

Ashok, K., Guan, Z., Saji, N., and Yamagata, T. (2004). Individual and combined influences of enso and the indian ocean dipole on the indian summer monsoon. *Journal of Climate*, 17(16):3141–3155.

Ashok, K. and Saji, N. (2007). On the impacts of enso and indian ocean dipole events on sub-regional indian summer monsoon rainfall. *Natural Hazards*, 42(2):273–285.

Beven, K. and Kirkby, M. J. (1979). A physically based, variable contributing area model of basin hydrology/un modèle à base physique de zone d'appel variable de l'hydrologie du bassin versant. *Hydrological Sciences Journal*, 24(1):43–69.

Bhat, G., Gadgil, S., Kumar, P. H., Kalsi, S., Madhusoodanan, P., Murty, V., Prasada Rao, C., Babu, V. R., Rao, L., Rao, R., et al. (2001). Bobmex: The bay of bengal monsoon experiment. *Bulletin of the American Meteorological Society*, 82(10):2217–2243.

Blandford, H. (1886). Rainfall of india, mem. *India Meteor. Dept*, 2:217–448.

Boyer, T. P., Garcia, H. E., Locarnini, R. A., Zweng, M. M., Mishonov, A. V., Reagan, J. R., Antonov, J. I., Baranova, O. K., Biddle, M. M., Johnson, D. R., et al. (2014). 2013 world ocean atlas aids high-resolution climate studies. *Eos, Transactions American Geophysical Union*, 95(41):369–370.

Bracco, A., Kucharski, F., Molteni, F., Hazeleger, W., and Severijns, C. (2005). Internal and forced modes of variability in the indian ocean. *Geophysical research letters*, 32(12).

Bracco, A., Kucharski, F., Molteni, F., Hazeleger, W., and Severijns, C. (2007). A recipe for simulating the interannual variability of the asian summer monsoon and its relation with enso. *Climate dynamics*, 28(5):441–460.

Chao, W. C. and Chen, B. (2001). The origin of monsoons. *Journal of the Atmospheric Sciences*, 58(22):3497–3507.

Chen, T.-C. and Chen, J.-M. (1993). The 10–20-day mode of the 1979 indian monsoon: Its relation with the time variation of monsoon rainfall. *Monthly Weather Review*, 121(9):2465–2482.

Cherchi, A., Gualdi, S., Behera, S., Luo, J. J., Masson, S., Yamagata, T., and Navarra, A. (2007). The influence of tropical indian ocean sst on the indian summer monsoon. *Journal of climate*, 20(13):3083–3105.

Cherchi, A. and Navarra, A. (2013). Influence of enso and of the indian ocean dipole on the indian summer monsoon variability. *Climate dynamics*, 41(1):81–103.

Clark, C. O., Cole, J. E., and Webster, P. J. (2000). Indian ocean sst and indian summer rainfall: Predictive relationships and their decadal variability. *Journal of Climate*, 13(14):2503–2519.

Collins, N., Theurich, G., Deluca, C., Suarez, M., Trayanov, A., Balaji, V., Li, P., Yang, W., Hill, C., and Da Silva, A. (2005). Design and implementation of components in the earth system modeling framework. *The International Journal of High Performance Computing Applications*, 19(3):341–350.

Coppola, E., Tomassetti, B., Mariotti, L., Verdecchia, M., and Visconti, G. (2007). Cellular automata algorithms for drainage network extraction and rainfall data assimilation. *Hydrological Sciences Journal*, 52:579–592.

Coppola, E., Verdecchia, M., Giorgi, F., Colaiuda, V., Tomassetti, B., and Lombardi, A. (2014). Changing hydrological conditions in the po basin under global warming. *Sci Total Environ*, 493:1183–96.

Danabasoglu, G., Yeager, S. G., Bailey, D., Behrens, E., Bentsen, M., Bi, D., Biastoch, A., Böning, C., Bozec, A., Canuto, V. M., et al. (2014). North atlantic simulations in coordinated ocean-ice reference experiments phase ii (core-ii). part i: mean states. *Ocean Modelling*, 73:76–107.

Dash, S., Kulkarni, M. A., Mohanty, U., and Prasad, K. (2009). Changes in the characteristics of rain events in india. *Journal of Geophysical Research: Atmospheres*, 114(D10).

Dash, S., Mamgain, A., Pattnayak, K., and Giorgi, F. (2013). Spatial and temporal variations in indian summer monsoon rainfall and temperature: an analysis based on regcm3 simulations. *Pure and Applied Geophysics*, 170(4):655–674.

Dash, S., Shekhar, M., and Singh, G. (2006). Simulation of indian summer monsoon circulation and rainfall using regcm3. *Theoretical and applied climatology*, 86(1-4):161–172.

De, U., Lele, R., and Natu, J. (1998). Breaks in southwest monsoon. *India Meteorological Department, Pre Published Sci Rep*, (1998/3):1–24.

Di Sante, F., Coppola, E., Farneti, R., and Giorgi, F. (2017). Assessing the role of local air- sea interaction over the south asia region in simulating the indian summer monsoon using the new earth system model regcm-es. *Climate Dynamics (In preparation)*.

Di Sante, F. and et al. (2017). One-year lead-time predictability of indian summer monsoon due to delayed enso impact. *Nature Geoscience (In preparation)*.

Dickinson, R. E., Kennedy, P., and Henderson-Sellers, A. (1993). *Biosphere-atmosphere transfer scheme (BATS) version 1e as coupled to the NCAR community climate model*. National Center for Atmospheric Research, Climate and Global Dynamics Division.

Du, Y., Xie, S.-P., Huang, G., and Hu, K. (2009). Role of air–sea interaction in the long persistence of el niño–induced north indian ocean warming. *Journal of Climate*, 22(8):2023–2038.

Fischer, A. S., Weller, R. A., Rudnick, D. L., Eriksen, C. C., Lee, C. M., Brink, K. H., Fox, C. A., and Leben, R. R. (2002). Mesoscale eddies, coastal upwelling, and the upper-ocean heat budget in the arabian sea. *Deep Sea Research Part II: Topical Studies in Oceanography*, 49(12):2231–2264.

Fu, X., Wang, B., and Li, T. (2002). Impacts of air–sea coupling on the simulation of mean asian summer monsoon in the echam4 model. *Monthly weather review*, 130(12):2889–2904.

Fu, X., Wang, B., Waliser, D. E., and Tao, L. (2007). Impact of atmosphere–ocean coupling on the predictability of monsoon intraseasonal oscillations. *Journal of the atmospheric sciences*, 64(1):157–174.

Gadgil, S. (2003). The indian monsoon and its variability. *Annual Review of Earth and Planetary Sciences*, 31(1):429–467.

Gadgil, S. and Joseph, P. (2003). On breaks of the indian monsoon. *Journal of Earth System Science*, 112(4):529–558.

Gadgil, S., Joshi, N., and Joseph, P. (1984). Ocean-atmosphere coupling over monsoon regions. *Nature*, 312(5990):141–143.

Gadgil, S. and Sajani, S. (1998). Monsoon precipitation in the amip runs. *Climate Dynamics*, 14(9):659–689.

Gadgil, S. and Srinivasan, J. (1990). Low frequency variation of tropical convergence zones. *Meteorology and Atmospheric Physics*, 44(1):119–132.

Gadgil, S., Vinayachandran, P., and Francis, P. (2003). Droughts of the indian summer monsoon: role of clouds over the indian ocean. *Current Science*, 85(12):1713–1719.

Gadgil, S., Vinayachandran, P., Francis, P., and Gadgil, S. (2004). Extremes of the indian summer monsoon rainfall, enso and equatorial indian ocean oscillation. *Geophysical Research Letters*, 31(12).

Gates, W. L. (1992). Amip: The atmospheric model intercomparison project. *Bulletin of the American Meteorological Society*, 73(12):1962–1970.

Gibson, J., Kalberg, P., Uppala, S., Nomura, A., Hernandez, A., and Serrano, E. (1997). Era description. ecmwf re-analysis project. *Report Series*, 1.

Giorgi, F. (1995). Perspectives for regional earth system modeling. *Global and Planetary Change*, 10(1-4):23–42.

Giorgi, F. (2006). Climate change hot-spots. *Geophysical research letters*, 33(8).

Giorgi, F. and Anyah, R. (2012). The road towards regcm4. *Climate Research*, 52:3–6.

Giorgi, F., Bi, X., and Pal, J. (2004). Mean, interannual variability and trends in a regional climate change experiment over europe. ii: climate change scenarios (2071–2100). *Climate Dynamics*, 23(7-8):839–858.

Giorgi, F., Coppola, E., Solmon, F., Mariotti, L., Sylla, M., Bi, X., Elguindi, N., Diro, G., Nair, V., Giuliani, G., et al. (2012). Regcm4: model description and preliminary tests over multiple cordex domains. *Climate Research*, 52:7–29.

Giorgi, F., Jones, C., Asrar, G. R., et al. (2009). Addressing climate information needs at the regional level: the cordex framework. *World Meteorological Organization (WMO) Bulletin*, 58(3):175.

Giorgi, F. and Lionello, P. (2008). Climate change projections for the mediterranean region. *Global and planetary change*, 63(2):90–104.

Giorgi, F., Marinucci, M. R., and Bates, G. T. (1993a). Development of a second-generation regional climate model (regcm2). part i: Boundary-layer and radiative transfer processes. *Monthly Weather Review*, 121(10):2794–2813.

Giorgi, F., Marinucci, M. R., Bates, G. T., and De Canio, G. (1993b). Development of a second-generation regional climate model (regcm2). part ii: Convective processes and assimilation of lateral boundary conditions. *Monthly Weather Review*, 121(10):2814–2832.

Goswami, B. (1994). Dynamical predictability of seasonal monsoon rainfall: Problems and prospects. *PROCEEDINGS-INDIAN NATIONAL SCIENCE ACADEMY PART A*, 60:101–101.

Goswami, B., Ajayamohan, R., Xavier, P. K., and Sengupta, D. (2003). Clustering of synoptic activity by indian summer monsoon intraseasonal oscillations. *Geophysical Research Letters*, 30(8).

Goswami, B., Rao, S. A., Sengupta, D., and Chakravorty, S. (2016). Monsoons to mixing in the bay of bengal. *Oceanography*, 29(2):18.

Goswami, P. and Mohapatra, G. (2014). A comparative evaluation of impact of domain size and parameterization scheme on simulation of tropical cyclones in the bay of bengal. *Journal of Geophysical Research: Atmospheres*, 119(1):10–22.

Graham, N. and Barnett, T. (1987). Sea surface temperature, surface wind divergence, and convection over tropical oceans. *Science*, 238(4827):657–660.

Grell, G. A., Dudhia, J., Stauffer, D. R., et al. (1994). A description of the fifth-generation penn state/ncar mesoscale model (mm5).

Hagemann, S. and Dümenil, L. (1997). A parametrization of the lateral waterflow for the global scale. *Climate Dynamics*, 14(1):17–31.

Hagemann, S. and Gates, L. D. (2001). Validation of the hydrological cycle of ecmwf and ncep reanalyses using the mpi hydrological discharge model. *Journal of Geophysical Research: Atmospheres*, 106(D2):1503–1510.

Haidvogel, D. B., Arango, H., Budgell, W. P., Cornuelle, B. D., Curchitser, E., Di Lorenzo, E., Fennel, K., Geyer, W. R., Hermann, A. J., Lanerolle, L., et al. (2008). Ocean forecasting in terrain-following coordinates: Formulation and skill assessment of the regional ocean modeling system. *Journal of Computational Physics*, 227(7):3595–3624.

Hill, C., DeLuca, C., Balaji, Suarez, M., and Silva, A. d. (2004a). The architecture of the earth system modeling framework. *Computing in Science & Engineering*, 6(1):18–28.

Hill, C., DeLuca, C., Balaji, V., Suarez, M., da Silva, A., Sawyer, W., Cruz, C., Trayanov, A., Zaslavsky, L., Hallberg, R., et al. (2004b). Implementing applications with the earth system modeling framework. In *International Workshop on Applied Parallel Computing*, pages 563–572. Springer.

Huffman, G. J., Adler, R. F., Morrissey, M. M., Bolvin, D. T., Curtis, S., Joyce, R., McGavock, B., and Susskind, J. (2001). Global precipitation at one-degree daily resolution from multisatellite observations. *Journal of Hydrometeorology*, 2(1):36–50.

Huffman, G. J., Bolvin, D. T., Nelkin, E. J., Wolff, D. B., Adler, R. F., Gu, G., Hong, Y., Bowman, K. P., and Stocker, E. F. (2007). The trmm multisatellite precipitation analysis (tmpa): Quasi-global, multiyear, combined-sensor precipitation estimates at fine scales. *Journal of Hydrometeorology*, 8(1):38–55.

Ihara, C., Kushnir, Y., Cane, M. A., and De La Peña, V. H. (2007). Indian summer monsoon rainfall and its link with enso and indian ocean climate indices. *International Journal of Climatology*, 27(2):179–187.

Izumo, T., Montégut, C. B., Luo, J.-J., Behera, S. K., Masson, S., and Yamagata, T. (2008). The role of the western arabian sea upwelling in indian monsoon rainfall variability. *Journal of Climate*, 21(21):5603–5623.

Jones, P. W. (1999). First-and second-order conservative remapping schemes for grids in spherical coordinates. *Monthly Weather Review*, 127(9):2204–2210.

Joseph, P. and Sabin, T. (2008). An ocean–atmosphere interaction mechanism for the active break cycle of the asian summer monsoon. *Climate dynamics*, 30(6):553–566.

Joseph, P. V., Eischeid, J. K., and Pyle, R. J. (1994). Interannual variability of the onset of the indian summer monsoon and its association with atmospheric features, el nino, and sea surface temperature anomalies. *Journal of Climate*, 7(1):81–105.

Ju, J. and Slingo, J. (1995). The asian summer monsoon and enso. *Quarterly Journal of the Royal Meteorological Society*, 121(525):1133–1168.

Kalnay, E., Kanamitsu, M., Kistler, R., Collins, W., Deaven, D., Gandin, L., Iredell, M., Saha, S., White, G., Woollen, J., et al. (1996). The ncep/ncar 40-year reanalysis project. *Bulletin of the American meteorological Society*, 77(3):437–471.

Kang, I.-S., Lee, J.-Y., and Park, C.-K. (2004). Potential predictability of summer mean precipitation in a dynamical seasonal prediction system with systematic error correction. *Journal of climate*, 17(4):834–844.

Kemball-Cook, S. and Wang, B. (2001). Equatorial waves and air–sea interaction in the boreal summer intraseasonal oscillation. *Journal of Climate*, 14(13):2923–2942.

Klein, S. A., Soden, B. J., and Lau, N.-C. (1999). Remote sea surface temperature variations during enso: Evidence for a tropical atmospheric bridge. *Journal of Climate*, 12(4):917–932.

Kosaka, Y., Xie, S.-P., Lau, N.-C., and Vecchi, G. A. (2013). Origin of seasonal predictability for summer climate over the northwestern pacific. *Proceedings of the National Academy of Sciences*, 110(19):7574–7579.

Krishnamurthy, V. and Ajayamohan, R. (2010). Composite structure of monsoon low pressure systems and its relation to indian rainfall. *Journal of Climate*, 23(16):4285–4305.

Krishnamurthy, V. and Shukla, J. (2000). Intraseasonal and interannual variability of rainfall over india. *Journal of Climate*, 13(24):4366–4377.

Krishnamurthy, V. and Shukla, J. (2007). Intraseasonal and seasonally persisting patterns of indian monsoon rainfall. *Journal of climate*, 20(1):3–20.

Krishnamurti, T. and Ardanuy, P. (1980). The 10 to 20-day westward propagating mode and âĂIJbreaks in the monsoonsâĂİ. *Tellus*, 32(1):15–26.

Krishnamurti, T. N. and Bhalme, H. (1976). Oscillations of a monsoon system. part i. observational aspects. *Journal of the Atmospheric Sciences*, 33(10):1937–1954.

Krishnamurti, T. N., Oosterhof, D., and Mehta, A. (1988). Air–sea interaction on the time scale of 30 to 50 days. *Journal of the atmospheric sciences*, 45(8):1304–1322.

Kucharski, F., Bracco, A., Barimalala, R., and Yoo, J. H. (2011). Contribution of the east–west thermal heating contrast to the south asian monsoon and consequences for its variability. *Climate dynamics*, 37(3-4):721–735.

Kucharski, F., Bracco, A., Yoo, J., and Molteni, F. (2007). Low-frequency variability of the indian monsoon–enso relationship and the tropical atlantic: the âĂIJweakeningâĂİ of the 1980s and 1990s. *Journal of Climate*, 20(16):4255–4266.

Kucharski, F., Molteni, F., and Yoo, J. (2006). Sst forcing of decadal indian monsoon rainfall variability. *Geophysical research letters*, 33(3).

Kumar, K. K., Rajagopalan, B., and Cane, M. A. (1999). On the weakening relationship between the indian monsoon and enso. *Science*, 284(5423):2156–2159.

Landman, W. A., Seth, A., and Camargo, S. J. (2005). The effect of regional climate model domain choice on the simulation of tropical cyclone–like vortices in the southwestern indian ocean. *Journal of Climate*, 18(8):1263–1274.

Large, W. G., McWilliams, J. C., and Doney, S. C. (1994). Oceanic vertical mixing: A review and a model with a nonlocal boundary layer parameterization. *Reviews of Geophysics*, 32(4):363–403.

Lawrence, D. M. and Webster, P. J. (2002). The boreal summer intraseasonal oscillation: Relationship between northward and eastward movement of convection. *Journal of the Atmospheric Sciences*, 59(9):1593–1606.

Li, C. and Yanai, M. (1996). The onset and interannual variability of the asian summer monsoon in relation to land–sea thermal contrast. *Journal of Climate*, 9(2):358–375.

Lighthill, M. and Whitham, G. (1955). On kinematic waves. i. flood movement in long rivers. In *Proceedings of the Royal Society of London A: Mathematical, Physical and Engineering Sciences*, volume 229, pages 281–316. The Royal Society.

Madec, G. et al. (2015). Nemo ocean engine.

Magana, V. and Webster, P. (1996). Atmospheric circulations during active and break periods of the asian monsoon. In *Preprints of the Eighth Conference on the Global Ocean-Atmosphere-Land System (GOALS), Amer. Meteorol. Soc., Atlanta, GA*.

Manning, R., Griffith, J. P., Pigot, T., and Vernon-Harcourt, L. F. (1890). *On the flow of water in open channels and pipes*.

Marshall, J., Adcroft, A., Hill, C., Perelman, L., and Heisey, C. (1997). A finite-volume, incompressible navier stokes model for studies of the ocean on parallel computers. *Journal of Geophysical Research: Oceans*, 102(C3):5753–5766.

Meehl, G. A., Covey, C., McAvaney, B., Latif, M., and Stouffer, R. J. (2005). Overview of the coupled model intercomparison project. *Bulletin of the American Meteorological Society*, 86(1):89–93.

Mishra, V., Smoliak, B. V., Lettenmaier, D. P., and Wallace, J. M. (2012). A prominent pattern of year-to-year variability in indian summer monsoon rainfall. *Proceedings of the National Academy of Sciences*, 109(19):7213–7217.

Montégut, C. B., Vialard, J., Shenoi, S. S., Shankar, D., Durand, F., Ethé, C., and Madec, G. (2007). Simulated seasonal and interannual variability of the mixed layer heat budget in the northern indian ocean. *Journal of Climate*, 20(13):3249–3268.

Mujumdar, M., Salunke, K., Rao, S. A., Ravichandran, M., and Goswami, B. (2011). Diurnal cycle induced amplification of sea surface temperature intraseasonal oscillations over the bay of bengal in summer monsoon season. *IEEE Geoscience and Remote Sensing Letters*, 8(2):206–210.

Murtugudde, R., McCreary, J. P., and Busalacchi, A. J. (2000). Oceanic processes associated with anomalous events in the indian ocean with relevance to 1997–1998. *Journal of Geophysical Research: Oceans*, 105(C2):3295–3306.

Nigam, S. and Shen, H.-S. (1993). Structure of oceanic and atmospheric low-frequency variability over the tropical pacific and indian oceans. part i: Coads observations. *Journal of climate*, 6(4):657–676.

Niu, G.-Y., Yang, Z.-L., Dickinson, R. E., and Gulden, L. E. (2005). A simple topmodel-based runoff parameterization (simtop) for use in global climate models. *Journal of Geophysical Research: Atmospheres*, 110(D21).

Nogherotto, R., Tompkins, A. M., Giuliani, G., Coppola, E., and Giorgi, F. (2016). Numerical framework and performance of the new multiple-phase cloud microphysics scheme in regcm4. 5: precipitation, cloud microphysics, and cloud radiative effects. *Geoscientific Model Development*, 9(7):2533–2547.

Oleson, K. W., Lawrence, D. M., Gordon, B., Flanner, M. G., Kluzek, E., Peter, J., Levis, S., Swenson, S. C., Thornton, E., Feddema, J., et al. (2010). Technical description of version 4.0 of the community land model (clm).

Pai, D., Bhate, J., Sreejith, O., and Hatwar, H. (2011). Impact of mjo on the intraseasonal variation of summer monsoon rainfall over india. *Climate Dynamics*, 36(1-2):41–55.

Pal, J., Giorgi, F., Bi, X., Elguindi, N., Solmon, F., Gao, X., Rauscher, S., Francisco, R., Zakey, A., Winter, J., et al. (2007a). The ictp regcm3 and regcnet: regional climate modeling for the developing world. bams 88: 1395–1409. doi: 10.1175. Technical report, BAMS-88-9-1395.

Pal, J. S., Giorgi, F., Bi, X., Elguindi, N., Solmon, F., Rauscher, S. A., Gao, X., Francisco, R., Zakey, A., Winter, J., et al. (2007b). Regional climate modeling for the developing world: the ictp regcm3 and regcnet. *Bulletin of the American Meteorological Society*, 88(9):1395–1409.

Pattnayak, K., Panda, S., Saraswat, V., and Dash, S. (2016). Relationship between tropospheric temperature and indian summer monsoon rainfall as simulated by regcm3. *Climate dynamics*, 46(9-10):3149–3162.

Raghavan, K. (1973). Break-monsoon over india. *Monthly Weather Review*, 101:33–43.

Rahman, S., Sengupta, D., and Ravichandran, M. (2009). Variability of indian summer monsoon rainfall in daily data from gauge and satellite. *Journal of Geophysical Research: Atmospheres*, 114(D17).

Rajeevan, M., Bhate, J., Kale, J., and Lal, B. (2006). High resolution daily gridded rainfall data for the indian region: Analysis of break and active. *Current Science*, 91(3).

Rajeevan, M., Gadgil, S., and Bhate, J. (2010). Active and break spells of the indian summer monsoon. *Journal of earth system science*, 119(3):229–247.

Ramamurthy, K. (1969). Monsoon of india: some aspects of the âĂŸbreakâĂŹin the indian southwest monsoon during july and august. *Forecasting manual*, 1(57):1–57.

Rao, Y. (1976). *Southwest monsoon*, volume 1. India Meteorological Department.

Rasmusson, E. M. and Carpenter, T. H. (1983). The relationship between eastern equatorial pacific sea surface temperatures and rainfall over india and sri lanka. *Monthly Weather Review*, 111(3):517–528.

Ratnam, J. V., Giorgi, F., Kaginalkar, A., and Cozzini, S. (2009). Simulation of the indian monsoon using the regcm3–roms regional coupled model. *Climate Dynamics*, 33(1):119–139.

Ratnam, J. V. and Kumar, K. K. (2005). Sensitivity of the simulated monsoons of 1987 and 1988 to convective parameterization schemes in mm5. *Journal of climate*, 18(14):2724–2743.

Rayner, N., Parker, D. E., Horton, E., Folland, C., Alexander, L., Rowell, D., Kent, E., and Kaplan, A. (2003). Global analyses of sea surface temperature, sea ice, and night marine air temperature since the late nineteenth century. *Journal of Geophysical Research: Atmospheres*, 108(D14).

Roxy, M. K., Ritika, K., Terray, P., Murtugudde, R., Ashok, K., and Goswami, B. (2015). Drying of indian subcontinent by rapid indian ocean warming and a weakening land-sea thermal gradient. *Nature communications*, 6.

Sabeerali, C., Ramu Dandi, A., Dhakate, A., Salunke, K., Mahapatra, S., and Rao, S. A. (2013). Simulation of boreal summer intraseasonal oscillations in the latest cmip5 coupled gcms. *Journal of Geophysical Research: Atmospheres*, 118(10):4401–4420.

Saha, S. K., Pokhrel, S., Salunke, K., Dhakate, A., Chaudhari, H. S., Rahaman, H., Sujith, K., Hazra, A., and Sikka, D. (2016). Potential predictability of indian summer monsoon rainfall in ncep cfsv2. *Journal of Advances in Modeling Earth Systems*.

Saji, N., Goswami, B., Vinayachandran, P., and Yamagata, T. (1999). A dipole mode in the tropical indian ocean. *Nature*, 401(6751):360–363.

Samala, B. K., Banerjee, S., Kaginalkar, A., Dalvi, M., et al. (2013). Study of the indian summer monsoon using wrf–roms regional coupled model simulations. *Atmospheric Science Letters*, 14(1):20–27.

Samson, G., Masson, S., Lengaigne, M., Keerthi, M., Vialard, J., Pous, S., Madec, G., Jourdain, N. C., Jullien, S., Menkès, C., et al. (2014). The now regional coupled model: Application to the tropical indian ocean climate and tropical cyclone activity. *Journal of Advances in Modeling Earth Systems*, 6(3):700–722.

Seo, H., Xie, S.-P., Murtugudde, R., Jochum, M., and Miller, A. J. (2009). Seasonal effects of indian ocean freshwater forcing in a regional coupled model. *Journal of Climate*, 22(24):6577–6596.

Sharmila, S., Pillai, P., Joseph, S., Roxy, M., Krishna, R., Chattopadhyay, R., Abhilash, S., Sahai, A., and Goswami, B. (2013). Role of ocean–atmosphere interaction on northward propagation of indian summer monsoon intra-seasonal oscillations (miso). *Climate dynamics*, 41(5-6):1651–1669.

Shchpetkin, A. and McWilliams, J. (2005). The regional ocean modeling system: A split-explicit free-surface topography following coordinates ocean model. *Ocean Modelling*, 9:347–404.

Shenoi, S., Shankar, D., and Shetye, S. (2002). Differences in heat budgets of the near-surface arabian sea and bay of bengal: Implications for the summer monsoon. *Journal of Geophysical Research: Oceans*, 107(C6).

Sikka, D. (1980). Some aspects of the large scale fluctuations of summer monsoon rainfall over india in relation to fluctuations in the planetary and regional scale circulation parameters. *Proceedings of the Indian Academy of Sciences-Earth and Planetary Sciences*, 89(2):179–195.

Sikka, D. and Gadgil, S. (1980). On the maximum cloud zone and the itcz over indian, longitudes during the southwest monsoon. *Monthly Weather Review*, 108(11):1840–1853.

Singh, S., Ghosh, S., Sahana, A., Vittal, H., and Karmakar, S. (2016). Do dynamic regional models add value to the global model projections of indian monsoon? *Climate Dynamics*, pages 1–23.

Sitz, L. E., Di Sante, F., Farneti, R., Fuentes-Franco, R., Coppola, E., Mariotti, L., Reale, M., Sannino, G., Barreiro, M., Nogherotto, R., Giuliani, G., Graffino, G., Solidoro, C., Cossarini, C., and Giorgi, F. (2017). Description and evaluation of the eart system regional climate model (regcm-es). *J. Adv. Model. Earth Syst. (submitted)*.

Skamarock, W. C., Klemp, J. B., Dudhia, J., Gill, D. O., Barker, D. M., Wang, W., and Powers, J. G. (2005). A description of the advanced research wrf version 2. Technical report, DTIC Document.

Smith, W. H. and Sandwell, D. T. (1997). Global sea floor topography from satellite altimetry and ship depth soundings. *Science*, 277(5334):1956–1962.

Solmon, F., Nair, V., and Mallet, M. (2015). Increasing arabian dust activity and the indian summer monsoon. *Atmos. Chem. Phys*, 15(14):8051–8064.

Sperber, K. and Palmer, T. (1996). Interannual tropical rainfall variability in general circulation model simulations associated with the atmospheric model intercomparison project. *Journal of Climate*, 9(11):2727–2750.

Sperber, K. R. and Annamalai, H. (2008). Coupled model simulations of boreal summer intraseasonal (30–50 day) variability, part 1: Systematic errors and caution on use of metrics. *Climate Dynamics*, 31(2-3):345–372.

Sperber, K. R., Annamalai, H., Kang, I.-S., Kitoh, A., Moise, A., Turner, A., Wang, B., and Zhou, T. (2013). The asian summer monsoon: an intercomparison of cmip5 vs. cmip3 simulations of the late 20th century. *Climate Dynamics*, 41(9-10):2711–2744.

Stouffer, R. J., Taylor, K. E., and Meehl, G. A. (2011). Cmip5 long-term experimental design. *CLIVAR Exchanges*, 56:5–7.

Syed, F. S. and Kucharski, F. (2016). Statistically related coupled modes of south asian summer monsoon interannual variability in the tropics. *Atmospheric Science Letters*, 17(2):183–189.

Syed, F. S., Yoo, J. H., Körnich, H., and Kucharski, F. (2012). Extratropical influences on the inter-annual variability of south-asian monsoon. *Climate dynamics*, 38(7-8):1661–1674.

Taylor, K. E., Stouffer, R. J., and Meehl, G. A. (2012). An overview of cmip5 and the experiment design. *Bulletin of the American Meteorological Society*, 93(4):485–498.

Thadathil, P., Gopalakrishna, V., Muraleedharan, P., Reddy, G., Araligidad, N., and Shenoy, S. (2002). Surface layer temperature inversion in the bay of bengal. *Deep Sea Research Part I: Oceanographic Research Papers*, 49(10):1801–1818.

Trenberth, K. E., Stepaniak, D. P., and Caron, J. M. (2000). The global monsoon as seen through the divergent atmospheric circulation. *Journal of Climate*, 13(22):3969–3993.

Tumolo, G. and Bonaventura, L. (2015). A semi-implicit, semi-lagrangian discontinuous galerkin framework for adaptive numerical weather prediction. *Quarterly Journal of the Royal Meteorological Society*, 141(692):2582–2601.

Turner, A., Inness, P., and Slingo, J. (2007). The effect of doubled co2 and model basic state biases on the monsoon-enso system. i: Mean response and interannual variability. *Quarterly Journal of the Royal Meteorological Society*, 133(626):1143–1157.

Turuncoglu, U., Giuliani, G., Elguindi, N., and Giorgi, F. (2013). Modelling the caspian sea and its catchment area using a coupled regional atmosphere-ocean model (regcm4-roms): model design and preliminary results. *Geoscientific Model Development*, 6(2):283.

Turuncoglu, U. U. and Sannino, G. (2016). Validation of newly designed regional earth system model (regesm) for mediterranean basin. *Climate Dynamics*, pages 1–29.

Unnikrishnan, C., Rajeevan, M., Rao, S. V. B., and Kumar, M. (2013). Development of a high resolution land surface dataset for the south asian monsoon region. *Current Science*, 105(9):1235.

Valcke, S. and Redler, R. (2012). The oasis coupler. In *Earth System Modelling-Volume 3*, pages 23–32. Springer.

Varkey, M., Murty, V., and Suryanarayana, A. (1996). Physical oceanography of the bay of bengal and andaman sea.

Waliser, D. E., Graham, N. E., and Gautier, C. (1993). Comparison of the highly reflective cloud and outgoing longwave radiation datasets for use in estimating tropical deep convection. *Journal of Climate*, 6(2):331–353.

Walker, G. T. (1925). Correlation in seasonal variations of weatherâĂŤa further study of world weather 1. *Monthly Weather Review*, 53(6):252–254.

Walker, G. T. and Bliss, E. (1932). World weather. *V. Mem. Roy. Meteor. Soc.*, 4:53–84.

Wang, B., Ding, Q., Fu, X., Kang, I.-S., Jin, K., Shukla, J., and Doblas-Reyes, F. (2005). Fundamental challenge in simulation and prediction of summer monsoon rainfall. *Geophysical Research Letters*, 32(15).

Wang, B., Kang, I.-S., and Lee, J.-Y. (2004). Ensemble simulations of asian–australian monsoon variability by 11 agcms. *Journal of Climate*, 17(4):803–818.

Wang, B., Wu, R., and Li, T. (2003). Atmosphere–warm ocean interaction and its impacts on asian–australian monsoon variation. *Journal of Climate*, 16(8):1195–1211.

Wang, B., Xiang, B., and Lee, J.-Y. (2013). Subtropical high predictability establishes a promising way for monsoon and tropical storm predictions. *Proceedings of the National Academy of Sciences*, 110(8):2718–2722.

Wang, B. and Xie, X. (1997). A model for the boreal summer intraseasonal oscillation. *Journal of the Atmospheric Sciences*, 54(1):72–86.

Webster, P. J. and Chou, L. C. (1980a). Low-frequency transitions of a simple monsoon system. *Journal of the Atmospheric Sciences*, 37(2):368–382.

Webster, P. J. and Chou, L. C. (1980b). Seasonal structure of a simple monsoon system. *Journal of the Atmospheric Sciences*, 37(2):354–367.

Webster, P. J., Magana, V. O., Palmer, T., Shukla, J., Tomas, R., Yanai, M., and Yasunari, T. (1998). Monsoons: Processes, predictability, and the prospects for prediction. *Journal of Geophysical Research: Oceans*, 103(C7):14451–14510.

Webster, P. J., Moore, A. M., Loschnigg, J. P., and Leben, R. R. (1999). Coupled ocean–atmosphere dynamics in the indian ocean during 1997–98. *Nature*, 401(6751):356–360.

Webster, P. J. and Yang, S. (1992). Monsoon and enso: Selectively interactive systems. *Quarterly Journal of the Royal Meteorological Society*, 118(507):877–926.

Xie, S.-P., Annamalai, H., Schott, F. A., and McCreary Jr, J. P. (2002). Structure and mechanisms of south indian ocean climate variability. *Journal of Climate*, 15(8):864–878.

Xie, S.-P., Hu, K., Hafner, J., Tokinaga, H., Du, Y., Huang, G., and Sampe, T. (2009). Indian ocean capacitor effect on indo–western pacific climate during the summer following el niño. *Journal of Climate*, 22(3):730–747.

Xie, S.-P., Kosaka, Y., Du, Y., Hu, K., Chowdary, J. S., and Huang, G. (2016). Indo-western pacific ocean capacitor and coherent climate anomalies in post-enso summer: A review. *Advances in Atmospheric Sciences*, 33(4):411–432.

Yang, J., Liu, Q., Xie, S.-P., Liu, Z., and Wu, L. (2007). Impact of the indian ocean sst basin mode on the asian summer monsoon. *Geophysical Research Letters*, 34(2).

Yasunari, T. (1979). Cloudiness fluctuations associated with the northern hemisphere summer monsoon. *Journal of the Meteorological Society of Japan. Ser. II*, 57(3):227–242.

Yasunari, T. (1980). A quasi-stationary appearance of 30 to 40 day period in the cloudiness fluctuations during the summer monsoon over india. *Journal of the Meteorological Society of Japan. Ser. II*, 58(3):225–229.

Yasunari, T. (1981). Structure of an indian summer monsoon system with around 40-day period. *Journal of the Meteorological Society of Japan. Ser. II*, 59(3):336–354.

Zeng, X., Zhao, M., and Dickinson, R. E. (1998). Intercomparison of bulk aerodynamic algorithms for the computation of sea surface fluxes using toga coare and tao data. *Journal of Climate*, 11(10):2628–2644.

Zhou, T., Turner, A., Kinter, J., Wang, B., Qian, Y., Chen, X., Wu, B., Wang, B., Liu, B., Zou, L., et al. (2016). Gmmip (v1. 0) contribution to cmip6: Global monsoons model inter-comparison project, geosci. model dev., 9, 3589–3604.

Zuo, H., Balmaseda, M. A., and Mogensen, K. (2015). The new eddy-permitting orap5 ocean reanalysis: description, evaluation and uncertainties in climate signals. *Climate Dynamics*, pages 1–21.